Finite Element Analysis of Structures at High Temperatures with Special Application to Plane Steel Beams and Frames

Peterson, Anders

1984

Document Version:
Publisher's PDF, also known as Version of record

LUND INSTITUTE OF TECHNOLOGY
Division of Structural Mechanics
Report TVSM-1001
LUND SWEDEN 1984

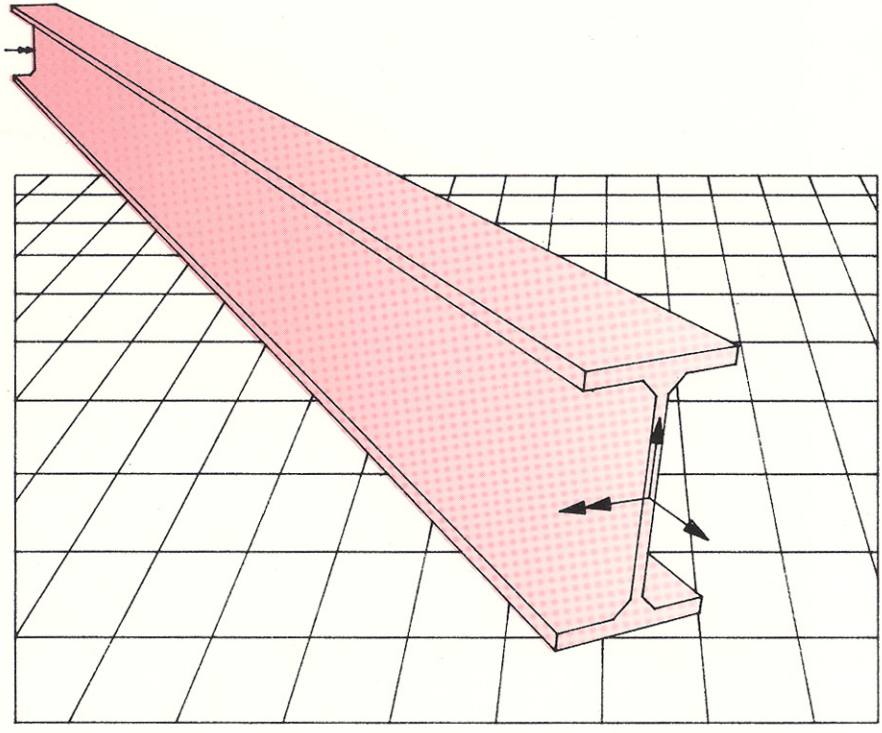

ANDERS PETERSON

FINITE ELEMENT ANALYSIS OF STRUCTURES AT HIGH TEMPERATURES

with special application to plane steel beams and frames

LUND INSTITUTE OF TECHNOLOGY
Division of Structural Mechanics
Report TVSM-1001
CODEN: LUTVDG/(TVSM-1001)/1-151/(1984)

ANDERS PETERSON

FINITE ELEMENT ANALYSIS OF STRUCTURES AT HIGH TEMPERATURES

with special application to plane steel beams and frames

Printed in Sweden
Studentlitteratur
Lund 1984

To Boel

ACKNOWLEDGEMENTS

The research work presented in this thesis has been carried out at the Division of Structural Mechanics, Lund Institute of Technology, Lund.

I wish to express my deep gratitude to Professor Hans Petersson and Docent Sven Thelandersson for their guidance and support during the course of this study and for proposing several improvements of the original manuscript.

Special acknowledgements are also directed to Tekn. Lic. Ola Dahlblom for his cooperation in computer programming, improvements of the manuscript and for many valuable discussions. Improvements of the manuscript have also been proposed by Tekn. Lic. Mats Olsson. His help is appreciated.

The author would like to thank Mrs. Tarja Aunola-Möller and Miss Cecilia Nyqvist for their skill and never failing patience in typing the manuscript, Mr. Bo Zadig for preparing the figures and Civ. Ing. Pål Hansson for the computer drawing on the cover.

I also wish to express my thanks to all other friends at the Division of Structural Mechanics for their support and interest. They have helped to create an atmosphere in which I could finish the work presented in this thesis.

In addition, I wish to thank Mr. Charles Brand for checking the English language.

To my wife Boel and our children Elin, Axel and Olof special thanks are directed for their support and patience during the course of this study.

Financial support given by the Swedish Council for Building Research is acknowledged.

Lund, September 1984

Anders Peterson

CONTENTS PAGE

ABSTRACT

Nonlinear analysis of structures at high temperatures is studied. Both geometric and material nonlinearities are taken into account.

Continuum mechanics relations are used to derive general finite element equations. An alternative formulation to Total Lagrangian (TL) and Updated Lagrangian (UL) formulations named Partially updated Lagrangian (PL) formulation is presented.

An isotropic small strain constitutive model using the von Mises yield criterion is derived for high temperature conditions. The model developed can be characterized as combined elastic-plastic-viscoplastic. The strain components are treated separately but plastic strains and viscoplastic (creep) strains are allowed to interact.

A new formulation of the creep behaviour is given. Both primary and secondary creep are considered.

As an application of the derived finite element equations and the constitutive model steel beams and frames are studied. The theory is implemented in a computer program, CAMFEM. The program operates on a command language with possibilities to store user-defined matrices on files and to create macro commands.

Comparison with experimental observations shows that the present theory well describes experimentally observed phenomena.

Key words: Finite element method, constitutive model, high temperature, plasticity, visco-plasticity, creep, steel, beams, frames, computer program, command language, macro command.

1. INTRODUCTION

1.1 General remarks

High temperatures are characteristic for the operating conditions in many industrial processes and in engineering applications such as combustion engines and nuclear reactors. In such cases special attention must be given to the choice of materials and the design of structural components.

Severe mechanical and thermal loading may also result from accidental situations. The design of structural members with regard to fire is a classical example. Another example is the nuclear power industry where rigorous safety requirements have made it necessary to consider a variety of conceivable accidents, many of which involve thermal shock loading. In many cases the consequences of failure are such that extreme care must be taken to ensure safe and economic design. These applications require methods of analysis which can account for thermal effects in a proper way. Knowledge of the performance of structural materials at high temperatures is also of great importance.

Structural behaviour is mostly predicted by the finite element method (FEM). In high temperature technology the results obtained from such an analysis depend strongly upon the modelling of the nonlinear material behaviour such as plasticity and creep.

In the present investigation special interest is focused on the combined elastic-plastic-thermal-creep behaviour of steel and the finite element formulation of beams in order to establish a procedure that can be adopted in the analysis of plane steel beams and frames in the temperature range 0-700^{o}C. A building steel structure exposed to fire is a typical special application.

1.2 Aim and scope of the present investigation

The analysis of plane steel frames at high temperatures is generally complex due to the many nonlinearities involved. Before the advent

of high speed digital computers, the analysis had to be performed with very crude approximations.

The aim of this investigation is to give a reliable and uniform approach to the analysis of plane steel frames at elevated temperature. Special emphasis is therefore given to a refined constitutive model for the case of small strains, in order to take into account plasticity and creep. An attempt is made to formulate the interaction between plasticity and creep that is observed in experiments. In addition the time dependent behaviour is given a new description.

Starting from a general continuum, the finite element equations for a beam with seven degrees of freedom are derived.

A computer program, based on the theory presented in this report, has been developed. This program facilitates the nonlinear analysis of beam members.

1.3 Summary of the contents

In Chapter 2 the basic equations for nonlinear, static problems are derived from general continuum mechanics. An alternative approach to the commonly used Total Lagrangian (TL) and Updated Lagrangian (UL) formulations named Partially updated Lagrangian (PL) formulation is suggested.

In Chapter 3 a general isotropic, small strain constitutive relation applicable to steel at high temperatures is formulated. The proposed model can be characterized as combined elastic-plastic-viscoplastic. The strain components (elastic, plastic, thermal, creep) are treated separately, but plastic and creep strains are allowed to interact.

In addition, a new formulation of the creep behaviour is given. Both primary and secondary creep are considered.

Based on the general finite element expressions derived in Chapter 2, the corresponding expressions for the beam element considered are given in Chapter 4.

During the course of this study the computer program, CAMFEM, was developed. In Chapter 5 a description of the program is given.

High temperature applications are studied in Chapter 6. Numerical results are compared with measured results from fire tests and/or results obtained by other investigators. A parameter study on a thermally exposed column is performed together with an analysis of a large plane frame using substructure technique.

Finally, Chapter 7 contains concluding remarks and suggestions for future developments.

1.4 Notations

Tensors are generally written in component form with indicial notation. If not otherwise indicated, the summation convention is used. For programming purposes, matrix notations are generally most convenient. Thus, from Chapter 4, the expressions are given in matrix form.

Notations and symbols in the text are explained when they first occur. In addition, notations and symbols are listed in Appendix A.

2. BASIC EQUATIONS OF NONLINEAR PROBLEMS

2.1 Introduction

In structural design linear theories are often used to predict structural behaviour. However, the study of nonlinear behaviour is important in a realistic assessment of the loadbearing capacity of a structure. The nonlinear behaviour is due to two sources, namely material and geometric nonlinearities. The first type of nonlinearity emanates from nonlinear constitutive relations and is described in Chapter 3. The second type appears in that the deformed geometry must be considered when the equlibrium equations are established.

Some fundamental relations in structural mechanics are dealt with in this chapter. For a more comprehensive treatment of continuum mechanics, see Refs. [1] - [8].

2.2 Description of motion

In solving nonlinear problems incremental theories are usually employed. The formulation of an incremental theory begins by dividing the loading path of the body into a number of equilibrium states. When the *Lagrangian description of motion* is chosen, the path of one material point is followed through the various configurations of the body and every position is defined in relation to a reference configuration. All state quantities such as displacements, strains and stresses are assumed to be known with respect to the reference configuration.

A Cartesian reference frame is chosen throughout this study. The motion of a particle in the body can symbolically be written

$$\underset{\sim}{x} = \underset{\sim}{x}(\underset{\sim}{X},t) \tag{2.1}$$

with the rectangular components

$$x_i = x_i(X_1,X_2,X_3,t) \tag{2.2}$$

where X_1, X_2 and X_3 are the *material coordinates* of the particle (coordinates in the reference configuration). The coordinates of its position x_1, x_2 and x_3 are called *spatial coordinates* giving the current position at time t. The material and the spatial coordinates are in the following measured with respect to the same reference axes.

2.3 Displacements, strains and stresses

The Cartesian components of the displacement vector are denoted u_i, defined by

$$x_i = X_i + u_i \tag{2.3}$$

Introducing the *deformation gradient tensor* $\underset{\sim}{F}$ defined by

$$F_{iJ} = \frac{\partial x_i}{\partial X_J} = \delta_{iJ} + \frac{\partial u_i}{\partial X_J} \tag{2.4}$$

the *Green strain tensor* describing the deformation in the current configuration relative to the reference configuration can be expressed as (see [1])

$$\underset{\sim}{E} = \frac{1}{2}(\underset{\sim}{F}^T \cdot \underset{\sim}{F} - \underset{\sim}{I}) \tag{2.5}$$

where $\underset{\sim}{I}$ is the unit tensor. In Eq. (2.4) δ_{iJ} denotes the Kronecker delta. The same deformation can also be measured relative to the current configuration by the *Almansi strain tensor*

$$\underset{\sim}{E}^* = \frac{1}{2}[\underset{\sim}{I} - (\underset{\sim}{F}^{-1})^T \cdot \underset{\sim}{F}^{-1}] \tag{2.6}$$

In rectangular components $\underset{\sim}{E}$ and $\underset{\sim}{E}^*$ can be written as

$$E_{IJ} = \frac{1}{2}\left(\frac{\partial x_k}{\partial X_I}\frac{\partial x_k}{\partial X_J} - \delta_{IJ}\right) \tag{2.7a}$$

$$E^*_{ij} = \frac{1}{2}\left(\delta_{ij} - \frac{\partial X_J}{\partial x_i}\frac{\partial X_J}{\partial x_j}\right) \tag{2.7b}$$

or expressed in displacements u_i

$$E_{IJ} = \frac{1}{2}\left(\frac{\partial u_J}{\partial X_I} + \frac{\partial u_I}{\partial X_J} + \frac{\partial u_k}{\partial X_I}\frac{\partial u_k}{\partial X_J}\right) \tag{2.8a}$$

$$E^*_{ij} = \frac{1}{2}\left(\frac{\partial u_i}{\partial x_j} + \frac{\partial u_j}{\partial x_i} - \frac{\partial u_k}{\partial x_i}\frac{\partial u_k}{\partial x_j}\right) \tag{2.8b}$$

When the displacement gradients are small compared to unity (small strains and rotations) the product terms of the strain tensors are normally negligible. In small displacement analysis the distinction between the strain tensors is usually ignored.

To establish the constitutive equations using the Green strain tensor $\underset{\sim}{E}$, a stress tensor with the same reference is needed. The *second Piola-Kirchhoff stress tensor* $\underset{\sim}{\tilde{T}}$ is such a *symmetric tensor* defined by (see [1]).

$$d\tilde{P}_I = \tilde{T}_{JI}\,\hat{N}_J\,dS^0 \tag{2.9}$$

where $d\underset{\sim}{\tilde{P}}$ is a fictitious force vector related to the reference configuration. $\underset{\sim}{\hat{N}}$ is the outward unit normal vector to the surface dS^0 in the reference configuration. The fictitious force $d\underset{\sim}{\tilde{P}}$ is related to the physical force $d\underset{\sim}{P}$ in the current configuration by

$$d\underset{\sim}{\tilde{P}} = \underset{\sim}{F}^{-1}\cdot d\underset{\sim}{P} \tag{2.10a}$$

or in component form

$$d\tilde{P}_I = \frac{\partial X_I}{\partial x_i}\,dP_i \tag{2.10b}$$

where $d\underset{\sim}{P}$ is defined by the component relation

$$dP_i = T_{ji}\,\hat{n}_j\,dS \tag{2.11}$$

The tensor $\underset{\sim}{T}$ is the *Cauchy stress tensor* and $\underset{\sim}{\hat{n}}$ is the outward unit normal vector to the surface area dS in the current con-

figuration. Now by using the relation between dS and dS^0 given by the expression known as *Nanson's formula* [1]

$$\hat{n}_j \, dS = \det \left| \frac{\partial x_m}{\partial X_N} \right| \frac{\partial X_J}{\partial x_j} \hat{N}_J \, dS^0 \tag{2.12}$$

the relation between the second Piola-Kirchhoff stress tensor and the Cauchy stress tensor may be written as

$$\tilde{T}_{IJ} = \det \left| \frac{\partial x_m}{\partial X_N} \right| \frac{\partial X_I}{\partial x_i} \frac{\partial X_J}{\partial x_j} T_{ij} \tag{2.13}$$

2.4 Equilibrium equations

The equilibrium of a body in the deformed configuration may be written as

$$\frac{\partial T_{ji}}{\partial x_j} + f_i = 0 \tag{2.14}$$

where f_i denotes a component of the body force vector per unit volume. The inertia effects are neglected in Eq. (2.14). A fundamental difficulty in the general application of Eq. (2.14) is that the deformed configuration of the body is unknown. In a Lagrangian formulation it is convenient to express the equilibrium equation in terms of variables referred to the reference configuration [1]

$$\frac{\partial}{\partial X_J} \left(\tilde{T}_{JI} \frac{\partial x_i}{\partial X_I} \right) + f_i^0 = 0 \tag{2.15}$$

Eq. (2.15) can now be multiplied by *weighting functions* $v_{im} = v_{im}(X_1, X_2, X_3)$ and integrated over the reference volume V^0

$$\int_{V^0} v_{im} \frac{\partial}{\partial X_J} \left(\tilde{T}_{JI} \frac{\partial x_i}{\partial X_I} \right) dV^0 + \int_{V^0} v_{im} f_i^0 \, dV^0 = 0 \tag{2.16}$$

The divergence theorem yields

$$\int_{V^0} \frac{\partial v_{im}}{\partial X_J} \tilde{T}_{JI} \frac{\partial x_i}{\partial X_I} dV^0 = \int_{V^0} v_{im} f_i^0 dV^0 + \int_{S^0} v_{im} \hat{N}_J \tilde{T}_{JI} \frac{\partial x_i}{\partial X_I} dS^0 \qquad (2.17)$$

where $\hat{N}_J$ denotes the direction cosine between the X_J-axis and the normal to the surface dS^0 in the reference configuration. The surface integral can alternatively be written as

$$\int_{S^0} v_{im} \hat{N}_J \tilde{T}_{JI} \frac{\partial x_i}{\partial X_I} dS^0 = \int_{S^0} v_{im} \tilde{t}_I \frac{\partial x_i}{\partial X_I} dS^0 = \int_{S^0} v_{im} t_i^0 dS^0 =$$

$$= \int_S v_{im} t_i dS \qquad (2.18)$$

where $\tilde{t}_I$ and t_i^0 are components of the second and first Piola-Kirchhoff traction vectors and t_i an actual force component in the current configuration.

An incremental form of Eq. (2.17) is

$$\int_{V^0} \frac{\partial v_{im}}{\partial X_J} d\tilde{T}_{JI} \frac{\partial x_i}{\partial X_I} dV^0 + \int_{V^0} \frac{\partial v_{im}}{\partial X_J} \tilde{T}_{JI} \frac{\partial (dx_i)}{\partial X_I} dV^0 = dP_m \qquad (2.19)$$

where

$$dP_m = \int_{V^0} v_{im} df_i^0 dV^0 + \int_{S^0} v_{im} d\tilde{t}_I \frac{\partial x_i}{\partial X_I} dS^0 + \int_{S^0} v_{im} \tilde{t}_I \frac{\partial (dx_i)}{\partial X_I} dS^0 =$$

$$= \int_{V^0} v_{im} df_i^0 dV^0 + \int_{S^0} v_{im} dt_i^0 dS^0 \qquad (2.20)$$

In Eq. (2.20) it is assumed that the loading is independent of the deformation (assumed to be valid throughout this study). The incremental relation between stress and strain is assumed to be given in a linearized form (see Chapter 3).

$$d\tilde{T}_{IJ} = C_{IJKL} dE_{KL} - d\tilde{T}_{IJ}^0 \qquad (2.21)$$

where $d\tilde{\tilde{T}}^0$ is an incremental initial or pseudo stress tensor, $\tilde{\tilde{C}}$ is the incremental material stiffness tensor evaluated at the current time referring to the reference configuration and

$$dE_{KL} = \frac{1}{2}\left[\frac{\partial(dx_i)}{\partial X_K}\frac{\partial x_i}{\partial X_L} + \frac{\partial x_i}{\partial X_K}\frac{\partial(dx_i)}{\partial X_L}\right] \tag{2.22}$$

is the increment of the Green strain tensor, see Eq. (2.7a). Eq. (2.3) gives

$$dx_i = du_i \tag{2.23}$$

and

$$\frac{\partial x_i}{\partial X_I} = \delta_{iI} + \frac{\partial u_i}{\partial X_I} \tag{2.24}$$

By use of Eqs. (2.23) and (2.24) $d\tilde{\tilde{E}}$ can be written as

$$dE_{KL} = \frac{1}{2}\left[\frac{\partial(du_i)}{\partial X_K}\left(\delta_{iL} + \frac{\partial u_i}{\partial X_L}\right) + \left(\delta_{iK} + \frac{\partial u_i}{\partial X_K}\right)\frac{\partial(du_i)}{\partial X_L}\right] \tag{2.25}$$

Substitution of Eqs. (2.21), (2.23) and (2.24) into (2.19) yields

$$\int_{V^0} \frac{\partial v_{im}}{\partial X_J}\left(\delta_{iI} + \frac{\partial u_i}{\partial X_I}\right) C_{IJKL}\, dE_{KL}\, dV^0 + \int_{V^0} \frac{\partial v_{im}}{\partial X_J}\tilde{T}_{JI}\frac{\partial(du_i)}{\partial X_I}\, dV^0$$

$$- \int_{V^0} \frac{\partial v_{im}}{\partial X_J}\, d\tilde{T}^0_{JI}\left(\delta_{iI} + \frac{\partial u_i}{\partial X_I}\right) dV^0 = dP_m \tag{2.26}$$

Finally the expression for the incremental Green strain tensor (Eq. (2.25)) is substituted in Eq. (2.26), yielding

$$\int_{V^0} \frac{\partial v_{im}}{\partial X_J}\left(\delta_{iI} + \frac{\partial u_i}{\partial X_I}\right) C_{IJKL}\left(\delta_{kK} + \frac{\partial u_k}{\partial X_K}\right)\frac{\partial(du_k)}{\partial X_L}\, dV^0 \tag{2.27}$$

$$+ \int_{V^0} \frac{\partial v_{im}}{\partial X_J}\tilde{T}_{JI}\frac{\partial(du_i)}{\partial X_I}\, dV^0 - \int_{V^0} \frac{\partial v_{im}}{\partial X_J}\, d\tilde{T}^0_{JI}\left(\delta_{iI} + \frac{\partial u_i}{\partial X_I}\right) dV^0 = dP_m$$

where it is assumed that the material stiffness tensor $\underset{\sim}{C}$ is symmetric ($C_{IJKL} = C_{KLIJ} = C_{JIKL} = C_{IJLK}$). Eq. (2.27) is the governing equation including both geometric and material non-linearities.

2.5 Finite element discretization

In finite element analysis the studied domain V^0 is divided into a number of subdomains V_n^0 which are called *finite elements*. For detailed discussions of the finite element method many text books are available. For more introductory reading, see Refs. [9] - [13]. The displacements u_i are usually chosen as basic unknowns and approximated within each element by use of nodal displacement variables $\bar{u}_n$ of the element, i.e.

$$u_i = \sum_n N_{in} \bar{u}_n \tag{2.28a}$$

if total displacements are the unknowns or

$$du_i = \sum_n N_{in} d\bar{u}_n \tag{2.28b}$$

when increments of displacements are unknowns. In Eq. (2.28) N_{in} are the *interpolation functions*. The summation index n in Eq. (2.28) normally exceeds 3. According to the *Galerkin method* [14] the interpolation functions are chosen as weighting functions, i.e.

$$v_{im} = N_{im} \tag{2.29}$$

Substitution of Eq. (2.28) and Eq. (2.29) into Eq. (2.27) and rearranging the equations gives

$$(K^0_{mn} + K^\sigma_{mn} + K^u_{mn})\, d\bar{u}_n = dR_m \tag{2.30}$$

where

$$K^0_{mn} = \int_{V^0} \frac{\partial N_{Im}}{\partial X_J} C_{IJKL} \frac{\partial N_{Kn}}{\partial X_L} dV^0 \tag{2.31a}$$

$$K^{\sigma}_{mn} = \int_{V^0} \frac{\partial N_{im}}{\partial X_J} \tilde{T}_{JI} \frac{\partial N_{in}}{\partial X_I} \, dV^0 \tag{2.31b}$$

$$K^{u}_{mn} = \int_{V^0} \frac{\partial N_{im}}{\partial X_J} \frac{\partial u_i}{\partial X_I} C_{IJKL} \frac{\partial N_{Kn}}{\partial X_L} \, dV^0 + \int_{V^0} \frac{\partial N_{Im}}{\partial X_J} C_{IJKL} \frac{\partial u_k}{\partial X_K} \frac{\partial N_{kn}}{\partial X_L} \, dV^0$$

$$+ \int_{V^0} \frac{\partial N_{im}}{\partial X_J} \frac{\partial u_i}{\partial X_I} C_{IJKL} \frac{\partial u_k}{\partial X_K} \frac{\partial N_{kn}}{\partial X_L} \, dV^0 \tag{2.31c}$$

$$dR_m = dP_m + \int_{V^0} \frac{\partial N_{im}}{\partial X_J} d\tilde{T}^0_{JI} \left(\delta_{iI} + \frac{\partial u_i}{\partial X_I}\right) dV^0 \tag{2.31d}$$

The matrix K^0 may be called *small displacement* stiffness matrix and the matrices K^{σ} and K^{u} the *initial stress* stiffness matrix and *initial displacement* stiffness matrix respectively.

2.6 Choice of reference configuration

With respect to the reference configuration for the incremental equations either the formulation termed *Total Lagrangian* (TL) or the one termed *Updated Lagrangian* (UL) is usually chosen. In principle, however, any previously calculated configuration may be selected as the reference configuration, although such a general approach may be more cumbersome.

In the TL-formulation all state quantities are referred to the initial undeformed configuration. The integrations are performed over the initial volume (and area), and the material stiffness tensor must be referred to the initial configuration.

The updated Lagrangian description of motion is based on the concept that quantities are updated with respect to the state at the end of each increment. A Lagrangian formulation is thus used with no initial displacements.

When the current configuration is chosen as the reference configuration, Eqs. (2.30)-(2.31) can be written as

$$(K^0_{mn} + K^\sigma_{mn})\ d\bar{u}_n = dR_m \tag{2.32}$$

$$K^0_{mn} = \int_V \frac{\partial N_{im}}{\partial x_j}\ c_{ijk\ell}\ \frac{\partial N_{kn}}{\partial x_\ell}\ dV \tag{2.33a}$$

$$K^\sigma_{mn} = \int_V \frac{\partial N_{km}}{\partial x_j}\ T_{ji}\ \frac{\partial N_{kn}}{\partial x_i}\ dV \tag{2.33b}$$

$$dR_m = dP_m + \int_V \frac{\partial N_{im}}{\partial x_j}\ dT^0_{ji}\ dV \tag{2.33c}$$

where $d\underset{\sim}{P}$ now contains the influence of tractions and body forces in the current configuration, i.e.

$$dP_m = \int_V N_{im}\ df_i\ dV + \int_S N_{im}\ dt_i\ dS \tag{2.34}$$

In Eqs. (2.33) and (2.34) the interpolation functions are calculated in the current configuration. The material stiffness $\underset{\sim}{c}$, referred to the current configuration, can be related to the material stiffness tensor $\underset{\sim}{C}$ in the TL-formulation by the transformation (see [3])

$$c_{ijk\ell} = \det\left|\frac{\partial X_N}{\partial x_n}\right|\ \frac{\partial x_i}{\partial X_P}\ \frac{\partial x_j}{\partial X_Q}\ C_{PQRS}\ \frac{\partial x_k}{\partial X_R}\ \frac{\partial x_\ell}{\partial X_S} \tag{2.35}$$

Finite element analyses of nonlinear problems by use of either the TL-formulation or the UL-formulation have been presented in a large number of papers, see for example Refs. [15] - [29].

According to Ref. [6] there is no theoretical difference between the TL- and UL-formulations and provided that appropriate material stiffness tensors are used they should give the same numerical result. In practice, the TL-formulation seems to be much more complicated than the UL-formulation as it contains more terms. It may, however, be more difficult to apply the UL-formulation in a correct way. This is due to that integrations have to

be performed with respect to the current volume V instead of the initial volumne V^0 and due to Eq. (2.35). A third approach, named *Partially updated Lagrangian (PL) formulation* outlined in Section 2.7, may therefore be found to be an attractive alternative.

2.7 Partially updated Lagrangian formulation

The considered region V^0 is divided into subregions (finite elements) and the notation for one such subregion is V^*. A local Cartesian coordinate system $\underset{\sim}{X}^*$ is referred to each subregion V^*. The motion of a particle within V^* can symbolically be written as

$$\underset{\sim}{x}^* = \underset{\sim}{x}^*(\underset{\sim}{X}^*, t) \tag{2.36}$$

or in component form

$$x_i^* = x_i^*(X_1^*, X_2^*, X_3^*, t) \tag{2.37}$$

where t denotes time.

The local coordinate system $\underset{\sim}{X}^*$ is translated and rotated relative to the fixed global Cartesian system $\underset{\sim}{x}$ as the deformation process proceeds. It is, however, not a true corotational system but remains fixed during each step (or iteration) in the computation procedure.

The components of the stress tensor $\underset{\sim}{\tilde{T}}$ depend on the chosen reference for material orientation but is not influenced by the choice of the local coordinate system $\underset{\sim}{X}^*$. The same holds for the components of the strain tensor $\underset{\sim}{E}$. The equlibrium equations, Eq. (2.15), can therefore equally well be written as

$$\frac{\partial}{\partial X_J^*}\left(\tilde{T}_{JI}\,\frac{\partial x_i^*}{\partial X_I^*}\right) + f_i^* = 0 \tag{2.38}$$

This corresponds, according to Eq. (2.19) and Eq. (2.20), to the incremental formulation

$$\int_{V^*} \frac{\partial v^*_{im}}{\partial X^*_J} \frac{\partial x^*_i}{\partial X^*_I} d\tilde{T}_{JI}\, dV^* + \int_{V^*} \frac{\partial v^*_{im}}{\partial X^*_J} \tilde{T}_{JI} \frac{\partial (dx^*_i)}{\partial X^*_I} dV^* = dP^*_m \tag{2.39}$$

$$dP^*_m = \int_{V^*} v^*_{im}\, df^*_i\, dV^* + \int_{S^*} v^*_{im}\, dt^{0*}_i\, dS^* \tag{2.40}$$

where V^* and S^* refer to the initial configuration (although translated and rotated) and t^{0*}_i is a component of the first Piola-Kirchhoff traction vector.

The quantity x^*_i is replaced by the displacement u^*_i,

$$dx^*_i = du^*_i \tag{2.41}$$

and

$$\frac{\partial x^*_i}{\partial X^*_I} = \delta_{iI} + \frac{\partial u^*_i}{\partial X^*_I} \tag{2.42}$$

which after substitution into Eq. (2.39) yields

$$\int_{V^*} \frac{\partial v^*_{im}}{\partial X^*_J} (\delta_{iI} + \frac{\partial u^*_i}{\partial X^*_I})\, d\tilde{T}_{JI}\, dV^* + \int_{V^*} \frac{\partial v^*_{im}}{\partial X^*_J} \tilde{T}_{JI} \frac{\partial (du^*_i)}{\partial X^*_I} dV^* = dP^*_m \tag{2.43}$$

The constitutive relation, Eq. (2.21), is still assumed to be valid

$$d\tilde{T}_{IJ} = C_{IJKL}\, dE_{KL} - d\tilde{T}^0_{IJ} \tag{2.44}$$

where the strain increment can be determined from

$$dE_{KL} = \frac{1}{2}\left[\frac{\partial (du^*_\ell)}{\partial X^*_K} (\delta_{\ell L} + \frac{\partial u^*_\ell}{\partial X^*_L}) + (\delta_{\ell K} + \frac{\partial u^*_\ell}{\partial X^*_K}) \frac{\partial (du^*_\ell)}{\partial X^*_L} \right] \tag{2.45}$$

in accordance with Eq. (2.25).

The substitution of Eqs. (2.44) and (2.45) into Eq. (2.43) yields (observing symmetric properties of the constitutive tensor $\underset{\sim}{C}$)

$$\int_{V^*} \frac{\partial v^*_{im}}{\partial X^*_J} (\delta_{iI} + \frac{\partial u^*_i}{\partial X^*_I}) C_{IJKL} (\delta_{\ell K} + \frac{\partial u^*_\ell}{\partial X^*_K}) \frac{\partial (du^*_\ell)}{\partial X^*_L} dV^*$$

$$+ \int_{V^*} \frac{\partial v^*_{im}}{\partial X^*_J} \underset{\sim}{T}_{JI} \frac{\partial (du^*_i)}{\partial X^*_I} dV^* = dR^*_m \qquad (2.46)$$

where

$$dR^*_m = \int_{V^*} \frac{\partial v^*_{im}}{\partial X^*_J} (\delta_{iI} + \frac{\partial u^*_i}{\partial X^*_I}) d\underset{\sim}{T}^{0}_{JI} + \int_{V^*} v^*_{im} df^*_i dV^* + \int_{S^*} v^*_{im} dt^{0*}_i dS^* \qquad (2.47)$$

The corresponding finite element formulation is in accordance with Section 2.5

$$(K^0_{mn} + K^\sigma_{mn} + K^u_{mn}) d\bar{u}^*_n = dR^*_m \qquad (2.48)$$

with

$$K^0_{mn} = \int_{V^*} \frac{\partial N_{Im}}{\partial X^*_J} C_{IJKL} \frac{\partial N_{Kn}}{\partial X^*_L} dV^* \qquad (2.49a)$$

$$K^\sigma_{mn} = \int_{V^*} \frac{\partial N_{im}}{\partial X^*_J} \underset{\sim}{T}_{JI} \frac{\partial N_{in}}{\partial X^*_I} dV^* \qquad (2.49b)$$

$$K^u_{mn} = \int_{V^*} \frac{\partial N_{im}}{\partial X^*_J} \frac{\partial u^*_i}{\partial X^*_I} C_{IJKL} \frac{\partial N_{Kn}}{\partial X^*_L} dV^* + \int_{V^*} \frac{\partial N_{Im}}{\partial X^*_J} C_{IJKL} \frac{\partial u^*_\ell}{\partial X^*_K} \frac{\partial N_{\ell n}}{\partial X^*_L} dV^*$$

$$+ \int_{V^*} \frac{\partial N_{im}}{\partial X^*_J} \frac{\partial u^*_i}{\partial X^*_I} C_{IJKL} \frac{\partial u^*_\ell}{\partial X^*_K} \frac{\partial N_{\ell n}}{\partial X^*_L} dV^* \qquad (2.49c)$$

$$dR_m^* = \int_{V^*} \frac{\partial N_{im}}{\partial X_J^*} \left(\delta_{iI} + \frac{\partial u_i^*}{\partial X_I^*}\right) d\tilde{T}_{JI}^0 \, dV^* + \int_{V^*} N_{im} \, df_i^* \, dV^* + \int_{S^*} N_{im} \, dt_i^{0*} \, dS^* \tag{2.49d}$$

It is remarkable that the term K^u in Eq. (2.48) is not normally considered in an updated incremental finite element analysis, even when local Cartesian coordinate systems are used. It corresponds to neglecting local element deformations, which may give rise to substantial errors, see for example Appendix D.2.

The formulation derived in this section is applied on plane beam elements in Chapter 4.

3. CONSTITUTIVE EQUATIONS

3.1 Introduction

In Chapter 2 the fundamental equations for solving nonlinear problems by the finite element method were derived. A successful application of these equations requires that the nonlinear material behaviour is adequately modelled.

In the present chapter an isotropic, small strain constitutive relation applicable to high temperature conditions is suggested.

The class of problems considered here involves nonlinear stress-strain relations which depend on temperature. In addition nonlinear creep type rate dependence has to be taken into account. The model proposed herein can be characterized as combined elastic-plastic-viscoplastic.

It is commonly assumed that instantaneous plastic strain and time dependent strain (creep) can be treated as independent components with separate hardening rules ([41] - [54]). This is not physically justified, however, since it is impossible to make a clear distinction between the two strain components. In the present model the strain components are also treated separately, but allowed to interact. A similar treatment is reported in Refs. [55] and [56].

In addition a completely new formulation of the creep behaviour is given. Both primary and secondary creep are considered.

Due to the potential applications the time scale considered is of the order of hours and days rather than months and years. On the other hand it is assumed that strain rates are sufficiently small to neglect dynamic rate dependence.

In the present chapter the engineering notations $\underset{\sim}{\sigma}$ and $\underset{\sim}{\varepsilon}$ are used for the stress tensor and the strain tensor respectively.

For a more detailed treatment of the basic concepts of the theory of creep and plasticity see Refs. [30] - [40].

3.2 Strain components

The total strain rate tensor $\dot{\underset{\sim}{\varepsilon}}$ is assumed to be decomposed into four parts

$$\dot{\varepsilon}_{k\ell} = \dot{\varepsilon}^{E}_{k\ell} + \dot{\varepsilon}^{P}_{k\ell} + \dot{\varepsilon}^{VP}_{k\ell} + \dot{\varepsilon}^{T}_{k\ell} \tag{3.1}$$

where $\dot{\underset{\sim}{\varepsilon}}^{E}$, $\dot{\underset{\sim}{\varepsilon}}^{P}$, $\dot{\underset{\sim}{\varepsilon}}^{VP}$ and $\dot{\underset{\sim}{\varepsilon}}^{T}$ are the elastic, plastic, viscoplastic (creep) and thermal strain rate tensors respectively. The decomposition (Eq. (3.1)) may be illustrated for uniaxial stress by Figure 3.1.

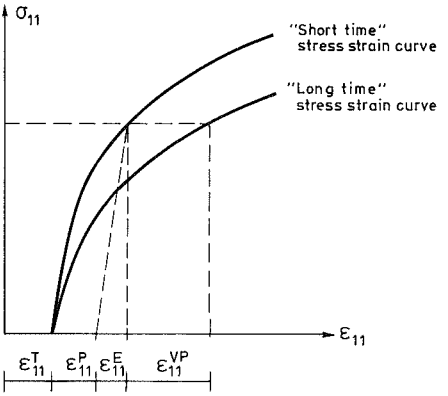

Figure 3.1 Strain components

Elastic components of strain are linearly related to the stress components by the generalized Hooke's law

$$\sigma_{ij} = C^{E}_{ijk\ell}\ \varepsilon^{E}_{k\ell} \tag{3.2}$$

where $\underset{\sim}{C}^{E}$ is the isotropic linear material stiffness tensor with the components

$$C^{E}_{ijk\ell} = \lambda\delta_{ij}\ \delta_{k\ell} + \mu(\delta_{ik}\ \delta_{j\ell} + \delta_{i\ell}\ \delta_{jk}) \tag{3.3}$$

In Eq. (3.3) λ and μ are the Lamé constants related to the elastic modulus E and Poisson's ratio ν by

$$\lambda = \frac{\nu E}{(1+\nu)(1-2\nu)} \tag{3.4a}$$

$$\mu = \frac{E}{2(1+\nu)} \tag{3.4b}$$

Both E and ν may in general be temperature dependent.

The stress rate can be expressed by taking the time derivate of Eq. (3.2) giving

$$\dot{\sigma}_{ij} = C^E_{ijk\ell}\,\dot{\varepsilon}^E_{k\ell} + \dot{C}^E_{ijk\ell}\,\varepsilon^E_{k\ell} \tag{3.5}$$

Solving Eq. (3.5) for the elastic strain rate yields

$$\dot{\varepsilon}^E_{k\ell} = F_{k\ell mn}\,(\dot{\sigma}_{mn} - \dot{C}^E_{mnpq}\,\varepsilon^E_{pq}) \tag{3.6}$$

where

$$F_{k\ell mn} = -\frac{\nu}{E}\,\delta_{k\ell}\,\delta_{mn} + \frac{1+\nu}{2E}\,(\delta_{km}\,\delta_{\ell n} + \delta_{kn}\,\delta_{\ell m}) \tag{3.7}$$

The thermal strain tensor is written as

$$\dot{\varepsilon}^T_{k\ell} = \delta_{k\ell}\,\alpha\,\dot{T} \tag{3.8}$$

where T is the temperature and α the coefficient of thermal expansion, which may depend on the temperature.

The plastic strain rate $\dot{\underset{\sim}{\varepsilon}}^P$ and the viscoplastic strain rate $\dot{\underset{\sim}{\varepsilon}}^{VP}$ will be discussed in later sections.

3.3 Plastic yield surface

The plastic *yield condition* defines stress states where plastic deformation occurs and can generally be expressed as

$$F^P(\underset{\sim}{\sigma}, T, \kappa^P) = 0 \tag{3.9}$$

where κ^P is a strain hardening parameter. Eq. (3.9) can be interpreted as a surface, called the *yield surface*, in the nine-dimensional stress space. The scalar function F^P is called the *yield function* or the *loading function*. When $F^P < 0$ the plastic strain rate is zero while plastic strain occurs when $F^P = 0$. Since stress states corresponding to $F^P > 0$ are not admissible the

consistency condition $\dot{F}^P = 0$ must hold for plastic straining.

A widely used yield condition for steel, is the one suggested by von Mises [57] in which yielding occurs when

$$F^P = \sqrt{3J_2'} - Y^P(T,\kappa^P) = 0 \tag{3.10}$$

where $Y^P(T,\kappa^P)$ is a scalar function and J_2' is the second invariant of the deviatoric stress tensor given by

$$J_2' = \frac{1}{2}\,\sigma'_{ij}\,\sigma'_{ij} \tag{3.11}$$

and

$$\sigma'_{ij} = \sigma_{ij} - \frac{1}{3}\,\delta_{ij}\,\sigma_{kk} \tag{3.12}$$

The scalar function $\sqrt{3J_2'}$ is also called *effective stress* $\bar{\sigma}$.

3.4 Flow rules

The plastic strain rate can be expressed by the *normality condition*

$$\dot{\varepsilon}^P_{ij} = \dot{\lambda}_1 \frac{\partial F^P}{\partial \sigma_{ij}} \tag{3.13}$$

where $\dot{\lambda}_1$ is a scalar function not yet determined and $\partial F^P/\partial \underset{\sim}{\sigma}$ is a normal to the surface $F^P = 0$. The relationship (3.13) is called an *associated flow rule*, since it is associated with the yield function F^P. When Eqs. (3.10) through (3.12) are used the normal to the yield surface is given by

$$\frac{\partial F^P}{\partial \sigma_{ij}} = \frac{\partial \bar{\sigma}}{\partial \sigma_{ij}} = \frac{3}{2}\,\frac{1}{\bar{\sigma}}\,\frac{\partial J_2'}{\partial \sigma_{ij}} = \frac{3}{2}\,\frac{\sigma'_{ij}}{\bar{\sigma}} \tag{3.14}$$

The viscoplastic strain rate is often defined by means of a flow rule similar to that of plasticity. The assumption of viscoplastic strain rate normal to a viscoplastic loading surface $F^{VP} = 0$ is normally adopted [32], i.e.

$$\dot{\varepsilon}_{ij}^{VP} = \dot{\lambda}_2 \frac{\partial F^{VP}}{\partial \sigma_{ij}} \tag{3.15}$$

where $\dot{\lambda}_2$ is a scalar function. The viscoplastic loading function F^{VP} is assumed to have the same form as F^P in Eq. (3.10), i.e.

$$F^{VP} = F^{VP}(\underset{\sim}{\sigma}, T, \kappa^{VP}) = \sqrt{3J_2'} - Y^{VP}(T, \kappa^{VP}) \tag{3.16}$$

where κ^{VP} is a hardening parameter describing the hardening of the viscoplastic loading surface.

It follows from Eq. (3.16) that

$$\frac{\partial F^{VP}}{\partial \sigma_{ij}} = \frac{\partial F^P}{\partial \sigma_{ij}} \tag{3.17}$$

and Eq. (3.15) can be rewritten as

$$\dot{\varepsilon}_{ij}^{VP} = \dot{\lambda}_2 \frac{\partial F^P}{\partial \sigma_{ij}} \tag{3.18}$$

The scalar function $\dot{\lambda}_2$ which governs the time dependent behaviour of the material will be described in Section 3.7.

3.5 Hardening rule

After initial yielding the stress states at which further plastic deformation occurs depend on the strain hardening parameter κ^P.

The isotropic hardening adopted in this study implies that the yield surface increases in size and maintains its original shape. It should be noted that the Bauschinger effect cannot be modelled by this hardening rule.

The current value of the loading function F^P under isotropic plastic flow can be calculated using the *strain-hardening hypothesis*. This hypothesis assumes that the hardening is a function of the plastic strain $\underset{\sim}{\varepsilon}^P$, i.e.

$$\kappa^P = \kappa^P(\underset{\sim}{\varepsilon}^P) \tag{3.19}$$

The following functional dependence is commonly used for steel

$$\kappa^P = \bar{\varepsilon}^P = \int \dot{\bar{\varepsilon}}^P \, dt \tag{3.20}$$

where

$$\dot{\bar{\varepsilon}}^P = \sqrt{\frac{2}{3} \dot{\varepsilon}^P_{ij} \dot{\varepsilon}^P_{ij}} \tag{3.21}$$

The scalar $\bar{\varepsilon}^P$ is the *effective plastic strain*. If Eqs. (3.13) and (3.14) are substituted into Eq. (3.21), the equivalent plastic strain rate is given by

$$\dot{\bar{\varepsilon}}^P = \sqrt{\frac{2}{3} (\dot{\lambda}_1 \frac{3}{2} \frac{\sigma'_{ij}}{\bar{\sigma}}) (\dot{\lambda}_1 \frac{3}{2} \frac{\sigma'_{ij}}{\bar{\sigma}})} = \dot{\lambda}_1 \sqrt{\frac{3}{2} \frac{\sigma'_{ij} \sigma'_{ij}}{\bar{\sigma}^2}} = \dot{\lambda}_1 \tag{3.22}$$

In this study an alternative approach is suggested. Figure 3.2 illustrates experimental curves reported in Refs. [37], [65] and [66].

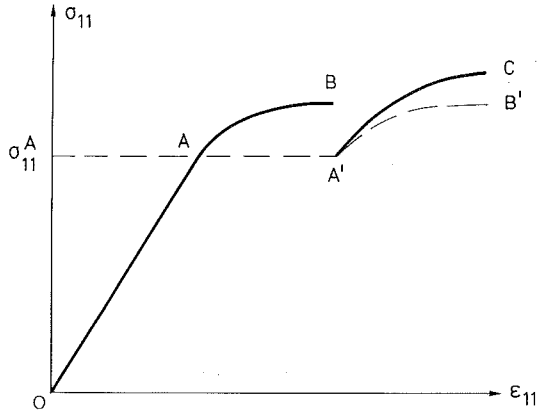

Figure 3.2 Experimentally obtained stress-strain relations

The curve O-A-B corresponds to instantaneous deformation at constant temperature with negligible creep. The result from a creep test at constant stress σ^A_{11} is showed by the dashed

line A-A'. If the creep test is followed by a further increase in stress, the observed response is described by the curve A'-C. If creep strain and instantaneous plastic strain had been uncoupled, as is often assumed, the response should be according to curve A'-B'. These tests clearly indicate that the plastic hardening is affected by the previously accumulated creep strain. To account for this behaviour the hardening parameter κ^P must be taken as a function of both plastic strain and creep strain, i.e.

$$\kappa^P = \kappa^P(\underset{\sim}{\varepsilon}^P, \underset{\sim}{\varepsilon}^{VP}) \tag{3.23}$$

As a natural and simple assumption κ^P may be taken as a function of the sum $\underset{\sim}{\varepsilon}^M$ of $\underset{\sim}{\varepsilon}^P$ and $\underset{\sim}{\varepsilon}^{VP}$. Then the strain hardening rule described in Eqs. (3.20) - (3.22) can be generalized as

$$\kappa^P = \bar{\varepsilon}^M = \int \dot{\bar{\varepsilon}}^M \, dt \tag{3.24}$$

where

$$\dot{\bar{\varepsilon}}^M = \sqrt{\frac{2}{3} \dot{\varepsilon}^M_{ij} \dot{\varepsilon}^M_{ij}} \tag{3.25}$$

in which

$$\dot{\varepsilon}^M_{ij} = \dot{\varepsilon}^P_{ij} + \dot{\varepsilon}^{VP}_{ij} \tag{3.26}$$

Inserting Eqs. (3.13), (3.18) and (3.26) into (3.25) one obtains

$$\dot{\bar{\varepsilon}}^M = \dot{\lambda}_1 + \dot{\lambda}_2 \tag{3.27}$$

Both hardening expressions, Eqs. (3.19) and (3.23), can be summarized by

$$\kappa^P = \int \dot{\kappa}^P \, dt \tag{3.28}$$

where now

$$\dot{\kappa}^P = \dot{\lambda}_1 + \xi \dot{\lambda}_2 \tag{3.29}$$

The scalar ξ is given unit value if the plastic hardening depends on the accumulated viscoplastic strain according to Eqs. (3.24) - (3.26) and zero if plastic and viscoplastic behaviour are uncoupled.

3.6 Stress-strain relation

During loading in the plastic region the stress point remains on the yield surface. The consistency condition must be satisfied, i.e.

$$\dot{F}^P = \frac{\partial F^P}{\partial \sigma_{ij}} \dot{\sigma}_{ij} + \frac{\partial F^P}{\partial T} \dot{T} + \frac{\partial F^P}{\partial \kappa^P} \dot{\kappa}^P = 0 \tag{3.30}$$

Eqs. (3.10), (3.28) and (3.29) yield

$$\frac{\partial F^P}{\partial \kappa^P} \dot{\kappa}^P = \frac{\partial F^P}{\partial Y^P} \frac{\partial Y^P}{\partial \kappa^P} (\dot{\lambda}_1 + \xi \dot{\lambda}_2) \tag{3.31}$$

Noting that $\partial F^P / \partial Y^P = -1$ and with the notation

$$H' = \frac{\partial Y^P}{\partial \kappa^P} \tag{3.32}$$

Eq. (3.31) yields

$$\frac{\partial F^P}{\partial \kappa^P} \dot{\kappa}^P = -H'(\dot{\lambda}_1 + \xi \dot{\lambda}_2) \tag{3.33}$$

By substitution of Eqs. (3.1), (3.5), (3.13) and (3.33) into Eq. (3.30) and solving for $\dot{\lambda}_1$ one obtains

$$\dot{\lambda}_1 = \frac{1}{s} \left[\frac{\partial F^P}{\partial \sigma_{ij}} \{ C^E_{ijk\ell} (\dot{\varepsilon}_{k\ell} - \dot{\varepsilon}^T_{k\ell} - \dot{\varepsilon}^{VP}_{k\ell}) + \dot{C}^E_{ijk\ell} \varepsilon^E_{k\ell} \} + \frac{\partial F^P}{\partial T} \dot{T} - H' \xi \dot{\lambda}_2 \right] \tag{3.34}$$

where the scalar s is defined by

$$s = \frac{\partial F^P}{\partial \sigma_{ij}} C^E_{ijk\ell} \frac{\partial F^P}{\partial \sigma_{k\ell}} + H' \tag{3.35}$$

It may be noticed that the scalar s contains two parts, one hardening independent part and one hardening dependent part.

A relation between stress rates and strain rates is now obtained by combination of Eqs. (3.1), (3.5), (3.13), (3.34) and (3.35)

$$\dot{\sigma}_{ij} = C^{EP}_{ijk\ell}\,\dot{\varepsilon}_{k\ell} - \dot{\sigma}^{0}_{ij} \tag{3.36}$$

where

$$C^{EP}_{ijk\ell} = C^{E}_{ijk\ell} - \beta\cdot\frac{1}{s}\,C^{E}_{ijmn}\,\frac{\partial F^{P}}{\partial \sigma_{mn}}\,\frac{\partial F^{P}}{\partial \sigma_{rs}}\,C^{E}_{rsk\ell} \tag{3.37}$$

and

$$\dot{\sigma}^{0}_{ij} = C^{EP}_{ijk\ell}\,(\dot{\varepsilon}^{T}_{k\ell} + \dot{\varepsilon}^{VP}_{k\ell}) + \beta\cdot\frac{1}{s}\Big[C^{E}_{ijk\ell}\,\frac{\partial F^{P}}{\partial \sigma_{k\ell}}\,(\frac{\partial F^{P}}{\partial T}\,\dot{T} - H'\xi\dot{\lambda}_{2})$$

$$+ C^{E}_{ijmn}\,\frac{\partial F^{P}}{\partial \sigma_{mn}}\,\frac{\partial F^{P}}{\partial \sigma_{rs}}\,\dot{C}^{E}_{rsk\ell}\,\varepsilon^{E}_{k\ell}\Big] - \dot{C}^{E}_{ijk\ell}\,\varepsilon^{E}_{k\ell} \tag{3.38}$$

The value of the coefficient β in Eqs. (3.37) and (3.38) depends on whether loading or unloading (neutral loading) is taking place, i.e.

$$\beta = \begin{cases} 1 & \text{if } \dfrac{\partial F^{P}}{\partial \sigma_{ij}}\,\dot{\sigma}_{ij} + \dfrac{\partial F^{P}}{\partial T}\,\dot{T} > 0 \quad \text{and } F^{P} = 0 \\ 0 & \text{otherwise} \end{cases} \tag{3.39}$$

The terms in Eq. (3.38) which contain $\dot{\underset{\sim}{C}}^{E}$ represent the stress increment due to a thermally induced change in the elastic constitutive tensor. The term containing $\partial F^{P}/\partial T$ in the same equation accounts for the stress increment caused by a modification in the yield surface due to a temperature change.

The quantity H' given by Eq. (3.32) can be interpreted as the slope of the stress-plastic strain diagram in a standard uniaxial tension test. Since dynamic rate dependence is not considered, such a test is representative for the instantaneous response upon loading.

The increment of the stress tensor can be calculated directly from Eqs. (3.36) - (3.38) when the behaviour during a time increment is either elastic ($\beta = 0$) or plastic ($\beta = 1$). The computational aspects of the stress calculation in the transition range from elastic to elastic-plastic behaviour are described in Appendix B.

Constitutive equations corresponding to Eqs. (3.36) - (3.38) with $\xi = 0$ have also been described by Refs. [42] - [44]. Other papers that can be mentioned in the field of constitutive modelling at high temperatures are Refs. [58] - [64] and [67] - [71].

3.7 Time dependent behaviour

In Section 3.4 the assumption of viscoplastic strain rate normal to the plastic yield surface was adopted. The viscoplastic strain rate thus can be expressed as

$$\dot{\varepsilon}_{ij}^{VP} = \dot{\lambda}_2 \frac{3}{2} \frac{\sigma'_{ij}}{\bar{\sigma}} \tag{3.40}$$

where Eq. (3.14) is used for the normal direction. The scalar $\dot{\lambda}_2$ can be evaluated from the special case of uniaxial creep. An explicit expression for $\dot{\lambda}_2$ can be deduced from any creep law relevant for the present problem.

In Ref. [59] different approaches for the scalar $\dot{\lambda}_2$ are discussed and in Ref. [72] a uniaxial law widely used in fire applications is described. In the following an alternative creep model will be proposed. In this model the coupling between plastic strain and viscoplastic strain is taken into account.

Assume that the scalar $\dot{\lambda}_2$ for the viscoplastic strain rate can be written as two additive components, i.e.

$$\dot{\lambda}_2 = g_1(\bar{\sigma}, T, \kappa^{VP}) + g_2(\bar{\sigma}, T) \tag{3.41}$$

where $\bar{\sigma}$ is the effective stress and κ^{VP} is a hardening function governing the viscoplastic strain rate cf. Eq. (3.16).

The second part of Eq. (3.41) concerns the secondary creep phase with a constant creep strain rate (stationary creep) and is assumed to be described by the Norton power law

$$g_2(\bar{\sigma}, T) = \gamma_2(T) \left(\frac{\bar{\sigma}}{E(20)}\right)^{n(T)} \tag{3.42}$$

where E(20) is the modulus of elasticity at $20^{\circ}C$. The fluidity parameter γ_2 and the exponent n can be determined from uniaxial tension creep tests ($\bar{\sigma} = \sigma_{11}$) at different temperatures and stress levels.

The primary creep phase corresponding to g_1 in Eq. (3.41) is characterized by an initially large strain rate which decreases due to the strain hardening. The viscoplastic loading function F^{VP} defined in Eq. (3.16) is used to describe the creep function g_1, and as a consequence of the coupling between plastic and viscoplastic behaviour described in Eqs. (3.24) - (3.27) it is logical to assume

$$\kappa^{VP} = \kappa^{P} = \bar{\varepsilon}^{M} \tag{3.43}$$

Thus Eq. (3.16) can be rewritten as

$$F^{VP}(\underset{\sim}{\sigma}, T, \kappa^{VP}) = \bar{\sigma} - Y^{VP}(T, \bar{\varepsilon}^{M}) \tag{3.44}$$

where Y^{VP} is a scalar function which can be obtained from uniaxial creep tests, see Figure 3.3. In Figure 3.3b the function Y^{P} defining the size of the yield surface is also shown.

It should be noted that for the case when plastic and viscoplastic strains are uncoupled $\bar{\varepsilon}^{M}$ is replaced by $\bar{\varepsilon}^{VP}$, defined in analogy with Eq. (3.21).

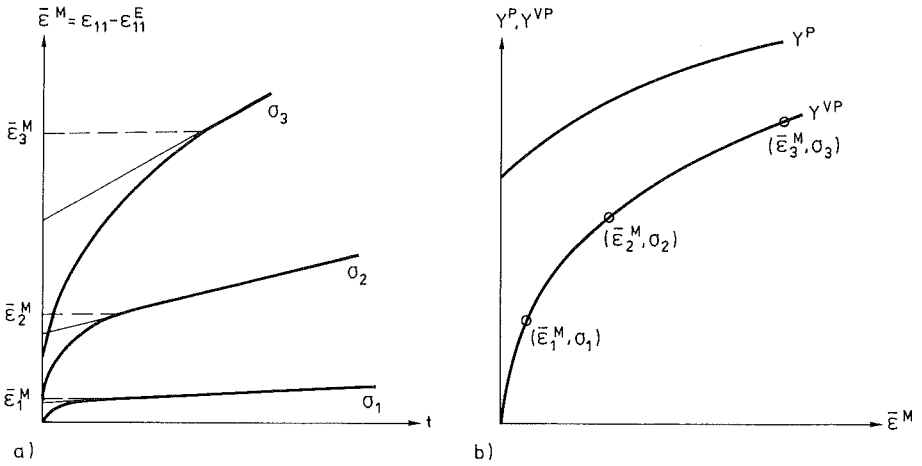

Figure 3.3 a) Creep curves at constant temperature
b) The function $Y^{VP}(T, \bar{\varepsilon}^M)$ obtained from the creep curves in a)

The function g_1 is now written as

$$g_1(\bar{\sigma}, T, \bar{\varepsilon}^M) = \gamma_1(T) < \phi(F^{VP}) > \tag{3.45}$$

where the brackets indicate that

$$<\phi(F^{VP})> = 0 \qquad \text{if } F^{VP} \leq 0 \tag{3.46}$$

$$<\phi(F^{VP})> = \phi(F^{VP}) \qquad \text{if } F^{VP} > 0$$

The scalar function ϕ is given in the simplified form

$$\phi(F^{VP}) = \frac{F^{VP}(\underline{\sigma}, T, \bar{\varepsilon}^M)}{E(20)} \tag{3.47}$$

or

$$\phi(F^{VP}) = \frac{\bar{\sigma} - Y^{VP}(T, \bar{\varepsilon}^M)}{E(20)} \tag{3.48}$$

At constant temperature and stress the function g_1 in most cases approaches zero within time since the numerator of Eq. (3.48) continuously decreases due to strain hardening. This is illustrated for the uniaxial case $\bar{\sigma} = \sigma^A_{11}$ in Figure 3.4.

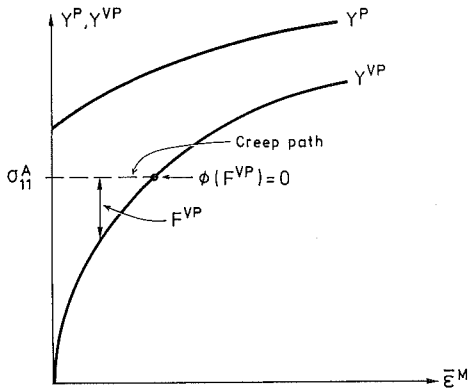

Figure 3.4 Strain hardening in primary creep

The fluidity parameter γ_1 can be determined from uniaxial tension tests and will not be further discussed.

3.8 Verification of the constitutive model

3.8.1 General remarks

In this section the constitutive model is applied in uniaxial stress and compared with test data. Ideally a quantitative calibration of the model requires a complete set of test data for temperatures in the range 0-700°C for any particular grade of steel. Much experimental information can be found in literature but a sufficiently complete data base is lacking in most cases.

The approach taken here is instead to identify the relative temperature dependence typical for the properties of mild structural steel. The properties of a particular steel quality can then be specified by standard properties at normal

temperature (20°C) like yield stress $\sigma_y(20)$ (= $Y^P(20,0)$), elastic modulus E(20) and coefficient of thermal expansion $\alpha(20)$.

The general temperature dependence of different material parameters as well as the numerical values of parameters used in the creep model are given in Appendix C. These parameters are assumed to give a general description of mild structural steel and are used throughout this thesis. Standard properties specified for different grades of steel are given separately for each particular application.

3.8.2 Creep tests

In this section the creep response of the model is compared with the tests used to determine the creep parameters [65]. Calculated creep curves for three different temperatures are shown together with experimental ones in Figures 3.5 - 3.7.

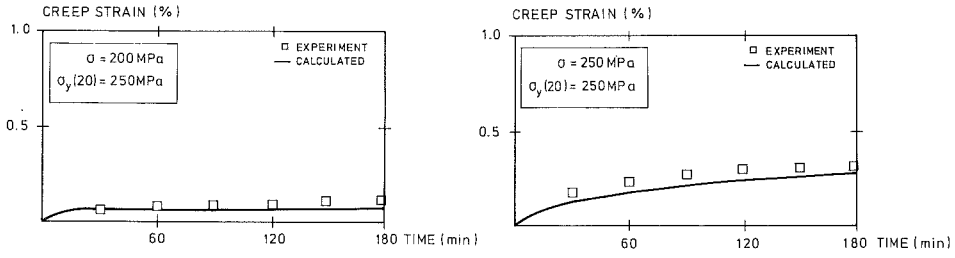

Figure 3.5 Creep curves at 400°C

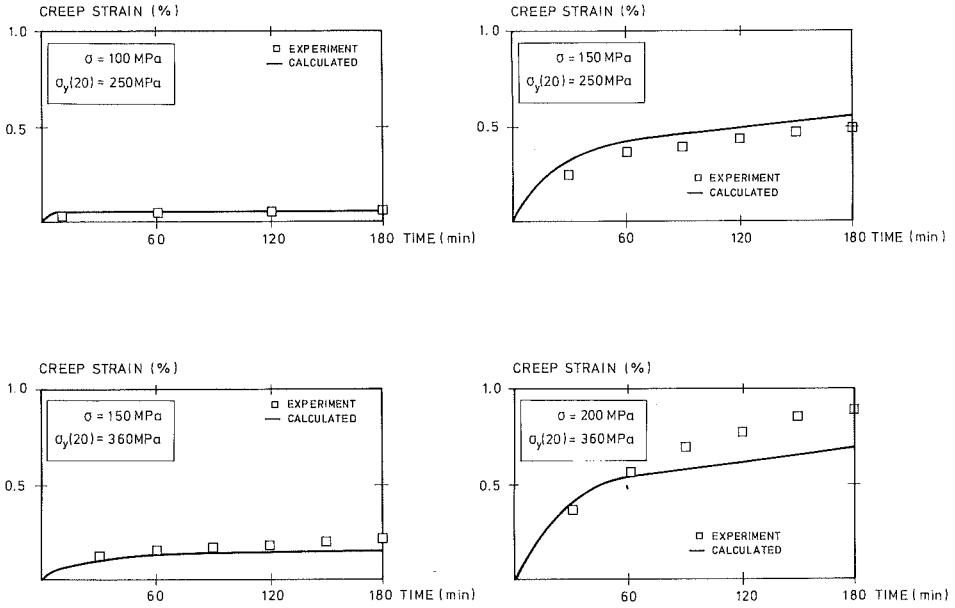

Figure 3.6 Creep curves at 500°C

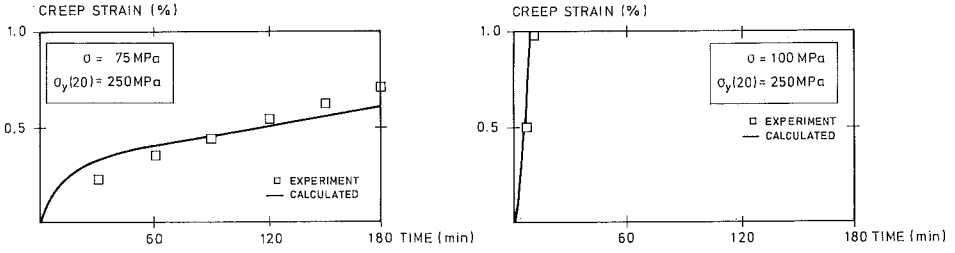

Figure 3.7 Creep curves at 600°C

With regard to the assumptions introduced the accuracy of the results presented in Figures 3.5 - 3.7 are satisfactory. Accurate fitting is very difficult to obtain for pure creep tests due to the many uncertain factors in the testing methods [73]. Practically, this may not be so important. A quantitative agreement with tests such as those described in Section 3.8.4 is, however, of great importance.

3.8.3 Influence of prior creep on subsequent plastic strain

As described in previous sections creep and plasticity influence each other. Tests show, for instance, that accumulated creep strain reduces the development of subsequent plastic strain through an increase of the yield stress, see Figure 3.2. The following example is a qualitative verification that the model describes this behaviour. None of the experiments reported that indicate this interaction are specified to the extent that a quantitative comparison is possible.

Assume constant temperature conditions ($T = 500^{\circ}C$), and consider the following stress history:

I Instantaneous loading up to a certain stress level ($\sigma_{11} = 100$ MPa $= 0.3\sigma_y(20)$)

II Constant stress during a time interval, so that creep strain will develop

III Subsequent instantaneous loading up to stress levels where yielding occurs.

The response of the model is shown in Figure 3.8, assuming on one hand that there is no interaction between creep and plasticity ($\xi = 0$) and on the other hand that when the hardening is dependent on both plastic strain and creep strain ($\xi = 1$).

When compared to Figure 3.2 the result clearly shows that the approach with a state variable $\bar{\varepsilon}^M$ that is a combined measure of plastic and creep straining gives a more realistic treatment of the plastic hardening.

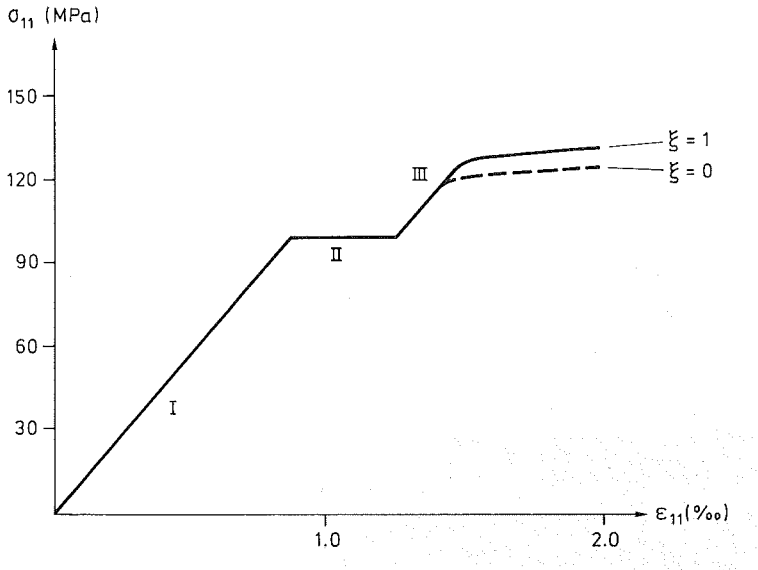

Figure 3.8 Effect of creep strain on subsequent yield

3.8.4 Nonisothermal behaviour

In the following example the model is applied for nonisothermal conditions. Test specimens have been loaded to a constant stress level and then the temperature has been increased at the rate $10^{\circ}C\ min^{-1}$, see Ref. [74]. The time independent part of the response in this kind of test can be visualized by cutting a plane at constant stress through the stress-strain-temperature surface as shown in Figure 3.9. A temperature-strain relation is obtained from the projection of the intersection line on the base plane.

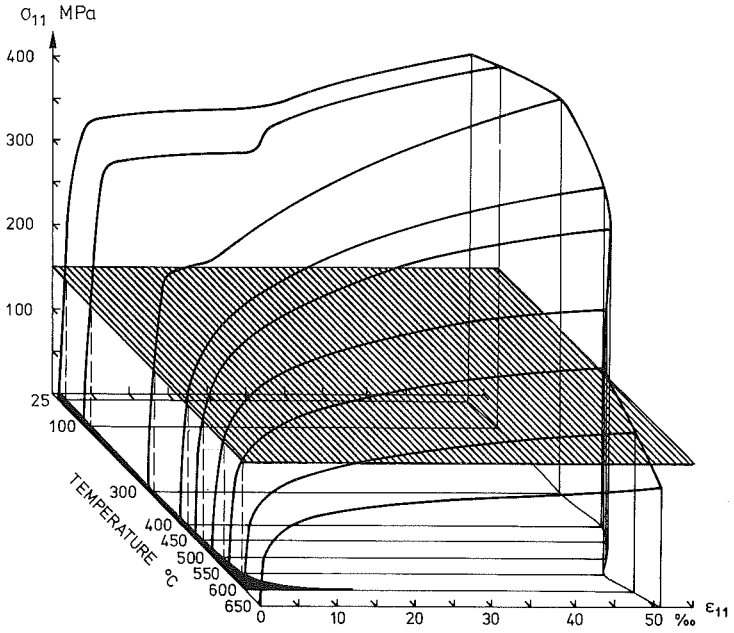

Figure 3.9 Stress-strain-temperature surface

By use of the present constitutive model the response under nonisothermal conditions was calculated. The results for four different stress levels are shown in Figure 3.10 and compared with test results. It should be noted that the temperature dependence of the material parameters used is quite independent of these tests.

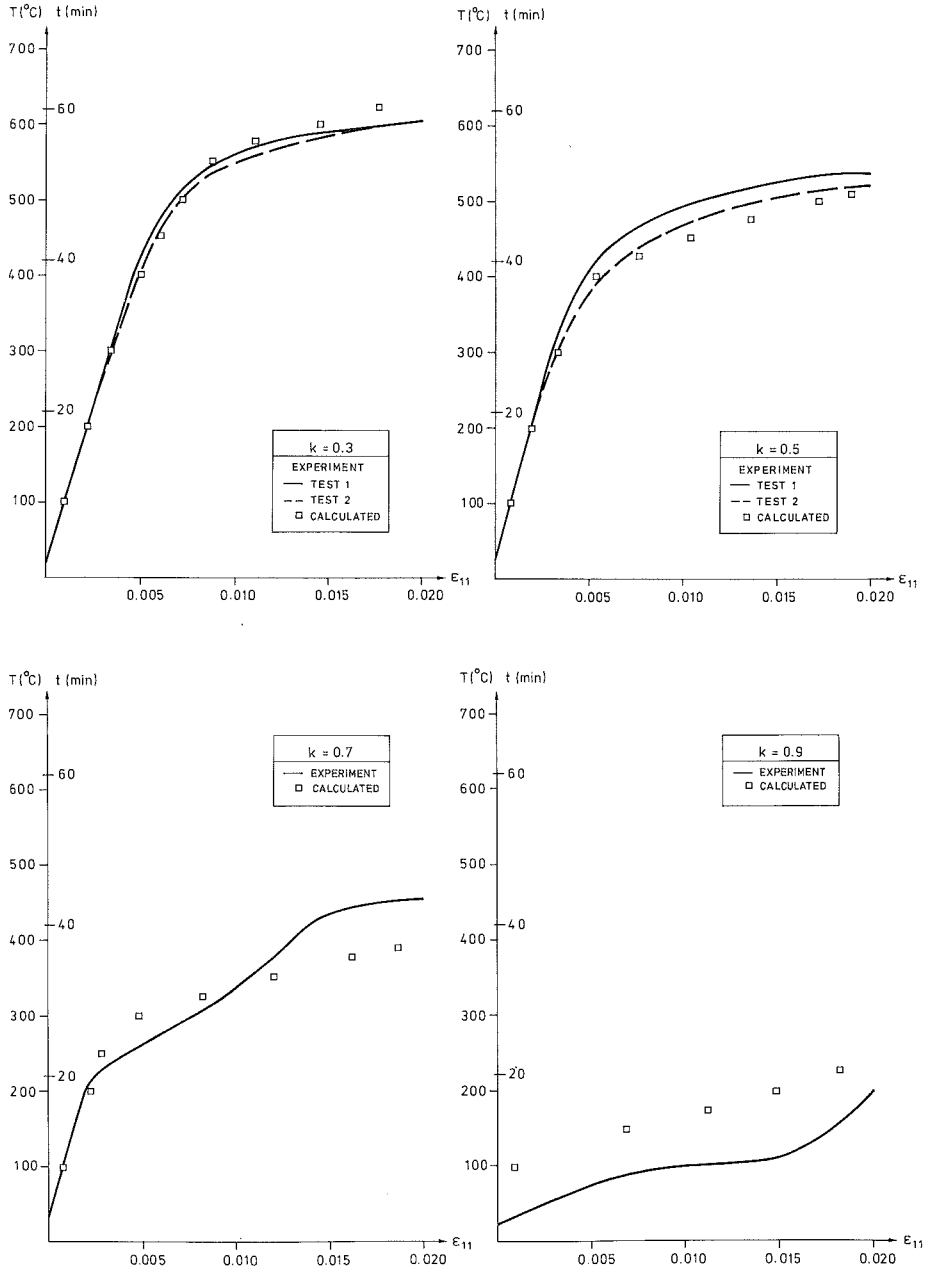

Figure 3.10 Comparison between experimental and calculated values. The ratio between actual stress and yield stress at room temperature ($\sigma_y(20)$ = 710 MPa) is denoted k

As can be seen in Figure 3.10 the agreement between calculated and experimental values is good for small values of k. The difference for higher values of k is mainly due to the material instability at high stress levels and low temperatures. In this range a transition from the marked yield plateau at normal temperature to a smooth stress-strain relation at high temperatures takes place, c.f. Figure 3.9.

It should be noted that this verification example is of considerable practical interest since it concerns an existing stress state combined with heating to high temperatures, which often is valid in practice.

3.9 Summary and conclusions

The scope of this chapter was to derive a material model for structural steel at high temperature conditions. The model is based on the theory of plasticity and viscoplasticity. It can be represented by a rheologic model where plastic strains and strains due to creep are treated as additive components (see Figure 3.11).

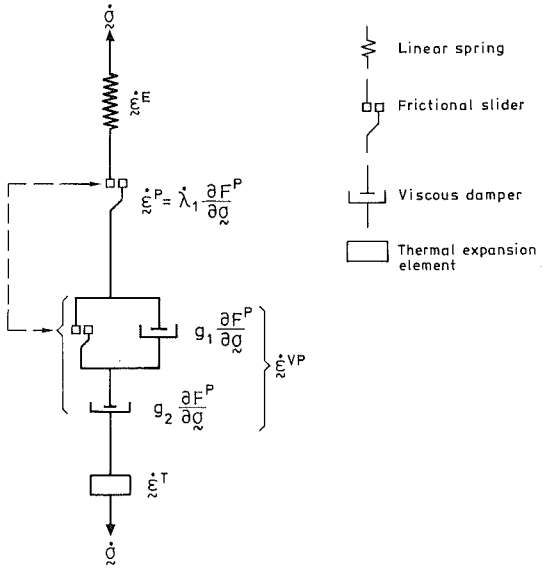

Figure 3.11 Rheologic model

Since there is no clear distinction between plastic and creep strain neither from experimental nor from a theoretical point of view, the plastic part and the viscoplastic part of the model are coupled through the hardening rules associated with them. This is indicated by the dashed line in Figure 3.11.

A main advantage with the proposed model is the well defined regions, see Table 3.1.

Region	F^P	F^{VP}	$\dot{\bar{\varepsilon}}^P$	$\dot{\lambda}_2$	
				g_1	g_2
I	<0	≤ 0	0	0	>0
II	<0	>0	0	>0	>0
III	=0	>0	>0	>0	>0

Table 3.1 State regions

Table 3.1 can be illustrated as in Figure 3.12.

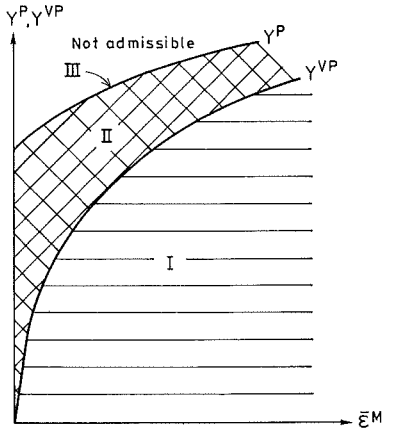

Figure 3.12 State regions

These three regions completely characterize the material behaviour at any stress state. Another important advantage is that all material parameters can be determined from well defined tests at isothermal conditions.

The validity of the proposed model is verified by comparison with experimental results. The agreement between calculated curves and experimental results is generally good in view of the limited amount of test data available to calibrate the model. The model is open for further development.

4. FINITE ELEMENT ANALYSIS OF PLANE BEAM STRUCTURES

4.1 Introduction

In this chapter finite element equations are derived for a straight, plane beam element and a computation procedure is outlined.

A local Cartesian coordinate system (X_1^*, X_2^*, X_3^*) refers to each element of the structure. This coordinate system may gradually be updated after each time (load) increment or iteration step. The plane bending occurs in the $X_1^* - X_3^*$-plane and the X_1^*-axis is oriented in the longitudinal direction of the beam element studied, see Figure 4.1.

In addition to the assumption of plane bending it is assumed that the influence of shear deformations and of the normal strains in transversal directions of the beam element are negligible. It is further assumed that the normal strain in the longitudinal direction is small and that the associated stress is substantially larger than any other stress component.

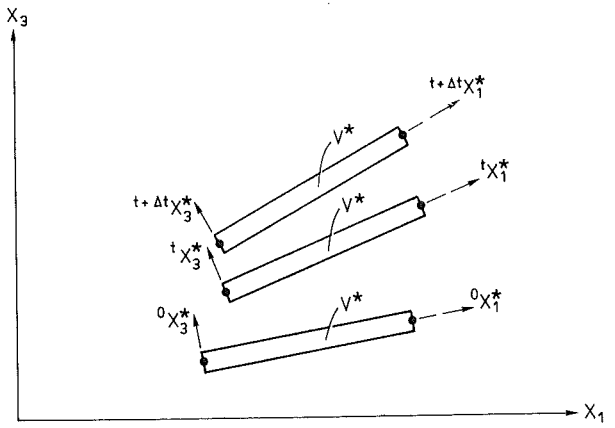

Figure 4.1 Gradually updated Cartesian coordinate system (X_1^*, X_2^*, X_3^*) for studied beam element. Locations of the integration volume V^* at three different time points are shown

Finite element formulations for nonlinear beam and frame analysis have been reported frequently, see for example [77] - [94]. The derivation given in this chapter is, however, believed to be novel as it starts from the general theory presented in Chapter 2 and is based on a partially updated Lagrangian formulation.

4.2 Basic beam theory formulation

The assumptions of negligible shear deformations and transversal normal strains correspond to the kinematic relation

$$u_1^* = u_0^*(X_1^*) - X_3^* \frac{\partial w^*(X_1^*)}{\partial X_1^*} \tag{4.1a}$$

$$u_2^* = 0 \tag{4.1b}$$

$$u_3^* = w^*(X_1^*) \tag{4.1c}$$

where u_0^* and w^* are displacements in the X_1^*- and X_3^*-directions referring to a longitudinal reference axis. The interpolation functions N_{in} defined by

$$u_i^* = N_{in}\, \bar{u}_n^* \tag{4.2}$$

are primarily related to u_0^* and w^*, i.e.

$$u_0^* = N_{un}(X_1^*)\, \bar{u}_n^* \tag{4.3a}$$

$$w^* = N_{wn}(X_1^*)\, \bar{u}_n^* \tag{4.3b}$$

Substitution of Eqs. (4.2) and (4.3) into Eq. (4.1) yields

$$N_{1n} = N_{un}(X_1^*) - X_3^* \frac{\partial N_{wn}(X_1^*)}{\partial X_1^*} \tag{4.4a}$$

$$N_{2n} = 0 \tag{4.4b}$$

$$N_{3n} = N_{wn}(X_1^*) \tag{4.4c}$$

It may especially be noted from Eqs. (4.1) and (4.4) that

$$\frac{\partial u_1^*}{\partial X_3^*} + \frac{\partial u_3^*}{\partial X_1^*} = 0 \tag{4.5a}$$

$$\frac{\partial N_{1n}}{\partial X_3^*} + \frac{\partial N_{3n}}{\partial X_1^*} = 0 \tag{4.5b}$$

Eq. (2.49a) can according to Eq. (4.4) be written as

$$K_{mn}^0 = \int_{V^*} \frac{\partial N_{1m}}{\partial X_1^*} C_T \frac{\partial N_{1n}}{\partial X_1^*} dV^* \tag{4.6}$$

Here the material quantity C_T is defined by the relation

$$d\tilde{T}_{11} = C_T \, dE_{11} - d\tilde{T}_{11}^0 \tag{4.7}$$

in accordance with Eq. (2.44) and with the assumption that only the longitudinal strain component E_{11} has an influence on $\tilde{T}_{11}$.

The assumption of small deformations ($|\frac{\partial u_1^*}{\partial X_1^*}| << 1$) and that the stress component $\tilde{T}_{11}$ geometrically has a substantially larger influence than any other stress component $\tilde{T}_{IJ}$ will now be applied. Eqs. (2.49b), (2.49c) and (2.49d) can finally be reduced to

$$K_{mn}^\sigma = \int_{V^*} \frac{\partial N_{3m}}{\partial X_1^*} \tilde{T}_{11} \frac{\partial N_{3n}}{\partial X_1^*} dV^* \tag{4.8}$$

$$K^{u}_{mn} = \int_{V^*} \frac{\partial N_{1m}}{\partial x_1^*} C_T \frac{\partial u_3^*}{\partial x_1^*} \frac{\partial N_{3n}}{\partial x_1^*} dV^* + \int_{V^*} \frac{\partial N_{3m}}{\partial x_1^*} \frac{\partial u_3^*}{\partial x_1^*} C_T \frac{\partial N_{1n}}{\partial x_1^*} dV^*$$

$$+ \int_{V^*} \frac{\partial N_{3m}}{\partial x_1^*} \frac{\partial u_3^*}{\partial x_1^*} C_T \frac{\partial u_3^*}{\partial x_1^*} \frac{\partial N_{3n}}{\partial x_1^*} dV^* \qquad (4.9)$$

$$dR_m^* = \int_{V^*} \left(\frac{\partial N_{1m}}{\partial x_1^*} + \frac{\partial N_{3m}}{\partial x_1^*} \frac{\partial u_3^*}{\partial x_1^*}\right) \tilde{dT}^0_{11} dV^* + \int_{V^*} (N_{1m} df_1^* + N_{3m} df_3^*) dV^*$$

$$+ \int_{S^*} (N_{1m} dt_1^{0*} + N_{3m} dt_3^{0*}) dS^* \qquad (4.10)$$

Substitution of Eq. (4.4) into Eqs. (4.6), (4.8), (4.9) and (4.10) gives with $X_1^* = x$, $X_3^* = z$ and $u_3^* = w^*$

$$K^{0}_{mn} = \int_{V^*} \begin{bmatrix} \frac{\partial N_{um}}{\partial x} & \frac{\partial^2 N_{wm}}{\partial x^2} \end{bmatrix} \left(C_T \begin{bmatrix} 1 & -z \\ -z & z^2 \end{bmatrix}\right) \begin{bmatrix} \frac{\partial N_{un}}{\partial x} \\ \frac{\partial^2 N_{wn}}{\partial x^2} \end{bmatrix} dV^* \qquad (4.11)$$

$$K^{\sigma}_{mn} = \int_{V^*} \frac{\partial N_{wm}}{\partial x} \tilde{T}_{11} \frac{\partial N_{wn}}{\partial x} dV^* \qquad (4.12)$$

$$K^{u}_{mn} = \int_{V^*} \begin{bmatrix} \frac{\partial N_{um}}{\partial x} & \frac{\partial^2 N_{wm}}{\partial x^2} \end{bmatrix} \left(C_T \frac{\partial w^*}{\partial x} \begin{bmatrix} 1 \\ -z \end{bmatrix}\right) \frac{\partial N_{wn}}{\partial x} dV^*$$

$$+ \int_{V^*} \frac{\partial N_{wm}}{\partial x} \left(C_T \frac{\partial w^*}{\partial x} \begin{bmatrix} 1 & -z \end{bmatrix}\right) \begin{bmatrix} \frac{\partial N_{un}}{\partial x} \\ \frac{\partial^2 N_{wn}}{\partial x^2} \end{bmatrix} dV^* + \int_{V^*} \frac{\partial N_{wm}}{\partial x} \left(\frac{\partial w^*}{\partial x} C_T \frac{\partial w^*}{\partial x}\right) \frac{\partial N_{wn}}{\partial x} dV^* \qquad (4.13)$$

$$dR_m^* = \int_{V^*} \left(\frac{\partial N_{um}}{\partial x} - z \frac{\partial^2 N_{wm}}{\partial x^2} + \frac{\partial N_{wm}}{\partial x} \frac{\partial w^*}{\partial x}\right) \tilde{dT}^0_{11} dV^* + \int_{V^*} \left[\left(N_{um} - z \frac{\partial N_{wm}}{\partial x}\right) df_1^* + \right.$$

$$\left. + N_{wm} df_3^*\right] dV^* + \int_{S^*} \left[\left(N_{um} - z \frac{\partial N_{wm}}{\partial x}\right) dt_1^{0*} + N_{wm} dt_3^{0*}\right] dS^* \qquad (4.14)$$

In these expressions N_{um} and N_{wm} are functions of the coordinate $x = X_1^*$ only, according to Eq. (4.4).

Matrix notations will now be used. Eq. (4.3) may be rewritten

$$\begin{bmatrix} u_0^* \\ w^* \end{bmatrix} = \begin{bmatrix} N_{u1}(x) & N_{u2}(x) \ldots\ldots\ldots\ldots N_{un}(x) \\ N_{w1}(x) & N_{w2}(x) \ldots\ldots\ldots\ldots N_{wn}(x) \end{bmatrix} \begin{bmatrix} \bar{u}_1^* \\ \bar{u}_2^* \\ \vdots \\ \bar{u}_n^* \end{bmatrix} = \begin{bmatrix} N_u \\ N_w \end{bmatrix} \bar{u}^* \qquad (4.15)$$

The beam element studied is initially straight and prismatic. The area of the cross section is denoted by A and the length by L ($V^* = AL$). If also the following notations are introduced

$$\begin{bmatrix} D_{11} & D_{12} \\ D_{21} & D_{22} \end{bmatrix} = \int_A C_T \begin{bmatrix} 1 & -z \\ -z & z^2 \end{bmatrix} dA \qquad (4.16)$$

$$H = \int_A \tilde{T}_{11} \, dA \qquad (4.17)$$

Eqs. (2.48), (4.11), (4.12) and (4.13) are written as

$$(K^0 + K^\sigma + K^u) \, d\bar{u}^* = dR^* \qquad (4.18)$$

$$K^0 = \int_L \begin{bmatrix} \frac{\partial N_u^T}{\partial x} & \frac{\partial^2 N_w^T}{\partial x^2} \end{bmatrix} \begin{bmatrix} D_{11} & D_{12} \\ D_{21} & D_{22} \end{bmatrix} \begin{bmatrix} \frac{\partial N_u}{\partial x} \\ \frac{\partial^2 N_w}{\partial x^2} \end{bmatrix} dx \qquad (4.19)$$

$$K^\sigma = \int_L \frac{\partial N_w^T}{\partial x} H \frac{\partial N_w}{\partial x} \, dx \qquad (4.20)$$

$$K^u = \int_L \left[\frac{\partial N_u^T}{\partial x} \quad \frac{\partial^2 N_w^T}{\partial x^2}\right] \left(\frac{\partial w^*}{\partial x} \begin{bmatrix} D_{11} \\ D_{21} \end{bmatrix}\right) \frac{\partial N_w}{\partial x}\, dx + \int_L \frac{\partial N_w^T}{\partial x} \left(\frac{\partial w^*}{\partial x} \begin{bmatrix} D_{11} & D_{12} \end{bmatrix}\right) \begin{bmatrix} \frac{\partial N_u}{\partial x} \\ \frac{\partial^2 N_w}{\partial x^2} \end{bmatrix} dx$$

$$+ \int_L \frac{\partial N_w^T}{\partial x} D_{11} \left(\frac{\partial w^*}{\partial x}\right)^2 \frac{\partial N_w}{\partial x}\, dx \qquad (4.21)$$

The incremental load dR^* is for a case with volume loads only

$$dR^* = \int_L \left[N_u^T \quad N_w^T \quad \frac{\partial N_w^T}{\partial x}\right] \left(\int_A \begin{bmatrix} df_1^* \\ df_3^* \\ -z df_1^* \end{bmatrix} dA\right) dx \qquad (4.22)$$

A similar expression is obtained for the contribution from the tractions dt_1^{0*} and dt_3^{0*} according to Eq. (4.14), while the contribution to dR^* of stress increment $d\tilde{T}_{11}^0$ is

$$dR_T^* = \int_L \left[\frac{\partial N_u^T}{\partial x} \quad \frac{\partial N_w^T}{\partial x} \quad \frac{\partial^2 N_w^T}{\partial x^2}\right] \left(\int_A \begin{bmatrix} 1 \\ \frac{\partial w^*}{\partial x} \\ -z \end{bmatrix} d\tilde{T}_{11}^0\, dA\right) dx \qquad (4.23)$$

4.3 Plane beam element with internal nodal displacement

The beam element that will be used in the following chapters is shown in Figure 4.2. A local coordinate system is introduced with $x = X_1^*$ and $z = X_3^*$. The cross section of the beam is assumed to be constant.

The nodal variables are deliberately marked to be located on a reference axis at an initial distance z_0 from the centroidal axis of the beam. In most applications z_0 will be set to zero. An internal nodal variable $\bar{u}_7^*$ is introduced in order to get a better approximation of the longitudinal strain distribution. This internal displacement can be eliminated by static conden-

sation on the element level before assembly of the global system of equations.

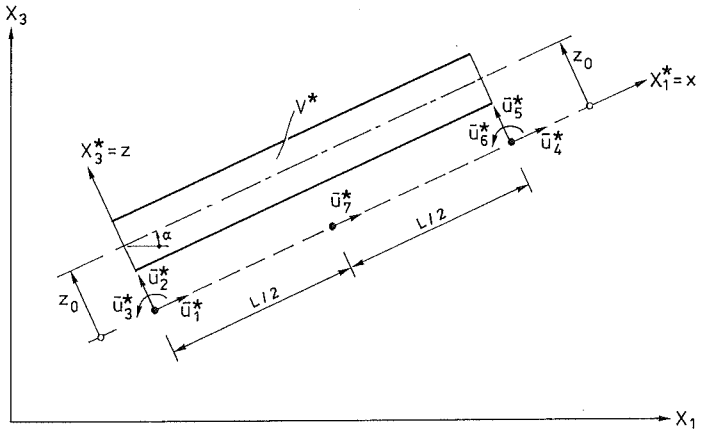

Figure 4.2 Nodal variables of beam element

The displacements $u_0^*(x)$ and $w^*(x)$ of the reference axis are approximated by polynominal functions

$$\begin{bmatrix} u_0^*(x) \\ w^*(x) \end{bmatrix} = \begin{bmatrix} 1 & x & x^2 & 0 & 0 & 0 & 0 \\ 0 & 0 & 0 & 1 & x & x^2 & x^3 \end{bmatrix} \begin{bmatrix} \alpha_1 \\ \alpha_2 \\ \vdots \\ \alpha_7 \end{bmatrix} \tag{4.24}$$

where α_1, $\alpha_2 \ldots \alpha_7$ can be expressed in the nodal variables $\bar{u}_1^*$, $\bar{u}_2^* \ldots \bar{u}_7^*$. According to Figure 4.2

$$u_0^*(0) = \bar{u}_1^* \qquad u_0^*(0.5L) = \bar{u}_7^* \qquad u_0^*(L) = \bar{u}_4^* \tag{4.25}$$

$$w^*(0) = \bar{u}_2^* \qquad w_{,x}^*(0) = \bar{u}_3^* \qquad w^*(L) = \bar{u}_5^* \qquad w_{,x}^*(L) = \bar{u}_6^*$$

where ,x denotes differentiation with respect to x. Thus

$$\begin{bmatrix}\alpha_1\\ \alpha_2\\ \alpha_3\\ \alpha_4\\ \alpha_5\\ \alpha_6\\ \alpha_7\end{bmatrix} = \begin{bmatrix} 1 & 0 & 0 & 0 & 0 & 0 & 0\\ -\frac{3}{L} & 0 & 0 & -\frac{1}{L} & 0 & 0 & \frac{4}{L}\\ \frac{2}{L^2} & 0 & 0 & \frac{2}{L^2} & 0 & 0 & -\frac{4}{L^2}\\ 0 & 1 & 0 & 0 & 0 & 0 & 0\\ 0 & 0 & 1 & 0 & 0 & 0 & 0\\ 0 & -\frac{3}{L^2} & -\frac{2}{L} & 0 & \frac{3}{L^2} & \frac{1}{L} & 0\\ 0 & \frac{2}{L^3} & \frac{1}{L^2} & 0 & -\frac{2}{L^3} & \frac{1}{L^2} & 0\end{bmatrix} \begin{bmatrix}\bar{u}_1^*\\ \bar{u}_2^*\\ \bar{u}_3^*\\ \bar{u}_4^*\\ \bar{u}_5^*\\ \bar{u}_6^*\\ \bar{u}_7^*\end{bmatrix} = G\bar{u}^* \qquad (4.26)$$

The row matrices N_u and N_w can according to Eqs. (4.16), (4.24) and (4.26) be expressed as

$$\begin{bmatrix}N_u\\ N_w\end{bmatrix} = \begin{bmatrix}1 & x & x^2 & 0 & 0 & 0 & 0\\ 0 & 0 & 0 & 1 & x & x^2 & x^3\end{bmatrix} G \qquad (4.27)$$

Derivation of Eq. (4.27) yields

$$\begin{bmatrix}\frac{\partial N_u}{\partial x}\\ \frac{\partial N_w}{\partial x}\\ \frac{\partial^2 N_w}{\partial x^2}\end{bmatrix} = \begin{bmatrix}0 & 1 & 2x & 0 & 0 & 0 & 0\\ 0 & 0 & 0 & 0 & 1 & 2x & 3x^2\\ 0 & 0 & 0 & 0 & 0 & 2 & 6x\end{bmatrix} G \qquad (4.28)$$

Substitution of Eqs. (4.27) and (4.28) into Eqs. (4.19) to (4.23) gives the expressions needed for the computation of the element equations

$$K\, d\bar{u}^* = d\bar{R}^* \qquad (4.29)$$

where according to Eq. (4.18)

$$K = K^0 + K^\sigma + K^u \tag{4.30}$$

Eq. (4.29) is written in a blocked form

$$\begin{bmatrix} K_{aa} & K_{ab} \\ K_{ba} & K_{bb} \end{bmatrix} \begin{bmatrix} d\bar{u}_a^* \\ d\bar{u}_b^* \end{bmatrix} = \begin{bmatrix} dR_a^* \\ dR_b^* \end{bmatrix} \tag{4.31}$$

where K_{aa} is a 6x6-matrix and K_{bb} an 1x1-matrix. The displacement $d\bar{u}_b^* = d\bar{u}_7^*$ is eliminated by static condensation so that a system of six element equations is obtained

$$\bar{K}_{aa}\, d\bar{u}_a^* = d\bar{R}_a^* \tag{4.32}$$

where

$$\bar{K}_{aa} = K_{aa} - K_{ab}\, K_{bb}^{-1}\, K_{ba} \tag{4.33}$$

$$d\bar{R}_a^* = dR_a^* - K_{ab}\, K_{bb}^{-1}\, dR_b^* \tag{4.34}$$

When $d\bar{u}_a^*$ has been computed $d\bar{u}_b^*$ can be determined from

$$d\bar{u}_b^* = K_{bb}^{-1}\,(dR_b^* - K_{ba}\, d\bar{u}_a^*) \tag{4.35}$$

In the assembly of the element equations into a global system of equations all nodal displacements need to be referred to a common X_1 - X_3-system, see Figure 4.2. The angle between the X_1-axis and the X_1^*-axis is denoted by α. The element equations, Eq. (4.32), are before assembly transformed into

$$G_\alpha^T\, \bar{K}_{aa}\, G_\alpha\, d\bar{u}_a = G_\alpha^T\, d\bar{R}_a^* \tag{4.36}$$

The relation between local and global displacements is given by

$$\bar{du}_a^* = \begin{bmatrix} \bar{du}_1^* \\ \bar{du}_2^* \\ \bar{du}_3^* \\ \bar{du}_4^* \\ \bar{du}_5^* \\ \bar{du}_6^* \end{bmatrix} = \begin{bmatrix} \cos\alpha & \sin\alpha & 0 & 0 & 0 & 0 \\ -\sin\alpha & \cos\alpha & 0 & 0 & 0 & 0 \\ 0 & 0 & 1 & 0 & 0 & 0 \\ 0 & 0 & 0 & \cos\alpha & \sin\alpha & 0 \\ 0 & 0 & 0 & -\sin\alpha & \cos\alpha & 0 \\ 0 & 0 & 0 & 0 & 0 & 1 \end{bmatrix} \begin{bmatrix} \bar{du}_1 \\ \bar{du}_2 \\ \bar{du}_3 \\ \bar{du}_4 \\ \bar{du}_5 \\ \bar{du}_6 \end{bmatrix} = G_\alpha \, \bar{du}_a \quad (4.37)$$

The vector $\bar{du}^*$ can thus easily be obtained from Eqs. (4.37) and (4.35) as soon as the quantities $\bar{du}_a$ have been calculated from the global system of equations.

Finally, the strain and stress increments dE_{11} and $d\tilde{T}_{11}$ have to be calculated. The assumption $|\frac{\partial u_1^*}{\partial X_1^*}| << 1$ yields

$$dE_{11} = \begin{bmatrix} 1 & \frac{\partial w^*}{\partial x} & -z \end{bmatrix} \begin{bmatrix} \frac{\partial N_u}{\partial x} \\ \frac{\partial N_w}{\partial x} \\ \frac{\partial^2 N_w}{\partial x^2} \end{bmatrix} \bar{du}^* \quad (4.38)$$

and according to Eq. (4.7)

$$d\tilde{T}_{11} = C_T \begin{bmatrix} 1 & \frac{\partial w^*}{\partial x} & -z \end{bmatrix} \begin{bmatrix} \frac{\partial N_u}{\partial x} \\ \frac{\partial N_w}{\partial x} \\ \frac{\partial^2 N_w}{\partial x^2} \end{bmatrix} \bar{du}^* - d\tilde{T}_{11}^0 \quad (4.39)$$

where the derivatives of N_u and N_w are expressed in Eq. (4.28).

4.4 Numerical integration

An important step in the nonlinear finite element analysis is the numerical integration of the element matrices. For the beam element studied this implies integration of Eqs. (4.11) - (4.15) or of Eqs. (4.19) - (4.23). Numerous methods for numerical integration are valid such as the trapezoidal rule, Simpson's rule, various types of Gaussian quadrature and Lobatto's integration formula. For a more detailed discussion on the subject, see Refs. [6] and [95]. Simpson's rule in combination with layer integration is adopted in this study and will be discussed in the following.

A typical expression for a non-zero term of the volume integrals is

$$\int_{V^*} f(x,z)\, dV^*$$

where f is a function of the position in the local Cartesian coordinate system. Application of Simpson's rule yields

$$\int_{V^*} f(x,z)\, dV^* = \left(\sum_{i=0}^{2m} a_i \int_A f(x_i,z)\, dA \right) \cdot L \tag{4.40}$$

where

$$a_0 = \frac{L}{6m}, \quad a_1 = \frac{4L}{6m}, \quad a_2 = \frac{2L}{6m}, \quad a_3 = \frac{4L}{6m}, \quad \ldots \quad a_{2m} = \frac{L}{6m} \tag{4.41}$$

and

$$x_i = \frac{iL}{2m} \tag{4.42}$$

where L is the length of the beam element, A is the area of the cross section and m is the number of subintervals for the numerical integration.

To solve the area integration in Eq. (4.40) the cross section is divided into a number of layers. The geometry of each layer

is defined by its area and distance from the reference axis, see Figure 4.3. The area integration is evaluated by simple summation, i.e.

$$\int_A f(x_i,z)\, dA = \sum_{j=1}^{n} f(x_i,z_j)\, A_j \qquad (4.43)$$

where n denotes the number of layers.

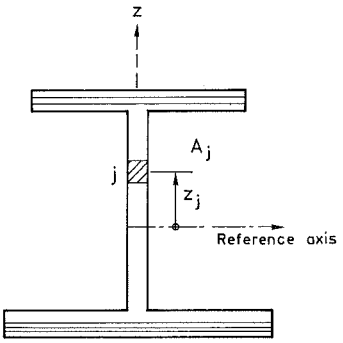

Figure 4.3 Division of cross section into layers

In this study one subinterval (i.e. m = 1) and 16-20 layers (i.e. $16 \leq n \leq 20$) are used in the calculations.

In the case of pure linear elastic material properties the integration is performed in an exact way.

4.5 Calculation procedure

The plane frame to be analysed is idealized as an assemblage of finite elements interconnected by nodal points. The nodal load history and the temperature distribution are prescribed. The problem is to determine nodal displacements, support reactions, internal forces, strains and stresses for each element as a function of time. In order to incorporate the time dependent properties, the time domain is divided into a discrete number of intervals and a time step integration is performed in which increments of displacements, strains and stresses are calculated and added to the previous ones. In each time (load) step the finite element method is used with respect to the

space domain. The nonlinear equilibrium equations for each element are established and element matrices and load vectors are transformed to a global coordinate reference frame in which the equilibrium equations for the entire structure are established giving a system of equations

$$K\,\Delta u = \Delta R \tag{4.44}$$

where K denotes a system matrix, Δu an incremental displacement vector and ΔR an incremental load vector.

The basic operations in each time step are

- calculation of element matrices and load vectors
- the solution of the system of equations
- calculation of internal quantities such as strain and stress

The present work does not include the calculation of the structural temperature distribution. This can, however, be performed by standard finite element programs for temperature analysis (see Refs. [96] - [98]). The temperature distribution may alternatively be given as experimental data. In the following the temperature histories in all elements are assumed to be known from the outset.

In the solution of a nonlinear problem the change in load during a time increment is applied in finite increments. The increments of the displacements are obtained by solving (4.44). The total displacements ${}^{t+\Delta t}u$ at time $t+\Delta t$ are

$${}^{t+\Delta t}u = {}^{t}u + \Delta u \tag{4.45}$$

The strains and stresses are calculated in the same way.

When using (4.44) to calculate the incremental displacements Δu, the problem is linearized in each time step. According to the material and geometric nonlinearities this linearization may result in an error which corresponds to an equilibrium unbalance of the system. Out-of-balance forces $\bar{P}$ appear as the difference between total applied loads and the internal

forces. When using a true incremental solution procedure these out-of-balance forces are ignored. A simple modified incremental method ([13]) is to add ${}^{t}\bar{P}$ from the previous step to the right side of Eq. (4.44) (a self-correcting incremental procedure)

$$K\,\Delta u = \Delta R + {}^{t}\bar{P} \tag{4.46}$$

An alternative procedure is to eliminate the out-of-balance forces by using an iteration method such as the Newton-Raphson procedure [6], [9], [99] - [102]. It should, however, be noted that for path dependent problems, undesired effects of artificial detours in the deformation process can occur when state variables are continuously updated during the iterations in the time steps. One way of handling this problem is described in Ref. [103].

In this work a true incremental or a self-correcting incremental procedure is used. These approaches are the most straight forward ones and are well adopted for computer implementation.

4.6 Substructuring

Nonlinear computer analysis of large structures can often be very expensive and available computer storage may not be sufficient. However, in many cases nonlinear behaviour is concentrated to a small part of the structure. This part can then often be treated as a substructure, while, in order to simplify the nonlinear analysis, the surrounding substructures must behave elastically. When stiffness properties of each substructure are determined, the substructures can be treated as complex structural elements and an ordinary assembly of structural analysis can be used for the partitioned structural model. The technique is exemplified by the frame in Figure 4.4.

The frame is subjected to high temperature conditions on the first floor. The nonlinear effects are assumed to be limited to elements included in substructure II (Figure 4.4b). The effect of substructure I, in which elastic behaviour is assumed, can be simulated by attaching "coupled springs" to substructure II at the boundary nodes (Figure 4.4c). The values of the "spring

stiffness" can be determined by statical condensation of the equations for substructure I, including all nodes. A description of substructural analysis is given in Refs. [104] - [105].

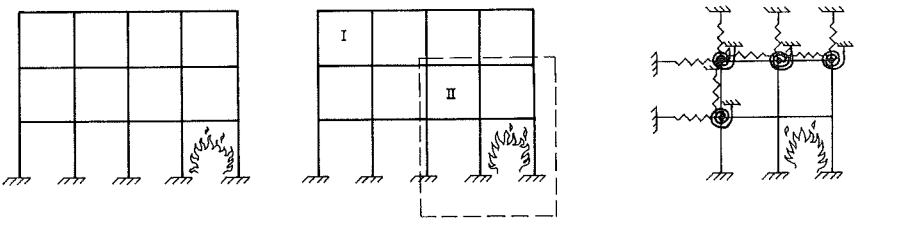

a) Real structure

b) Partitioning in substructures

c) Structure of nonlinear analysis

Figure 4.4 Substructure analysis

5. COMPUTER PROGRAM

5.1 Introduction

The development of new computer programs has often been a necessity for many researchers. A lot of work has been doubled, since previous experience have not been considered and existing computer codes have not been used. During the course of this study the computer program CAMFEM was developed [106]. The main purpose of the development of CAMFEM has been to create a problem independent program structure which easily can be connected to specific subroutines to form programs for analysis of different classes of problems, see Refs. [107]-[109]. The program structure includes general facilities needed in most calculations and much time can be saved because only the problem dependent parts have to be written. One objective has been to make the program structure as clear as possible in order to make it easy to introduce new parts in the program. The computer program is primarily intended to be a research tool.

All data used in the calculations are stored in matrices named by the user. This facilitates inspection and manipulation of the matrices at any stage of the calculation process. An internal data handling system in which all matrices are stored column-wise in one single array is adopted.

CAMFEM is based on a *command language*. The program is subdivided into a number of program modules, which are executed separately by commands given by the user. In general a command consists of a command name followed by arguments. The command name is a logical name of some operation (e.g. ADD = matrix addition, INV = matrix inversion) and the arguments are user-defined matrices, which contain either numerial values or alphanumeric text (to be used in macro commands). One facility of CAMFEM is the possibility to store the user-defined matrices on files. This makes it possible to stop the calculation at an arbitrary stage and later restart the calculation.

In a time stepping procedure the same sequence of commands is to be executed several times. Such a sequence of commands can be defined as a *macro command*. The calculation procedure is defined by a set of macro commands created by the user. Simply by rearranging the macro commands the calculation procedure can easily be changed. CAMFEM may therefore be seen as a high level language for analysis of structural behaviour. In a conventional finite element program a modification in the calculation procedure usually results in a lot of changes in the program code.

The program language is FORTRAN 77 and all calculation is performed in double precision.

It should be noted that in CAMFEM a concept is used where each node consists of only one nodal variable to describe the topology. This facilitates various arrangements of coupling between elements. Internal hinges are taken into account just by introducing additional degrees of freedom as described in Figure 5.1. It should be noted that no change of the program code has to be performed since these arrangements are completely handled by the user.

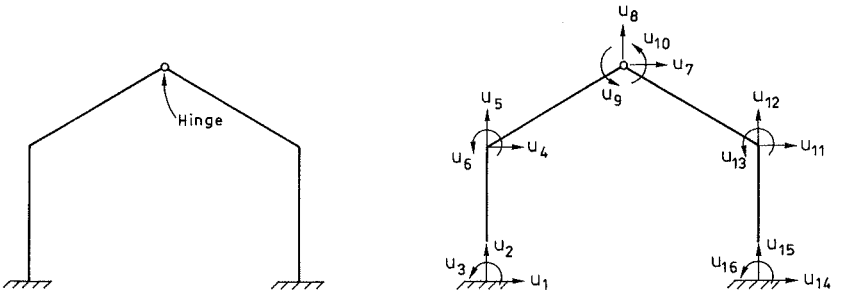

Figure 5.1 Internal hinge

The set of problem independent commands is briefly described in Section 5.2 and specific commands introduced in this work are described in Section 5.3. In Section 5.4 an example on the usage of the commands is given.

5.2 Problem independent commands

The problem independent commands can be divided into four groups. These commands can be linked together with problem dependent commands to a special prupose version of CAMFEM, see Figure 5.2.

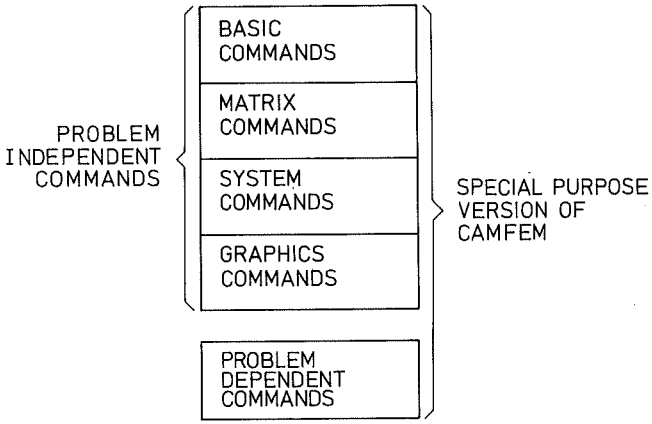

Figure 5.2 Groups of commands

In the following a brief description of the contents of the groups of commands will be given. A more detailed description is given in Appendix E.

The group of basic commands includes commands for control of execution, data handling and macros.

The commands for control of execution are

STOP	Stop execution
PRON	Turn printing on
PROFF	Turn printing off
QUON	Turn question mode on
QUOFF	Turn question mode off
C	Write a comment line

The commands for data handling are

LOAD	Load numeric matrix
LTEXT	Load text matrix
DELETE	Delete matrix
COPY	Copy one matrix into another
PRINT	Print matrix
SAVE	Store matrix on file
OLD	Read matrix from file
UNSAVE	Delete matrix on file
CREFIL	Create file
DELFIL	Delete file

The commands for macros are

EMACRO	Execute macro
PMACRO	Set parameters to macro
BMACRO	Break execution of macro

The second group consists of matrix commands that can be used for different matrix operations. The commands are

ADD	Add two matrices
SUB	Subtract one matrix from another
MULT	Multiply two matrices
INV	Calculate the inverse of a matrix
DET	Calculate the determinant of a matrix
EIGEN	Solve an eigenvalue problem
TRANS	Transponate a matrix
CONDRC	Reduce a matrix

To perform a finite element analysis some system commands for creation, condensation and solution of systems of equations are needed. The system commands are

ELIN	Assemble element matrices
CONDES	Perform static condensation
SOLVES	Solve a symmetric system of equations
SOLVTR	Perform Gaussian reduction
SOLVLM	Perform load vector modification
SOLVBS	Perform back-substitution

The fourth group contains graphic commands for generating plot information in device independent form on a direct access file, which later on can be interpreted by commands for visible output. These commands will not be further described here. The reader is referred to Ref. [106].

5.3 Problem dependent commands

For nonlinear analysis of plane beams and frames a special version of CAMFEM was created by introducing commands based on the theory described in the previous sections. The new commands basically deal with the calculation of element stiffness matrices, element load vectors and strains and stresses in the integration points. On the structural level mainly the problem independent commands are used. In the following a brief description of the commands used in this study is given.

The geometry and topology of each beam element being a part of a structure are defined by its length L, slope α and six global node variables (see Figure 5.2).

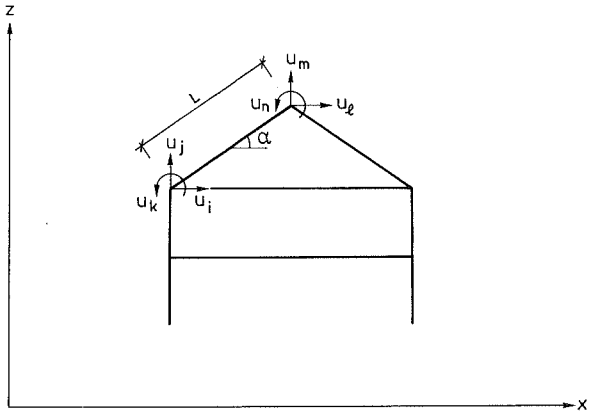

Figure 5.2 Element geometry and topology

The structural behaviour shows various nonlinearities in different parts of the structure. In order to take into account the range of nonlinearity that may appear, the calculation of the element stiffness matrix is performed by a command with different arguments:

```
BEAM2E EP EM
```

calculates the elastic element stiffness matrix EM from element properties stored in EP (contains the modulus of elasticity,

cross sectional area, element length, element slope...).

BEAM2E EP EM STATE GEOM

calculates the elastic-plastic element stiffness matrix EM by usage of EP (which now also contains information of the stress-strain relation), state variables (σ, $\bar{\varepsilon}^M$) stored in STATE and the cross sectional geometry (A_j, z_j c.f. Eq. (4.43)) stored in GEOM.

BEAM2E EP EM STATE GEOM TDMP TEMP EL

calculates the elastic-plastic-thermal element stiffness matrix EM and the element pseudo load vector EL based on temperature dependent material properties (T, E(T), σ_y(T)...) stored in TDMP and a temperature variation described by the matrix TEMP.

With regard to geometric nonlinearities different approaches for the element stiffness matrix EM are available, see Table 5.1.

Type of analysis	EM contains		
	K^0(Eq.(4.11))	K^σ(Eq.(4.12))	K^u(Eq.(4.13))
Small displacements	YES	YES/NO	NO
Large displacements (the "geometry" is updated)	YES	YES	YES/NO

Table 5.1 Alternative geometric nonlinearities.

For each element it is possible to choose which type of non-linearity that is to be taken into account. The choice is indicated by a number stored in EP.

When element matrices and load vectors have been assembled and the system of equations have been solved (see the problem independant commands ELIN, SOLVTR, SOLVLM and SOLVBS in Section 5.2 and Appendix E) strains, stresses and internal forces can be obtained by the command BEAM2S given with arguments corresponding to elastic, elastic-plastic and elastic-plastic-thermal calculation

```
BEAM2S EP EN DISP RINT CONV
BEAM2S EP EN DISP RINT CONV STATE GEOM
BEAM2S EP EN DISP RINT CONV STATE GEOM TDMP TEMP
```

where

EN contains the topology of the element

DISP contains total and incremental displacements

RINT contains the integrated internal forces

CONV specifies whether or not a convergence criterion is achieved (to be used in an iteration process)

An advantage with the present procedure is that elements that remain elastic throughout the analysis can be treated as elastic even in a nonlinear analysis. In a conventional nonlinear analysis all elements are often treated in the same way. It is also possible to change the assumed behaviour during the analysis.

It should be noted that for elastic elements no numerical integration is needed. Therefore, an exact integration was performed for elements with elastic properties only.

5.4 Example on the usage of CAMFEM commands

In order to demonstrate the usage of the commands in CAMFEM, the contents of two macro commands, STEP and ASSEM used for the solution of one loadstep, are shown in Figure 5.3. The structure to be analysed consists of two elastic beam elements only.

In Table 5.2 the contents of some of the user-defined matrices are explained.

The two macros are used in order to analyse the cantilever beam in Figure 5.4.

```
MATRIX STEP              20  ROWS
================================

   1 C
   2 C PERFORM ONE INCREMENTAL STEP
   3 C
   4 C Create global stiffness matrix
   5 LOAD K
   6 EMACRO ASSEM 1 EP1 EN1
   7 EMACRO ASSEM 1 EP2 EN2
   8 C Solve the system of equations
   9 SOLVTR K BOUND PIV TEST
  10 LOAD DU
  11 SOLVLM K DU DR BOUND PIV
  12 SOLVBS K DU DR BOUND
  13 C Update displacements
  14 ADD U DU U
  15 C Store incremental and total displacements in DISPL
  16 COPY DU DISPL POS1
  17 COPY U DISPL POS2
  18 C Calculate element forces
  19 BEAM2S EP1 EN1 DISPL DUMMY CONV
  20 BEAM2S EP2 EN2 DISPL DUMMY CONV


MATRIX ASSEM              4  ROWS
================================

   1 C Calculate and assemble element matrix
   2 PMACRO EP EN
   3 BEAM2E EP EM
   4 ELIN K EM EN
```

Figure 5.3 Macro commands

Matrix	Contents
K	Global stiffness matrix
BOUND	Boundary conditions
DU	Incremental displacements
DR	Incremental loads
U	Total displacements
EPi	Element properties for element i
ENi	Topology for element i

Table 5.2 Contents of matrices in Figure 5.3

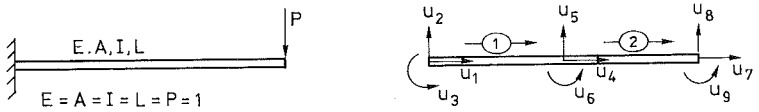

a) Load and geometry

b) Element numbers and global node variable numbers

Figure 5.4 Cantilever beam

The calculation procedure for a small displacement analysis is shown in the computer listing in Figure 5.5. It should be noted that the matrices to be used are previously created and stored on a file (BEAM) from which they are read by the command OLD.

```
***          CAMFEM          ***
***     VERSION JUNE 1984    ***
-----------------------------------
>OLD ALL BEAM
**OLD ALL BEAM
     1 ROWS      7 COLUMNS IN MATRIX EN1
     1 ROWS      7 COLUMNS IN MATRIX EN2
     1 ROWS     25 COLUMNS IN MATRIX EP1
     1 ROWS     25 COLUMNS IN MATRIX EP2
     1 ROWS      2 COLUMNS IN MATRIX POS1
     1 ROWS      2 COLUMNS IN MATRIX POS2
     1 ROWS      1 COLUMNS IN MATRIX CONV
     1 ROWS      1 COLUMNS IN MATRIX TEST
     1 ROWS      4 COLUMNS IN MATRIX BOUND
     9 ROWS      1 COLUMNS IN MATRIX DU
     9 ROWS      1 COLUMNS IN MATRIX U
     9 ROWS      9 COLUMNS IN MATRIX K
     9 ROWS      2 COLUMNS IN MATRIX DISPL
     9 ROWS      1 COLUMNS IN MATRIX DR
    20 ROWS IN MATRIX STEP
     4 ROWS IN MATRIX ASSEM
-----------------------------------
>EMACRO STEP
**EMACRO STEP
=================================================== START OF MACRO STEP
-----------------------------------
**C
-----------------------------------
**C PERFORM ONE INCREMENTAL STEP
-----------------------------------
**C
-----------------------------------
**C Create global stiffness matrix
-----------------------------------
**LOAD K
MATRIX K          PREVIOUSLY DEFINED
(    9 ROWS     9 COLUMNS)
ZERO MATRIX
-----------------------------------
**EMACRO ASSEM 1 EP1 EN1
=================================================== START OF MACRO ASSEM
-----------------------------------
**C Calculate and assemble element matrix
-----------------------------------
**PMACRO EP EN
-----------------------------------
**BEAM2E EP EM
-----------------------------------
**ELIN K EM EN
=================================================== END OF MACRO ASSEM
-----------------------------------
**EMACRO ASSEM 1 EP2 EN2
=================================================== START OF MACRO ASSEM
-----------------------------------
**C Calculate and assemble element matrix
-----------------------------------
**PMACRO EP EN
-----------------------------------
**BEAM2E EP EM
-----------------------------------
**ELIN K EM EN
=================================================== END OF MACRO ASSEM
-----------------------------------
**C Solve the system of equations
-----------------------------------
**SOLVTR K BOUND PIV TEST
-----------------------------------
**LOAD DU
MATRIX DU         PREVIOUSLY DEFINED
(    9 ROWS     1 COLUMNS)
ZERO MATRIX
-----------------------------------
**SOLVLM K DU DR BOUND PIV
-----------------------------------
**SOLVBE K DU DR BOUND
-----------------------------------
**C Update displacements
-----------------------------------
**ADD U DU U
-----------------------------------
**C Store incremental and total displacements in DISPL
-----------------------------------
**COPY DU DISPL POS1
-----------------------------------
**COPY U DISPL POS2
-----------------------------------
**C Calculate element forces
-----------------------------------
**BEAM2S EP1 EN1 DISPL DUMMY CONV
ELEMENT FORCES FOR EL. NO.    1
*******************************
     .0000       1.000       1.000       .0000      -1.000      -.5000
-----------------------------------
**BEAM2S EP2 EN2 DISPL DUMMY CONV
ELEMENT FORCES FOR EL. NO.    2
*******************************
     .0000       1.000       .5000       .0000      -1.000       .0000
=================================================== END OF MACRO STEP
-----------------------------------
>PRINT U
**PRINT U

MATRIX U                  9 ROWS     1 COLUMNS
=============================================

              1
   1   .000000
   2   .000000
   3   .000000
   4   .000000
   5  -.104167
   6  -.375000
   7   .000000
   8  -.333333
   9  -.500000

-----------------------------------
>STOP
**STOP

CALCULATION TERMINATED
```

Figure 5.5 Example of a computer list from CAMFEM

In a nonlinear analysis CAMFEM offers a great flexibility. A step-by-step procedure is obtained if the macro command STEP is executed repeatedly with a new incremental load vector DR in each load step. A Newton-Raphson iteration procedure can be obtained if commands calculating the out-of-balance forces are included in the macro command STEP. Similarly, a modified Newton-Raphson procedure can be established by simple modifications of the macros.

For a more detailed description of the usage of commands in CAMFEM, see Refs. [106] and [107].

5.5 Concluding remarks

A computer program, CAMFEM, has been developed. A set of problem independent commands is described in Appendix E. The program is extended with the nonlinear material model described in Chapter 3 and the beam element described in Chapter 4. In Appendix D the validity of the program for isothermal conditions is shown by some verification examples.

A number of applications involving temperature dependent material properties are given in Chapter 6.

6. NUMERICAL RESULTS

6.1 General remarks

In this chapter a number of examples concerning high temperature analysis of steel components are shown. In order to verify the present calculation model, numerical results are compared with results obtained from fire tests and/or other numerical studies on simply supported beams. In addition a parameter study on a single column is presented and the capability of the computer program to analyse large frame structures is demonstrated. In all examples the material parameters given in Appendix C are used.

6.2 Simply supported beams with no axial restraint

6.2.1 Short-time fire exposure

In Ref. [120] an experiment concerning a fire exposed IPE 80 steel beam is described. Geometry, load and boundary conditions are shown in Fig. 6.1.

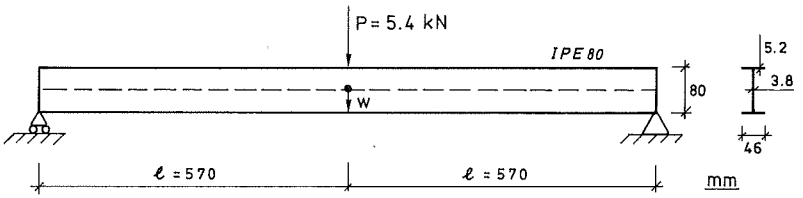

Figure 6.1 Fire exposed beam

In the test, the temperature was measured by four thermocouples along the length of the beam. The intention was to have a uniform temperature distribution all over the beam. If this was fulfilled or not is not reported. However, the average value of the temperature as a function of time is shown in Fig. 6.2.

Uniform temperature distribution with temperature values of Fig. 6.2 every 2.5 min is used as input data for the computer calculation. Linear interpolation is applied for intermediate times.

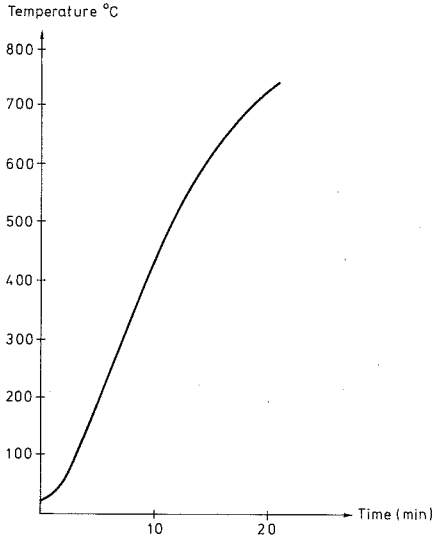

Figure 6.2 Average temperature of the beam vs time

According to measurements, the yield stress of the steel at room temperature was found to be 392 MPa (i.e. $\sigma_y(20) = 392$ MPa). Due to the symmetry of the beam only one half was modelled, see Fig. 6.3. Four beam elements were used in the analysis.

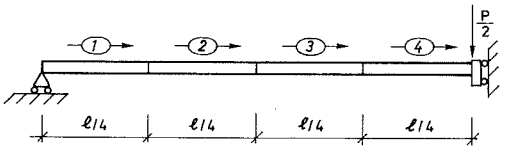

Figure 6.3 Finite element model

The cross sectional area was divided into 20 layers each described by the area and the distance from the centroidal axis.

A true incremental calculation was performed with a time step $\Delta t = 0.25$ min. In Fig. 6.4 the calculated midpoint displacement w is shown as a function of time. The displacement at time 0 is denoted w_o. In the same figure the experimentally obtained curve is also shown together with calculation results reported by Forsén [121].

As can be seen in Fig. 6.4 the discrepancies between the experimental curve and the curve obtained in this study are small.

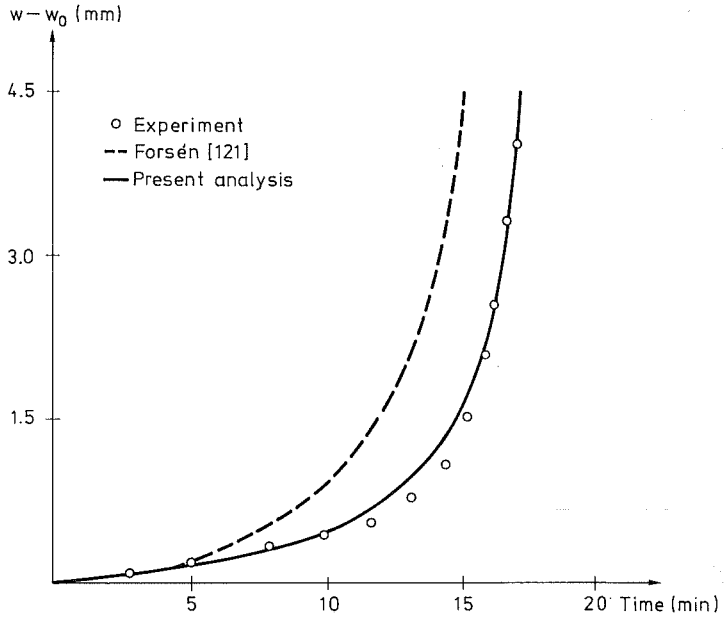

Figure 6.4 Midpoint displacement of the beam

6.2.2 Long-time fire exposure

A frequently used verification for thermal creep analysis is the experimental fire test results of a beam reported by Stanzak and Harmathy [122]. The beam was made of ASTM A36 grade steel, with W200x25 (AISC 8WF17) section and a simply supported span of 4.724 m (186 in.), see Fig. 6.5.

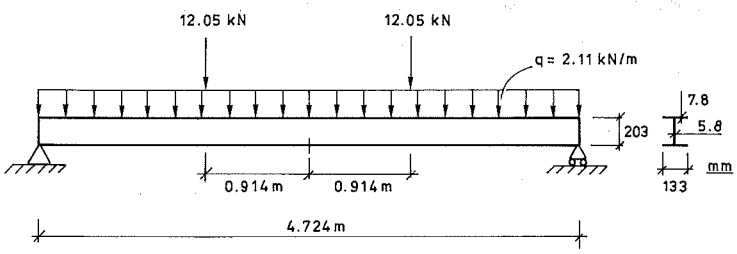

Figure 6.5 Simply supported test beam

The beam is loaded by a uniform load of 2.11 kN/m (120.6 lbs/in.) and by two concentrated loads equal to 12.05 kN (2707 lbs), each 0.914 m (36 in.) from the mid-span. In the test, the temperature distribution along the length of the beam was measured at the mid-span and the quarter-span sections. Fig. 6.6 shows the time-temperature variations measured at the mid-span for the top flange (T_t), the center line of the web (T_w) and the bottom flange (T_b). According to measurements the temperature distributions at the quarter-span sections were essentially the same at the mid-span.

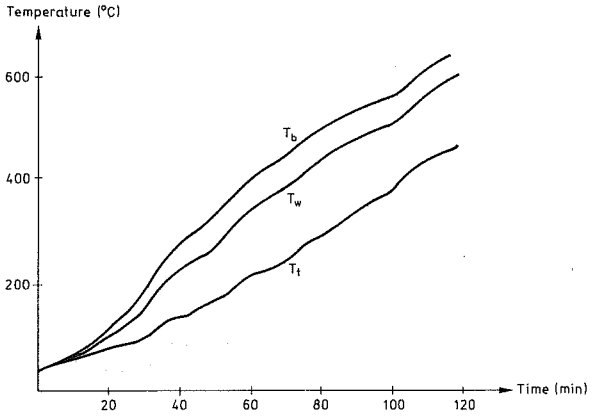

Figure 6.6 Time-temperature curves measured at the mid-span of the beam in Fig. 6.5

In the present analysis the temperature is assumed to be uniformly distributed in the longitudinal direction and varied quadratically in the transverse direction, i.e.

$$T(z) = T_w + \frac{z}{h}(T_t - T_b) - \frac{4z^2}{h^2}\left(T_w - \frac{T_t + T_b}{2}\right) \qquad (6.1)$$

in which z is the distance from the centroid axis and h is the height of the beam (203 mm). The temperatures T_t, T_w and T_b are taken from Fig. 6.6.

Taking the symmetry into account, one half of the beam is divided into four finite elements as shown in Fig. 6.7.

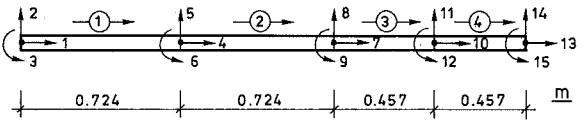

Figure 6.7 Finite element model of one half of the beam shown in Fig. 6.5

The cross sectional area of the beam is divided into 16 layers. The temperature in each layer is calculated by use of Eq. 6.1 and Fig. 6.6 for seven discrete times. The results are given in Table 6.1 and are used as input data for the computer calculation. The temperature distribution for times other than those shown in Table 6.1 is obtained by linear interpolation.

	Temperature (°C)						
z (mm)	0 min	20 min	40 min	60 min	80 min	100 min	120 min
100.52500	20.	70.	126.	206.	282.	367.	467.
98.57500	20.	71.	128.	209.	285.	370.	470.
95.65000	20.	71.	130.	212.	290.	375.	474.
87.84375	20.	72.	138.	222.	303.	388.	486.
76.13125	20.	74.	148.	236.	322.	407.	503.
58.56250	20.	77.	163.	256.	348.	432.	526.
35.13750	20.	80.	181.	281.	380.	463.	555.
11.71250	20.	84.	197.	304.	408.	489.	579.
- 11.71250	20.	86.	212.	325.	431.	510.	600.
- 35.13750	20.	89.	226.	345.	451.	527.	617.
- 58.56250	20.	91.	238.	363.	467.	539.	630.
- 76.13125	20.	93.	245.	375.	476.	545.	638.
- 87.84375	20.	94.	250.	382.	481.	548.	642.
- 95.65000	20.	95.	253.	387.	483.	549.	644.
- 98.57500	20.	95.	254.	388.	484.	550.	644.
-100.52500	20.	95.	255.	389.	485.	550.	645.

Table 6.1 Input time-temperature values for different layers

In Ref. [123] stress-strain curves for an ASTM A36 steel at elevated temperatures are reported. According to the results shown the yield stress at 20°C can be set to 310 MPa.

The uniformly distributed load is simply replaced by lumped concentrated loads.

A true incremental time-stepping procedure with $\Delta t = 1$ min was employed. The midspan displacement (corresponding to nodal variable number 14) is shown in Fig. 6.8 as a function of time. In the

same figure the experimental curve is also shown together with results obtained by other investigators.

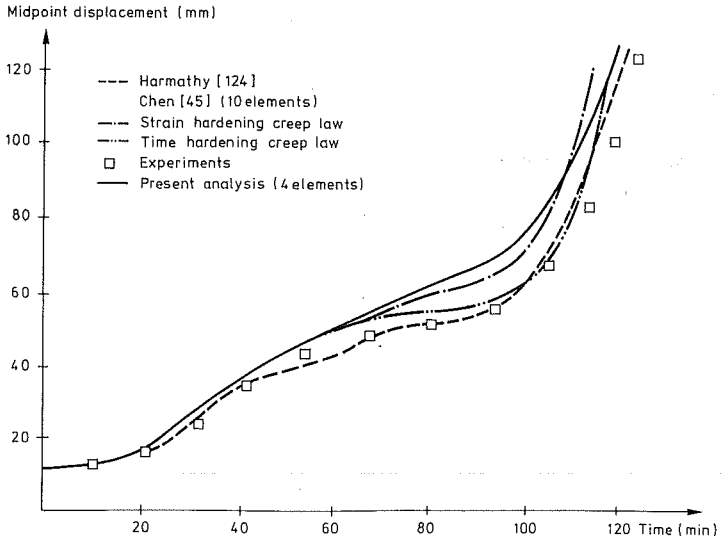

Figure 6.8 Midpoint displacement vs time for fire tested beam

Both Harmathy [124] and Cheng [45] used a set of material parameters related to the test on ASTM A36 steel reported in [123]. Harmathy used a finite difference method only applicable to simply supported beams. Cheng used a finite element method and an incremental solution method with Newton-Raphson iterations to analyse the beam. Considering the independent set of material data and the number of finite elements used in the present study the results obtained are acceptable.

In Fig. 6.9 the calculated stress distribution for the mid-section is shown after 110 min and compared with the one obtained by Cheng [45].

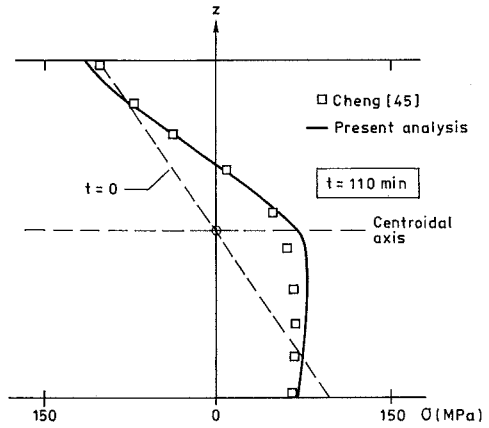

Figure 6.9 Stress distribution at mid-section

6.3 Simply supported beam with fixed supports

The simply supported beam described in Section 6.2 was free to move in the longitudinal direction. In this section the present model is compared with numerical results for a simply supported axially restrained, fire protected beam reported by Furumura ([125]) and shown in Fig. 6.10.

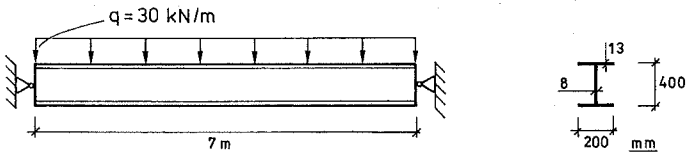

Figure 6.10 Simply supported beam with axially fixed supports

In Ref. [125] a computer program has been used in order to determine the temperature distribution in the beam when the temperature outside the fire protection was raised in the manner for fire tests. The result is given in Fig. 6.11, where the subscripts t, w and b on the temperature denote top flange, centerline of web and bottom flange respectively.

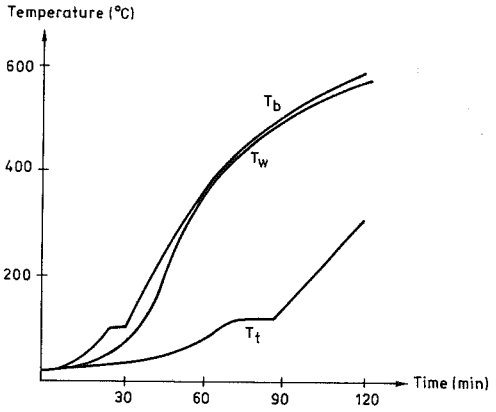

Figure 6.11 Calculated time-temperature curves ([125])

As temperature input values for T_t, T_w and T_b every 10 min are used. A linear temperature distribution between T_t and T_w and between T_w and T_b is used in the numerical studies in Ref. [125] and also adopted herein.

The yield stress at $20^{\circ}C$ is in Ref. [125] assumed to be 340 MPa (i.e. $\sigma_y(20) = 340$ MPa) and is valid as input in the present analysis.

One half of the beam is divided into four equal beam elements and a true incremental procedure ($\Delta t = 1$ min) is used. The result for the midpoint displacement is shown in Fig. 6.12 and compared with those reported by Furumura.

In Fig. 6.13 the axial restraint force at the support is shown. The force increases rapidly until the beam begins to yield after about 30 minutes. The rate of displacement at the midpoint increases markedly at the same time (Fig. 6.12).

In Fig. 6.14 comparison is also shown for the midpoint moment.

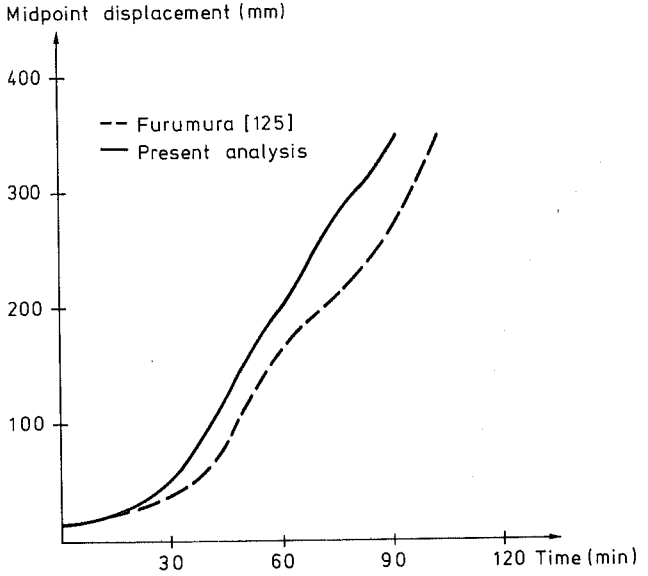

Figure 6.12 Calculated midpoint displacement

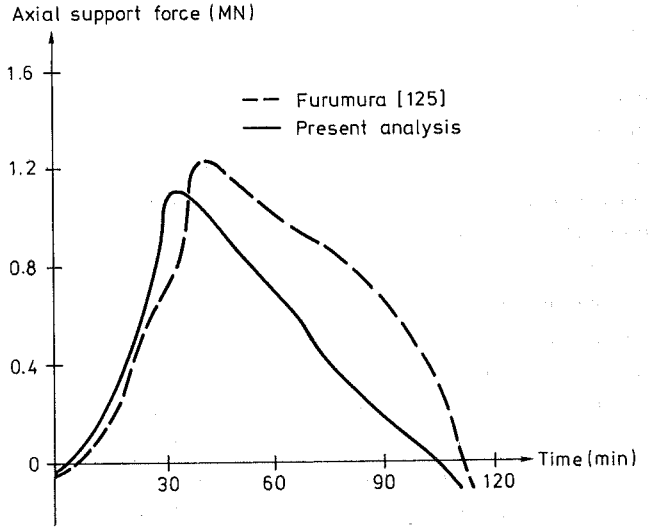

Figure 6.13 Axial support force

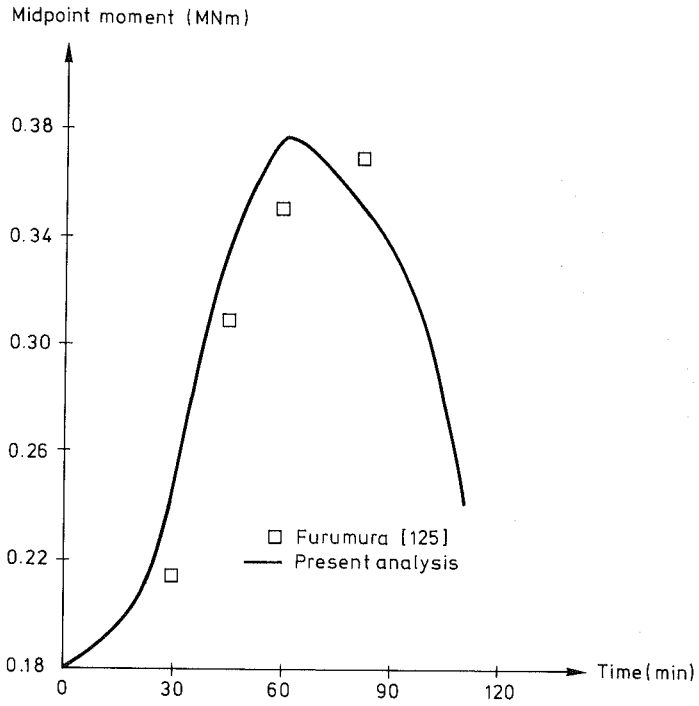

Figure 6.14 Midpoint moment

The differences between the results obtained in this study and those reported in Ref. [125] are in the author's opinion mainly due to the different stress-strain descriptions used. In Ref. [125] the yield stress is assumed to be less temperature dependent than the general concept adopted in this study. For instance, at 300°C the yield stress is about 10 percent higher than the corresponding value used in the present analysis. In addition, the stress-strain relations after initial yield are assumed to be linear. This implies that, if yield stress levels Y^P are determined from these relations, higher values than those suggested in this study, will be obtained. The somewhat earlier yield and the differences in the calculated displacement and forces (cf. Fig. 6.12 and 6.14) are results from the above mentioned differences in material parameters.

This example demonstrates rather clearly the influence of the description of the nonlinear material behaviour. Although discrepancies occur, the behaviour is to a large extent the same.

6.4 Single column at high temperature conditions

6.4.1 Problem description

In this section a parameter study on the behaviour of a single column exposed to a temperature rise is performed. The column is shown in Fig. 6.15.

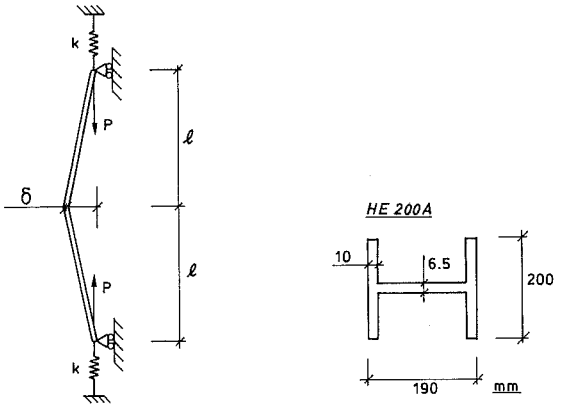

Figure 6.15 Single column

The column of length 2ℓ and with an initial displacement δ at the midlength is centrically loaded by an axial force P. The extent of axial restraint of the column is described by an axial spring with stiffness k, i.e. k = 0 means that the support is free to move while k = ∞ corresponds to a fixed support.

The temperature is assumed to be uniformly distributed in the column and the temperature rise is given by Fig. 6.16.

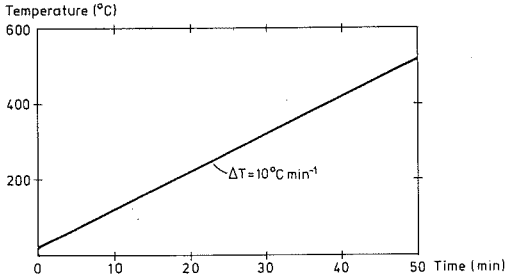

Figure 6.16 Temperature in column

Due to the symmetry in geometry and loading only one half of the beam is studied using four beam elements of equal length (see Fig. 6.17).

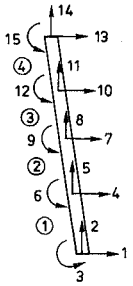

Figure 6.17 Element subdivision and nodal variable numbers

In the finite element model (Fig. 6.17) displacements corresponding to nodal variable numbers 1, 14 and 15 are prescribed to zero.

Furthermore, the cross sectional area of each beam was divided into 20 layers and the yield stress at room temperature was chosen to be 340 MPa.

The calculation procedure took place as follows. The column was first loaded by the axial force P (no restraints). Starting with this state of stress as initial condition a true incremental method is used in order to determine the behaviour of the column when the temperature is raised. The influence of three parameters has mainly been studied:

- the effect of axial restraint (value of spring stiffness k)
- influence of initial displacement δ
- influence of the column slenderness.

The calculated horizontal displacement at midlength (corresponding to nodal variable number 13) and the axial support (corresponding to nodal variable number 14) are compared with a reference column in the following subsections.

The calculations are terminated either after 50 minutes or if the axial support force decreases below the value of the initially applied external load.

6.4.2 Reference column

As a reference column the one shown in Fig. 6.18 is used. In this reference case the supports are assumed fixed (k = ∞).

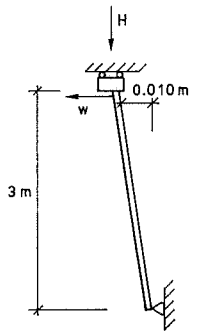

Figure 6.18 Reference column

The results for the horizontal displacement w and the axial support force H are shown in Fig. 6.19. Note that the axial force H is initially equal to the applied load P = 0.5 MN.

In Fig. 6.19 it can be seen, that when the column yields after about 8 minutes, the horizontal displacement increases very rapidly for this rather slender column. This rapid increase is due to the fact that when yield occurs in the midpoint section many material points are affected at the same time since strains are mainly due to the axial displacements (no bending). As also can be seen the support force decreases drastically after the maximum value is reached.

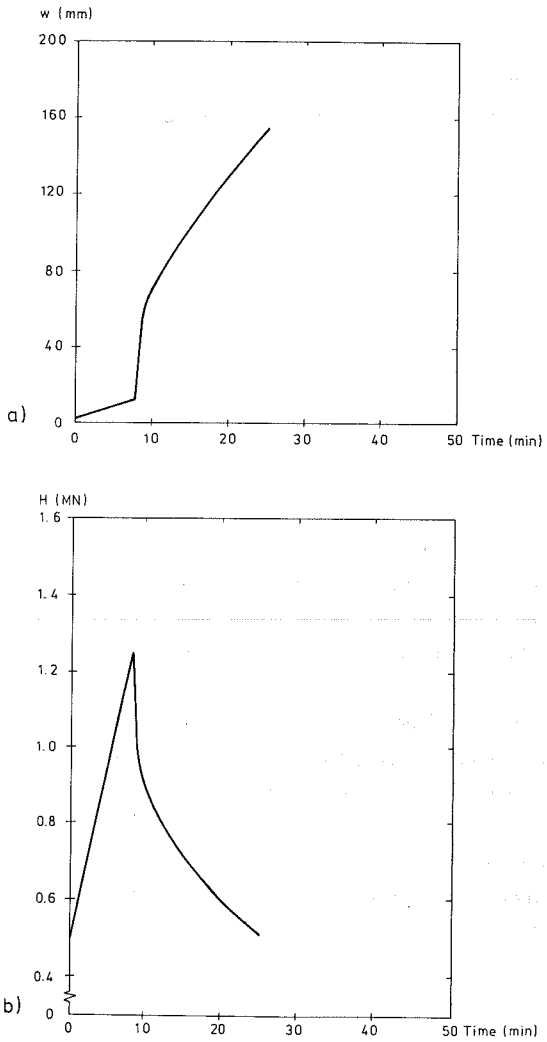

Figure 6.19 Results for the reference column
a) Horizontal displacement
b) Axial support force

6.4.3 Influence of axial restraint

In this subsection the influence of the axial restraint is studied. Calculations for three different values of the spring stiffness have been performed. The results are shown in Fig. 6.20.

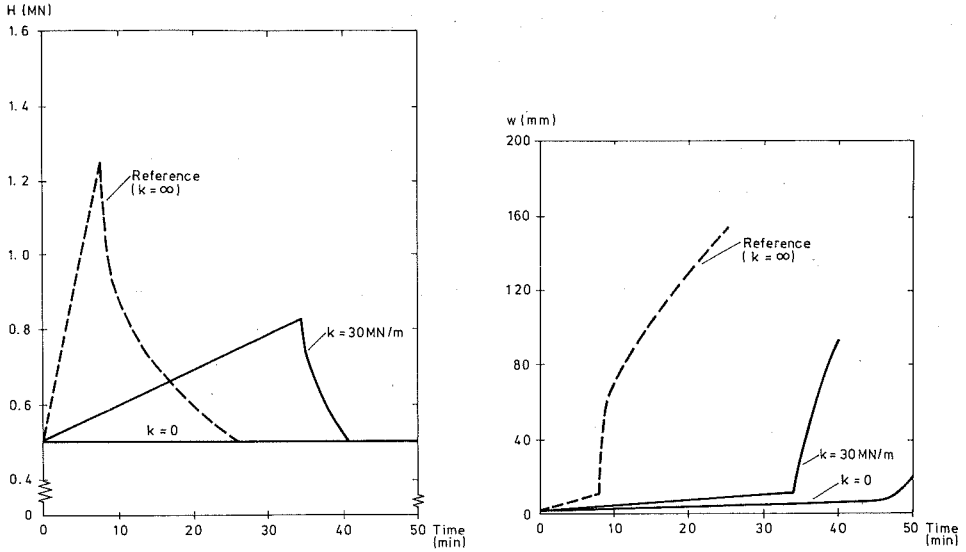

a) Axial support force

b) Horizontal displacement

Figure 6.20 Influence of axial restraints

The axial stiffness k = 30 MN/m corresponds to the stiffness experienced by a column in a ten to twelwe storey frame.

A decrease of the axial stiffness means that the initial yield occurs later, at a higher temperature, since now the column is able to expand. A calculation model where it is assumed that the column is free to move may differ very much from "reality", although axial restraints corresponding to fixed supports (k = ∞) very seldom can be found in a real structure. As seen in Fig. 6.20 even a moderate restraint may cause buckling of the column leading to an earlier failure. Axial restraint is of practical interest for multistorey and/or multibay systems locally exposed to high temperatures. In such cases the thermal expansion of the heated member will be resisted by the surrounding structural system, which may have a significant stiffness.

The influence of axial restraints on concrete beams under fire conditions have been studied by Forsén [126].

6.4.4 Influence of initial displacement

In the reference case the initial displacement δ of the mid-point of the column is very small. This leads to simultaneous yield in a major part of the cross section, essentially caused by axial overloading.

In Fig. 6.21 it is shown that for larger values of δ, yield occurs earlier, now due to bending effects in the outer fibres. The very rapid increase of the horizontal displacement disappears, the displacement curves become smoother as do the curves describing the axial support force. The peak values of the latter curves are also significantly smaller for larger values of δ.

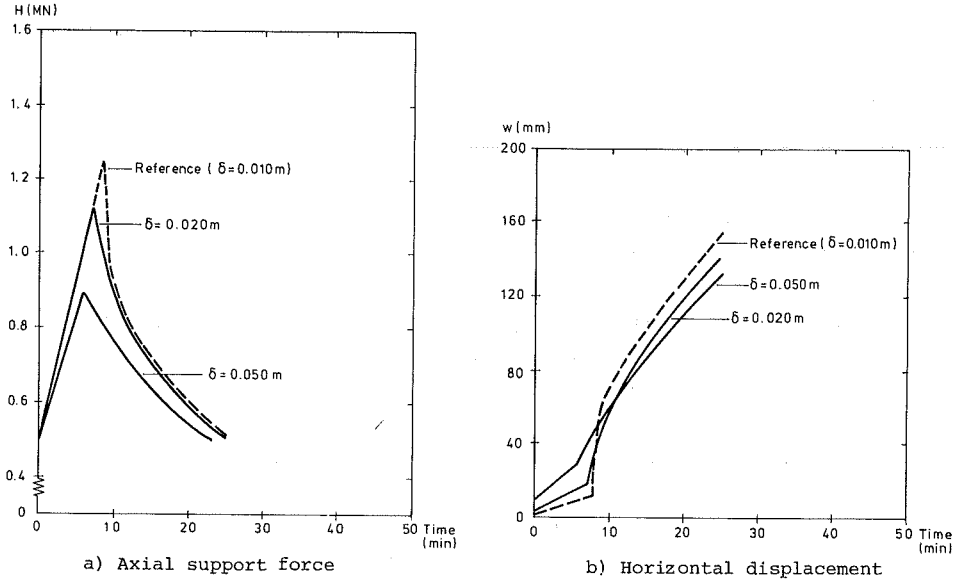

Figure 6.21 Influence of initial displacement

6.4.5 Influence of the slenderness of the column

In this subsection the effect of a decrease of the slenderness of the column is studied. The slenderness ratio is reduced to half

the value of the reference case, simply by changing the length of the column. Since the design stress increases with decreasing ratios the applied external load is changed in proportion. According to the Swedish Regulations for Steel Structures, 1970 [127] the design stress for the slenderness of the reference case is about 140 MPa while, if the slenderness ratio is halved, the design stress is about 200 MPa. The applied load is therefore increased proportionally, giving P = 0.70 MN. In Fig. 6.22 the results for this new column are shown for the axial support force and the horizontal displacement.

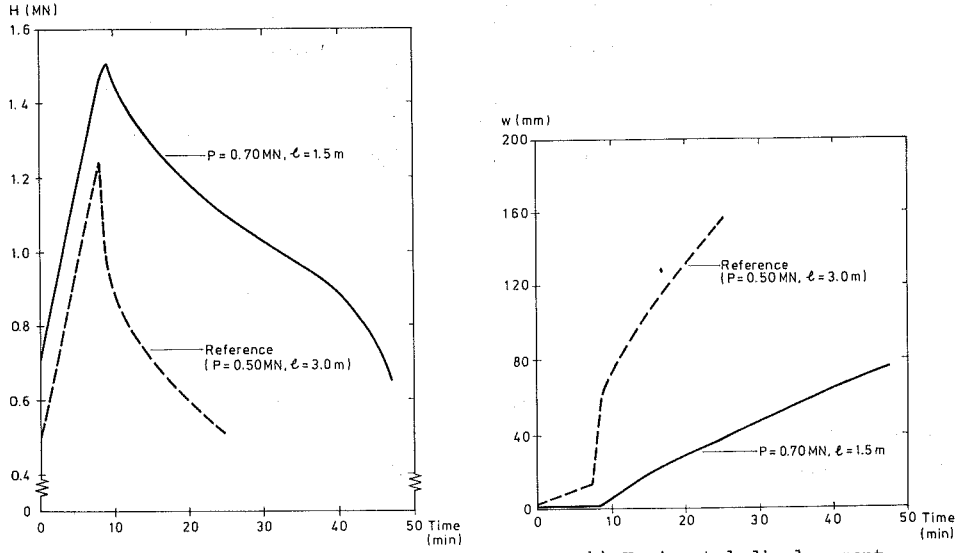

a) Axial support force

b) Horizontal displacement

Figure 6.22 Results for column with decreased slenderness

Fig. 6.22 shows that slender columns are more sensitive to axial restraint. The horizontal displacement for the shorter column does not increase in the same manner after yield. Here the yield is mainly due to the axial compressive load and does not occur in the mid-section only.

6.5 Large scale frame structure

6.5.1 Problem definition

In order to demonstrate the capability of the present version of the computer program an analysis of a four storey frame will be shown. The geometrical properties of the frame and the permanent external load are shown in Fig. 6.23.

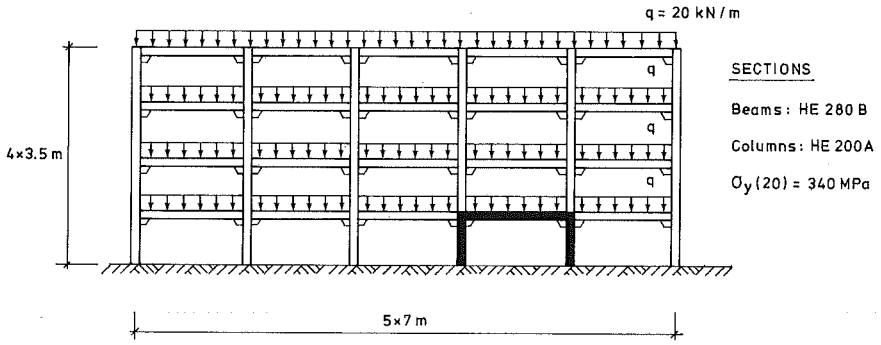

Figure 6.23 Geometrical layout of the frame

The load consists of the uniformly distributed load and of a temperature rise in the shaded members in Fig. 6.23. The temperature is assumed to be uniformly distributed in this part and the rate of heating is assumed to be $10^{\circ}C/min$.

6.5.2 Structural model

The nonlinear behaviour is assumed to be concentrated to the part of the frame exposed to elevated temperature while the surrounding structure is assumed to behave elastically, see Fig. 6.24.

The hinges are assumed to be centrically located.

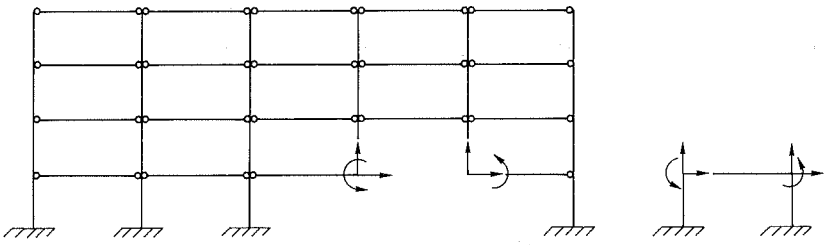

a) Elastic part b) Nonlinear part

Figure 6.24 Subdivision of the frame

By a statical condensation procedure the elastic part is treated as a substructure and is used as an ordinary structural element now with degrees of freedom valid at the boundary nodes between the elastic and nonlinear part. The finite element model of the nonlinear part is shown in Fig. 6.25.

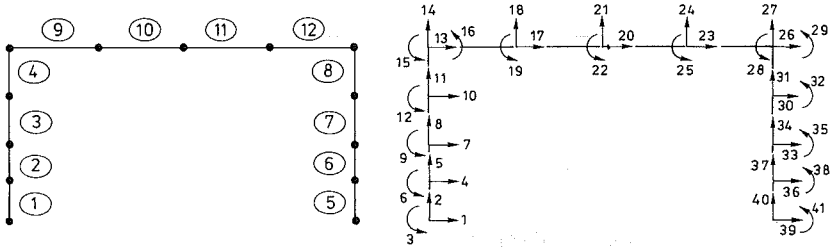

Figure 6.25 Element subdivision and global node variable numbers

Thus the structural element for the elastic part only influences the stiffness corresponding the nodal variable numbers 13, 14, 15, 26, 27 and 29. It should be noted that the hinges are taken into account just by introducing additional rotational degrees of freedom (for example nodal variable number 15 and 16 for the upper left hinge in Figure 6.25).

6.5.3 Numerical results

The output data from the nonlinear analysis was extensive. The intention here is only to demonstrate some of the characteristics of the behaviour rather than account for all details of the results.

In Fig. 6.26 the calculated displacement patterns for the non-linear part of the frame at various times are shown.

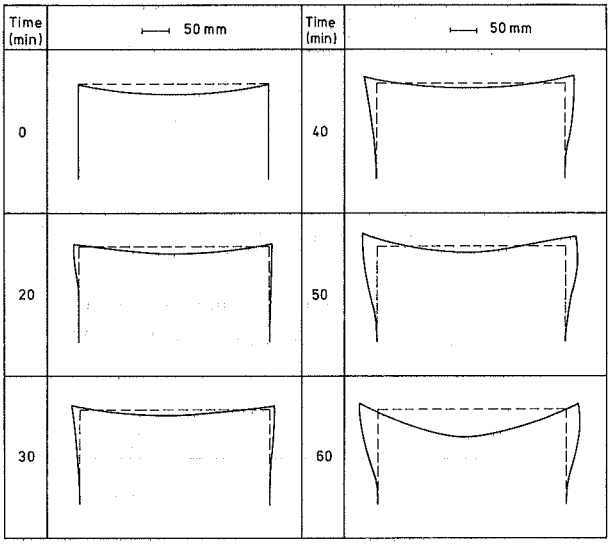

Figure 6.26 Displacement patterns

In Fig. 6.27 the midpoint displacement w and the right end horizontal displacement h of the beam are shown separately together with the elongation u of the left column.

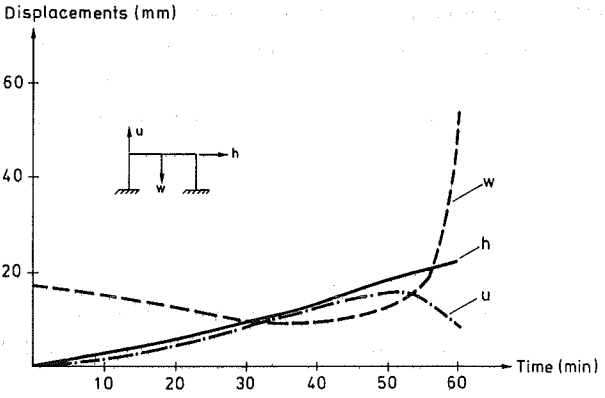

Figure 6.27 Calculated displacements

As can be seen the horizontal displacement h increases almost linearly with time. The midpoint displacement of the beam w firstly decreases due to the thermal expansion of the columns but when yield occurs in the mid-section this displacement very rapidly increases until collapse. The elongation of the column starts to decrease after about 50 min due to further yield. The approximate spread of yielded zones is shown in Figure 6.28.

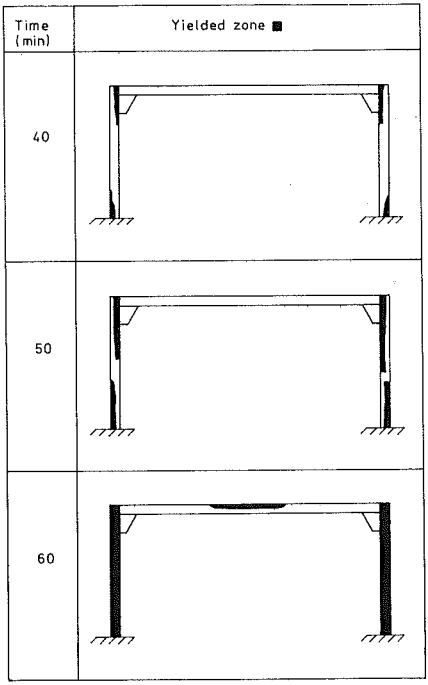

Figure 6.28 Spread of yielded zones

Finally, the moments at the fixed supports are shown in Figure 6.29 and normal forces in the left column and the beam are shown in Figure 6.30.

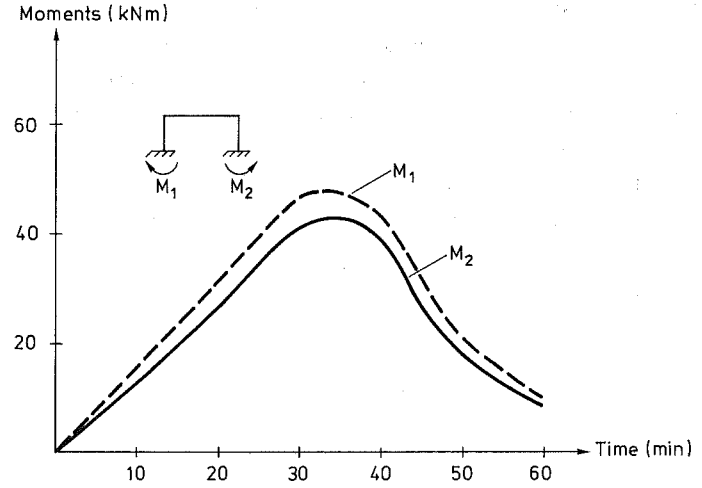

Figure 6.29 Moments at the fixed supports

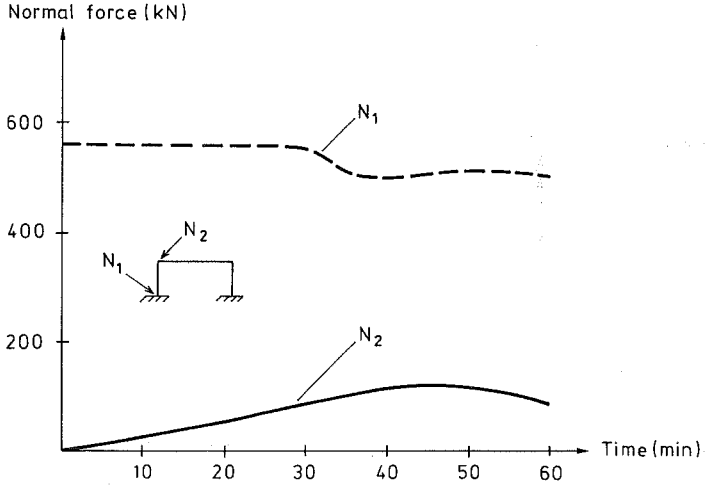

Figure 6.30 Normal forces

7. CONCLUDING REMARKS

7.1 Discussion and conclusions

The research work described in this thesis is concerned with finite element analysis of structures at high temperature with special application to steel beams and frames.

Based on the general expressions for the Partially updated Lagrangian formulation (PL) derived in Chapter 2 the corresponding matrices are derived for a plane beam element with an internal degree of freedom in Chapter 4. Results indicate that if a coarse element subdivision is used, the PL-formulation is more accurate than in a UL-formulation, where the local element deformations are ignored.

The elastic-plastic-viscoplastic constitutive model derived in Chapter 3 is verified for uniaxial stress for nonisothermal conditions. The agreement between numerical results and experimental values is quite satisfactory. It is also shown that the experimentally observed increase in yield stress due to prior creep can be taken into account. This is because both plastic strains and creep strains are treated as interacting non-elastic strains.

The computer program CAMFEM developed during the course of this study is based on a command language. Experience has shown that the modularized program structure is very useful in a research environment where new fields of application are studied. The user-defined matrices and macro commands offer a large flexibility.

The finite element equations for beams in combination with the uniaxial form of the presented constitutive model are used to predict the behaviour for steel skeletal structures. Although quite independent material parameters are used, the numerical results are in satisfactory agreement with experimentally observed results.

7.2 Future developments

A crucial point in the analysis of structures at high temperatures is the modelling of the nonlinear material behaviour. Although a theoretical description in many cases can be derived, the need for more experimental work is essential, especially determination of the creep parameters. The present constitutive model is restricted to small strain isotropic conditions. It might be of interest also to derive expressions for large deformations. In addition, a constitutive model with kinematic hardening would be necessary in order to take into account the Bauschinger effect.

In this work plane steel skeletal structures are studied, assuming the temperature to be uniformly distributed over the width. An improved description of the behaviour is to include effects as torsion, buckling of the flanges and the effect of shear deformations.

The calculation procedure adopted here is a true incremental one. This can give differences from the real behaviour if not sufficiently small time steps are used. Further developments of efficient and stable numerical procedures for problems involving both material and geometric nonlinearities are of interest.

APPENDIX A. NOTATIONS

Notations and symbols are explained in the text where they first occur. Most of the notations used are given in this appendix as well.

Latin letters

A	cross sectional area
$\underset{\sim}{C}$	material stiffness tensor
$\underset{\sim}{C}^{E}$	elastic material stiffness tensor
$\underset{\sim}{C}^{EP}$	elastic-plastic material stiffness tensor
C_T	material tangent modulus
D_{ij}	cross sectional functions
$\underset{\sim}{E}$	Green strain tensor
$\underset{\sim}{E}^{*}$	Almansi strain tensor
E	modulus of elasticity
$\underset{\sim}{F}$	deformation gradient tensor, material flexibility tensor
F^{P}	plastic loading function
F^{VP}	viscoplastic loading function
G	matrix related to element geometry
G_α	transformation matrix
H	normal force
H'	slope of an effective stress-strain curve
$\underset{\sim}{I}$	unit tensor
I	moment of inertia
J_2'	second invariant of the deviatoric stress tensor
K^{0}	small displacement stiffness matrix
K^{σ}	initial stress stiffness matrix
K^{u}	initial displacement stiffness matrix

L	beam length
N_i	interpolation functions
$\hat{\underset{\sim}{N}}$	outward unit normal in the initial configuration
$\tilde{\underset{\sim}{p}}$	pseudo force vector
$\underset{\sim}{p}$	physical force vector
R	element nodal force vector
R^*	element nodal force vector in a partially updated configuration
S	surface in the current configuration
S^0	surface in the initial configuration
S^*	surface in a partially updated configuration
$\underset{\sim}{\tau}$	Cauchy stress tensor
$\tilde{\underset{\sim}{T}}$	second Piola-Kirchhoff stress tensor
$\tilde{\underset{\sim}{T}}^0$	initial stress tensor
T	temperature
V	volume in the current configuration
V^0	volume in the initial configuration
V^*	volume in a partially updated configuration
$\underset{\sim}{X}$	material coordinate vector
$\underset{\sim}{X}^*$	material coordinate vector for a partially updated configuration
Y^P	yield stress level
Y^{VP}	primary creep stress level
a_i	integration constants
$\underset{\sim}{\mathfrak{C}}$	material stiffness tensor referred to the current configuration
f_i	body force component per unit volume in the current configuration
f_i^0	body force component per unit volume in the initial configuration
f_i^*	body force component per unit volume in a partially updated configuration

g_1 creep function for primary creep

g_2 creep function for secondary creep

n creep exponent

$\underset{\sim}{\hat{n}}$ outward unit normal in the current configuration

t time

$\tilde{t}_i$ component of the second Piola-Kirchhoff traction vector

t_i^0 component of the first Piola-Kirchhoff traction vector

t_i^{0*} component of the first Piola-Kirchhoff traction vector with respect to a partially updated configuration

$\underset{\sim}{u}$ displacement vector referred to the initial configuration

$\underset{\sim}{u}^*$ displacement vector referred to a partially updated configuration

$\bar{u}$ nodal displacement vector referred to the initial configuration

$\bar{u}^*$ nodal displacement vector referred to a partially updated configuration

u_0^* axial displacement along the reference axis in a partially updated configuration

v_i weighting function in the initial configuration

v_i^* weighting function in a partially updated configuration

w^* lateral displacement in a partially updated configuration

$\underset{\sim}{x}$ spatial coordinates

$\underset{\sim}{x}^*$ spatial coordinates in a partially updated configuration

x,z coordinates

Greek letters

α coefficient of thermal expansion, load factor, slope

$\alpha_1,\alpha_2\ldots$ coefficients

β scalar

γ_1 fluidity parameter (primary creep)

γ_2 fluidity parameter (secondary creep)

δ	initial displacement
δ_{ij}	Kronecker's delta
$\underset{\sim}{\varepsilon}$	total strain tensor
$\underset{\sim}{\varepsilon}^{E}$	elastic strain tensor
$\underset{\sim}{\varepsilon}^{P}$	plastic strain tensor
$\underset{\sim}{\varepsilon}^{T}$	thermal strain tensor
$\underset{\sim}{\varepsilon}^{VP}$	viscoplastic strain tensor
$\bar{\varepsilon}^{P}$	effective plastic strain
$\bar{\varepsilon}^{M}$	effective permanent strain
$\underset{\sim}{\sigma}$	stress tensor
$\underset{\sim}{\sigma}^{0}$	initial stress tensor
$\underset{\sim}{\sigma}'$	deviatoric stress tensor
$\bar{\sigma}$	effective stress
σ_{y}	uniaxial yield stress
κ^{P}	hardening parameter for the plastic loading function F^{P}
κ^{VP}	hardening parameter for the viscoplastic loading function F^{VP}
μ	Lame's elasticity constant, temperature dependent scalar
ν	Poisson's ratio
λ	Lame's elasticity constant, loading parameter
$\dot{\lambda}_{1}$	scalar function for plastic strains
$\dot{\lambda}_{2}$	scalar function for viscoplastic strains
ξ,η	scalars
ϕ	scalar function

Other notations

$\underset{\sim}{\cdot}$	tensor (wavy underscore)
${}^{t}(\cdot)$	indices denoting time (left superindex)
${}^{t+\Delta t}(\cdot)$	
$(\cdot)^{T}$	transpose of $(\cdot)$
$\det(\cdot)$	determinant of $(\cdot)$
$\dot{\cdot}$	time differentiation $(\partial/\partial t)$
$,x$	partial differentiation $(\partial/\partial x)$
$\Delta(\cdot)$	increment of $(\cdot)$
$d(\cdot)$	differential of $(\cdot)$

APPENDIX B. CALCULATION OF STRESS IN THE TRANSITION RANGE FROM ELASTIC TO PLASTIC BEHAVIOUR

B.1 General remarks

Consider a time increment Δt between t and $t+\Delta t$. The corresponding temperatures are ${}^{t}T$ and ${}^{t+\Delta t}T$ while the increments of the total, thermal and viscoplastic strain tensors are denoted $\Delta\underset{\sim}{\varepsilon}$, $\Delta\underset{\sim}{\varepsilon}^{T}$ and $\Delta\underset{\sim}{\varepsilon}^{VP}$ respectively. The actual stress tensor is ${}^{t}\underset{\sim}{\sigma}$ and the elastic strain tensor ${}^{t}\underset{\sim}{\varepsilon}^{E}$. In the following the stress calculation is described both in the general three-dimensional case and for the special case of uniaxial stress.

B.2 General formulation

Assume that the behaviour is elastic and calculate a trial stress increment tensor, cf. Eqs. (3.1) and (3.5)

$$\Delta\hat{\sigma}_{ij} = {}^{t+\Delta t}C^{E}_{ijk\ell}(\Delta\varepsilon_{k\ell} - \Delta\varepsilon^{T}_{k\ell} - \Delta\varepsilon^{VP}_{k\ell}) + \Delta C^{E}_{ijk\ell}\,{}^{t}\varepsilon^{E}_{k\ell} \tag{B.1}$$

where $\Delta\underset{\sim}{C}^{E}$ is the change of the elastic material stiffness tensor $\underset{\sim}{C}^{E}$ during the time interval. The stress increment $\Delta\hat{\underset{\sim}{\sigma}}$ is added to the stress state at the start of the increment i.e.

$${}^{t+\Delta t}\hat{\sigma}_{ij} = {}^{t}\sigma_{ij} + \Delta\hat{\sigma}_{ij} \tag{B.2}$$

The plastic yield function for this stress at the end of the time increment is written as

$${}^{t+\Delta t}\hat{F}^{P}({}^{t+\Delta t}\hat{\underset{\sim}{\sigma}},\ {}^{t+\Delta t}T,\ {}^{t+\Delta t}\kappa) = f({}^{t+\Delta t}\hat{\underset{\sim}{\sigma}}) - {}^{t+\Delta t}\hat{Y}^{P} \tag{B.3}$$

where

$${}^{t+\Delta t}\hat{Y}^{P} = Y^{P}({}^{t+\Delta t}T,\ {}^{t+\Delta t}\kappa) \tag{B.4}$$

is the value of Y^{P} at time $t+\Delta t$ provided that plastic yield does not occur. It should be noted that the hardening due to incremental viscoplastic strains is taken into account in (B.4).

If the yield function is less than or equal to zero, i.e. if ${}^{t+\Delta t}\hat{F}^P \leq 0$, the predicted stress increment is correct, but if ${}^{t+\Delta t}\hat{F}^P > 0$ yielding occurs during the time increment and one must determine the stress and strain at the level of the initial yield surface.

To obtain the stress increment necessary to cause yield, write the yield condition Eq. (3.10) as

$$({}^{t}\sigma'_{ij} + \eta\Delta\hat{\sigma}'_{ij})({}^{t}\sigma'_{ij} + \eta\Delta\hat{\sigma}'_{ij}) - \frac{2}{3}({}^{t+\eta\Delta t}Y^P)^2 = 0 \qquad \text{(B.5)}$$

in which primes indicate deviatoric components and $\eta\Delta\hat{\underline{g}}'$ is the portion of the stress increment necessary to cause yield. Assuming that

$${}^{t+\eta\Delta t}Y^P = {}^{t}Y^P + \eta\Delta\hat{Y}^P \qquad \text{(B.6)}$$

where

$$\Delta\hat{Y}^P = {}^{t+\Delta t}\hat{Y}^P - {}^{t}Y^P \qquad \text{(B.7)}$$

the scalar η can now be solved to yield

$$\eta = \frac{-b + (b^2 - 4ac)^{1/2}}{2a} \qquad \text{(B.8)}$$

in which

$$\begin{aligned} a &= \Delta\hat{\sigma}'_{ij}\Delta\hat{\sigma}'_{ij} - \frac{2}{3}\Delta\hat{Y}^P \cdot \Delta\hat{Y}^P \\ b &= 2\,{}^{t}\sigma'_{ij}\Delta\hat{\sigma}'_{ij} - \frac{4}{3}\Delta\hat{Y}^P \cdot {}^{t}Y^P \\ c &= {}^{t}\sigma'_{ij}\,{}^{t}\sigma'_{ij} - \frac{2}{3}\,{}^{t}Y^P \cdot {}^{t}Y^P \end{aligned} \qquad \text{(B.9)}$$

The corresponding strain increment tensor necessary to cause yield can be determined noting that the material behaves elastically up to yield. The following relation is valid

$$\bar{t}\varepsilon^{E}_{k\ell} = \bar{t}F_{k\ell mn}({}^{t}\sigma_{mn} + \eta\Delta\hat{\sigma}_{mn}) \tag{B.10}$$

where an expression for the flexibility tensor $\bar{t}_{\tilde{F}}$ is given in Eq. (3.7) and $\bar{t} = t + \eta\Delta t$ is the time for initial yield. The strain increment $\Delta\bar{\tilde{\varepsilon}}^{E}$ is then obtained from

$$\Delta\bar{\varepsilon}^{E}_{k\ell} = \bar{t}\varepsilon^{E}_{k\ell} - {}^{t}\varepsilon^{E}_{k\ell} \tag{B.11}$$

where

$${}^{t}\varepsilon^{E}_{k\ell} = {}^{t}F_{k\ell mn}\,{}^{t}\sigma_{mn} \tag{B.12}$$

The stress and temperature states at initial yield are now known and the remaining stress increment $\Delta\overset{*}{\tilde{\sigma}}$ occurring after yield is to be determined. The elastic-plastic portion of the strain increment after yield is given by

$$\Delta\overset{*}{\varepsilon}_{k\ell} = \Delta\varepsilon_{k\ell} - \Delta\varepsilon^{T}_{k\ell} - \Delta\varepsilon^{VP}_{k\ell} - \Delta\bar{\varepsilon}^{E}_{k\ell} \tag{B.13}$$

where $\Delta\bar{\tilde{\varepsilon}}^{E}$ is given by Eq. (B.11). The consistency condition gives

$$\bar{t}\left(\frac{\partial F^{P}}{\partial\sigma_{ij}}\right)\Delta\overset{*}{\sigma}_{ij} + \bar{t}\left(\frac{\partial F^{P}}{\partial\kappa^{P}}\right)\Delta\kappa^{P} + \bar{t}\left(\frac{\partial F^{P}}{\partial T}\right)\Delta\overset{*}{T} = 0 \tag{B.14}$$

where the asterisks indicate increments after yield and the partial derivates of F^{P} should be evaluated at the time for initial yield. The stress increment $\Delta\overset{*}{\tilde{\sigma}}$ is written as

$$\Delta\overset{*}{\sigma}_{ij} = {}^{t+\Delta t}C^{E}_{ijk\ell}(\Delta\overset{*}{\varepsilon}_{k\ell} - \Delta\lambda_{1}\,\bar{t}a_{k\ell}) + \Delta C^{*E}_{ijk\ell}\,\bar{t}\varepsilon^{E}_{k\ell} \tag{B.15}$$

in which the normality condition is used for the plastic strain tensor and the notation $\bar{t}_{\tilde{a}}$ is used for the gradient of the yield surface at time $\bar{t}$. The second term in Eq. (B.14) is obtained from Eq. (3.33) as

$$\bar{t}\left(\frac{\partial F^{P}}{\partial\kappa^{P}}\right)\Delta\kappa^{P} = -\bar{t}H'(\Delta\lambda_{1} + \xi\Delta\overset{*}{\lambda}_{2}) \tag{B.16}$$

Substitution of Eqs. (B.15) and (B.16) into Eq. (B.13) and solving for $\Delta\lambda_{1}$ yields

$$\Delta\lambda_1 = \frac{1}{s}[\bar{t}a_{ij}\{{}^{t+\Delta t}C^{E}_{ijk\ell}\Delta\varepsilon^{*}_{k\ell} + \Delta C^{*E}_{ijk\ell}\,\bar{t}\varepsilon^{E}_{k\ell}\} + \bar{t}(\frac{\partial F^{P}}{\partial T})\Delta T^{*} - \bar{t}_{H'}\xi\Delta\lambda^{*}_{2}] \quad (B.17)$$

where

$$s = \bar{t}a_{ij}\,{}^{t+\Delta t}C^{E}_{ijk\ell}\,\bar{t}a_{k\ell} + \bar{t}_{H'} \quad (B.18)$$

Substitution of $\Delta\lambda_1$ into (B.15) gives

$$\Delta\sigma^{*}_{ij} = ({}^{t+\Delta t}C^{E}_{ijk\ell} - \frac{1}{s}\,{}^{t+\Delta t}C^{E}_{ijmn}\,\bar{t}a_{mn}\,\bar{t}a_{rs}\,{}^{t+\Delta t}C^{E}_{rsk\ell})\Delta\varepsilon^{*}_{k\ell}$$
$$- \frac{1}{s}\{{}^{t+\Delta t}C^{E}_{ijk\ell}\,\bar{t}a_{k\ell}(\bar{t}(\frac{\partial F^{P}}{\partial T})\Delta T^{*} - \bar{t}_{H'}\xi\Delta\lambda^{*}_{2}) + {}^{t+\Delta t}C^{E}_{ijmn}\,\bar{t}a_{mn}\,\bar{t}a_{rs}\Delta C^{*E}_{rsk\ell}\,\bar{t}\varepsilon^{E}_{k\ell}\}$$
$$+ \Delta C^{*E}_{ijk\ell}\,\bar{t}\varepsilon^{E}_{k\ell} \quad (B.19)$$

A corresponding expression for the case when the stress point already lies on the yield surface at time t is given in rate form in Eqs. (3.36)-(3.38).

Finally the stress state and hardening parameter at the end of the time increment can be obtained by

$${}^{t+\Delta t}\sigma_{ij} = {}^{t}\sigma_{ij} + \eta\Delta\hat{\sigma}_{ij} + \Delta\sigma^{*}_{ij} \quad (B.20)$$

$${}^{t+\Delta t}\kappa = {}^{t}\kappa + \Delta\lambda_1 + \xi\Delta\lambda_2 \quad (B.21)$$

and used as initial values for the next time increment.

B.3 Uniaxial stress state

For the sake of simplicity the index 11 is dropped in the following. The trial stress increment is for uniaxial stress given as

$$\Delta\hat{\sigma} = {}^{t+\Delta t}E(\Delta\varepsilon - \Delta\varepsilon^{T} - \Delta\varepsilon^{VP}) + \Delta E\,{}^{t}\varepsilon \quad (B.22)$$

in which

$$\Delta E = {}^{t+\Delta t}E - {}^{t}E \quad (B.23)$$

is the change of the elastic modulus during the time interval Δt. Then the trial stress is

$$\hat{\sigma} = {}^{t}\sigma + \Delta\hat{\sigma} \tag{B.24}$$

To check whether or not the yield criterion is satisfied, calculate

$${}^{t+\Delta t}\hat{F}^{P} = |\hat{\sigma}| - {}^{t+\Delta t}\hat{\sigma}_{y} \tag{B.25}$$

where ${}^{t+\Delta t}\hat{\sigma}_{y} = \sigma_{y}({}^{t+\Delta t}\kappa, {}^{t+\Delta t}T)$ is the yield stress at time $t+\Delta t$ if plastic yield does not occur. If ${}^{t+\Delta t}\hat{F}^{P}$ is greater than zero yield occurs and the portion of the stress increment to cause yield can be determined from

$$\eta = \frac{{}^{t}\sigma_{y} - |{}^{t}\sigma|}{|\Delta\hat{\sigma}| - \Delta\hat{\sigma}_{y}} \tag{B.26}$$

where

$$\Delta\hat{\sigma}_{y} = {}^{t+\Delta t}\sigma_{y} - {}^{t}\sigma_{y}$$

The corresponding elastic strain increment is given by

$$\Delta\bar{\varepsilon}^{E} = \frac{\eta\Delta\hat{\sigma}}{\bar{t}_{E}} + (\frac{1}{\bar{t}_{E}} - \frac{1}{t_{E}}){}^{t}\sigma$$

The elastic-plastic strain increment after yield is calculated as

$$\Delta\varepsilon^{*} = \Delta\varepsilon - \Delta\varepsilon^{T} - \Delta\varepsilon^{VP} - \Delta\bar{\varepsilon}^{E} \tag{B.27}$$

and the stress increment after yield can now be obtained from

$$\Delta\sigma^{*} = {}^{t+\Delta t}E\{\Delta\varepsilon^{*} - \frac{1}{s}[{}^{t+\Delta t}E\Delta\varepsilon^{*} + \Delta E^{*}\bar{t}_{\varepsilon}{}^{E} - \mathrm{sgn}\,\bar{t}_{\sigma}\,(\bar{t}_{H'}\xi\Delta\lambda^{*}_{2} + \Delta\sigma^{*}_{y})]\}$$

$$+ \Delta E^{*}\bar{t}_{\varepsilon}{}^{E} \tag{B.28}$$

in which

$$\Delta\sigma^{*}_{y} = \sigma_{y}(\bar{t}_{\kappa}, {}^{t+\Delta t}T) - \sigma_{y}(\bar{t}_{\kappa}, \bar{t}_{T}) \tag{B.29}$$

$$\Delta E^{*} = {}^{t+\Delta t}E - \bar{t}_{E} \tag{B.30}$$

$$s = {}^{t+\Delta t}E + \bar{t}_{H'} \tag{B.31}$$

since

$$\bar{t}\left(\frac{\partial F}{\partial T}\right)\Delta T^{*} = \bar{t}\left(\frac{\partial F^{P}}{\partial Y^{P}}\right)\bar{t}\left(\frac{\partial Y^{P}}{\partial T}\right)\Delta T^{*} = -\Delta\sigma_{y}^{*} \tag{B.32}$$

and

$$\bar{t}a_{11} = \bar{t}\left(\frac{\partial F}{\partial \sigma_{11}}\right) = \mathrm{sgn}\,\bar{t}\sigma \tag{B.33}$$

The scalar parameter $\Delta\lambda_1$ describing the hardening due to plastic strain is finally given by

$$\Delta\lambda_1 = \frac{\mathrm{sgn}\,\bar{t}\sigma\left({}^{t+\Delta t}E\Delta\varepsilon^{*} + \Delta E^{*}\bar{t}\varepsilon E - \Delta\sigma_{y}^{*} - \bar{t}_{H'}\xi\Delta\lambda_2^{*}\right)}{{}^{t+\Delta t}E + \bar{t}_{H'}} \tag{B.34}$$

The calculation procedure adopted in this study is summarized by the steps a)-l) below. The simpler superscripts "1" and "2" are used to indicate time t and t+Δt respectively.

a) Calculate trial stress increment

$$\Delta\hat{\sigma} = {}^{2}E(\Delta\varepsilon - \Delta\varepsilon^{T} - \Delta\varepsilon^{VP}) + \left(\frac{{}^{2}E}{{}^{1}E} - 1\right){}^{1}\sigma$$

b) Calculate accumulated trial stress

$${}^{2}\hat{\sigma} = {}^{1}\sigma + \Delta\hat{\sigma}$$

c) Calculate loading function

$$F^{P} = |{}^{2}\hat{\sigma}| - \hat{\sigma}_{y}({}^{2}\hat{\kappa},\ {}^{2}T)$$

where

$${}^{2}\hat{\kappa} = {}^{1}\kappa + \Delta\lambda_2 \qquad \Delta\lambda_2 = (g_1 + g_2)\Delta t$$

d) If $F^{P} \leq 0$ the calculated stress is correct. Jump to l.

e) Yielding occurs. Determine the portion of stress up to yield

$$\eta = \frac{\sigma_y({}^{1}\kappa,\ {}^{1}T) - |{}^{1}\sigma|}{|\Delta\hat{\sigma}| - \Delta\hat{\sigma}_y}$$

in which

$$\Delta\hat{\sigma}_y = \sigma_y({}^2\hat{\kappa},\ {}^2T) - \sigma_y({}^1\kappa,\ {}^1T)$$

f) Assume that

$$\bar{t}_E = {}^1E + \eta({}^2E - {}^1E)$$

$$\bar{t}_T = {}^1T + \eta({}^2T - {}^1T)$$

$$\Delta\lambda_2^* = (1-\eta)\Delta\lambda_2 \Rightarrow \bar{t}_\kappa = {}^1\kappa + \eta\Delta\lambda_2$$

where

$$\bar{t} = {}^1t + \eta\Delta t$$

g) Calculate elastic strain increment up to yield

$$\Delta\bar{\varepsilon}^E = \frac{\eta\Delta\hat{\sigma}}{\bar{t}_E} - \left(\frac{\bar{t}_E - {}^1E}{\bar{t}_E\,{}^1E}\right){}^1\sigma$$

and the elastic-plastic strain increment after yield

$$\Delta\varepsilon^* = \Delta\varepsilon - \Delta\varepsilon^T - \Delta\varepsilon^{VP} - \Delta\bar{\varepsilon}^E$$

h) Calculate

$$\Delta\sigma_y^* = \sigma_y(\bar{t}_\kappa,\ {}^2T) - \sigma_y(\bar{t}_\kappa,\ \bar{t}_T)$$

$$\Delta E^* = {}^2E - \bar{t}_E$$

$$\bar{t}_\sigma = {}^1\sigma + \eta\Delta\hat{\sigma}$$

i) Calculate scalar function $\Delta\lambda_1$

$$\Delta\lambda_1 = \frac{\operatorname{sgn}\bar{t}_\sigma\left({}^2E\Delta\varepsilon^* + \Delta E\,\frac{\bar{t}_\sigma}{t_E}\right) - \Delta\sigma_y^* - \bar{t}_{H'}\xi\Delta\lambda_2}{{}^2E + \bar{t}_{H'}}$$

j) Determine stress increment after yield

$$\Delta\sigma^{*} = {}^{2}E(\Delta\varepsilon^{*} - \Delta\lambda_{1}\mathrm{sgn}\,\bar{t}_{\sigma}) + \Delta E^{*}\frac{\bar{t}_{\sigma}}{\bar{t}_{E}}$$

k) Calculate total stress increment

$$\Delta\sigma = \eta\Delta\hat{\sigma} + \Delta\sigma^{*}$$

l) Update state variables

$${}^{2}\sigma = {}^{1}\sigma + \Delta\sigma$$

$${}^{2}\kappa = {}^{1}\kappa + \Delta\lambda_{1} + \xi\Delta\lambda_{2}$$

B.4 Concluding remarks

The stress calculation for the transition range from elastic to plastic behaviour has been described. It should be noted that the derived expressions are also valid if the material already behaves plastically at the start of the time interval. In that case the scalar η gives zero value.

The new stress state obtained may depart from the yield surface. This discrepancy can be practically eliminated if the increments considered are sufficiently small. Alternative procedures to ensure that the yielding condition is satisfied are presented in Ref. [34].

APPENDIX C. TEMPERATURE DEPENDENT MATERIAL PARAMETERS

C.1 Introduction

Tests on mild structural steel at different temperatures [75] with $\sigma_y(20) = 340$ MPa and $E(20) = 2.1 \cdot 10^5$ MPa are used to determine the general temperature dependence of the modulus of elasticity and the plastic hardening function Y^P. The temperature dependence of the coefficient of thermal expansion is determined from tests reported in [76] while creep parameters are obtained from tests reported in [65].

As a general concept parameters are required for discrete temperatures and linear interpolation is used to calculate parameters for intermediate temperatures. Special arrangements have been introduced to describe the scalar function Y^P and the creep parameters.

C.2 Plastic hardening function Y^P

For each discrete temperature the function $Y^P(T, \bar{\varepsilon}^M)$ is specified by its values in four points viz. $\bar{\varepsilon}^M = 0$, $\bar{\varepsilon}^M = 0.2\%$, $\bar{\varepsilon}^M = 1.0\%$ and $\bar{\varepsilon}^M = 3.0\ \%$. For intermediate values of $\bar{\varepsilon}^M$ a third order polynomial is used.

C.3 Creep parameters

In Section 3.7 the scalar function Y^{VP} was introduced to describe the primary part of the creep strain rate. The principle adopted in this study is to take Y^{VP} as a fraction of Y^P for all temperatures and stresses, i.e.

$$Y^{VP} = \mu(T) \cdot Y^P \qquad (C.1)$$

This approximation is shown in Fig. C.1.

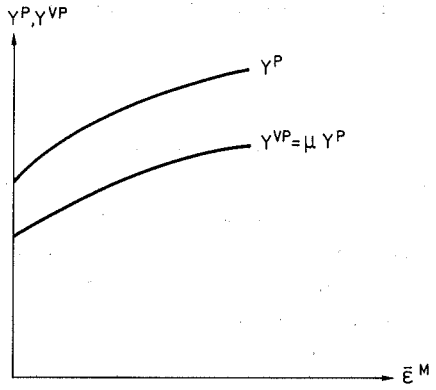

Figure C.1 Approximation of the scalar function Y^{VP}

The chosen variation of the parameter μ with the temperature is shown in Fig. C.2. As can be seen in the figure primary creep is neglected for temperatures below $400^{\circ}C$.

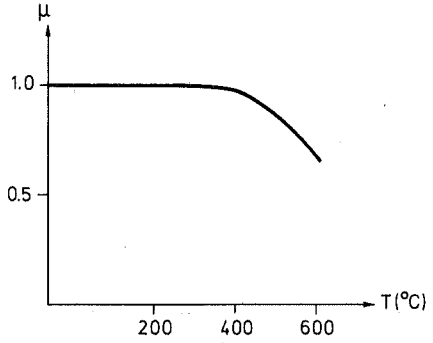

Figure C.2 Variation of the parameter μ in Eq. (C.1) with temperature

The exponent n(T) in Eq. (3.42) for the secondary creep phase is assumed to have a constant value. The temperature effect on secondary creep is described by the fluidity parameter $\gamma_2(T)$.

C.4 Numerical values of material properties

Numerical values of various material parameters at different temperatures in the range 20-700°C are given in Table C.1. Values for the elastic modulus E and the plastic hardening function Y^P are given in relative form.

The creep tests used to determine the creep parameters were performed in the temperature range 400-600°C. Therefore, the creep parameters given outside this range have been obtained by extrapolation and to some extent pure judgement.

The values given in Table C.1 are used in all numerical applications presented in this thesis. The temperature dependence represented by those values may be considered as generally representative for the behaviour of mild structural steel.

T (°C)	$\frac{E(T)}{E(20^oC)}$	$\frac{Y^P(T,0)}{Y^P(20,0)}$	$\frac{Y^P(T,0.002)}{Y^P(20,0)}$	$\frac{Y^P(T,0.01)}{Y^P(20,0)}$	$\frac{Y^P(T,0.03)}{Y^P(20,0)}$
20	1.00	1.00	1.00	1.01	1.03
100	0.97	0.93	0.94	1.00	1.13
300	0.83	0.68	0.75	0.94	1.23
400	0.70	0.58	0.65	0.84	1.13
500	0.56	0.35	0.43	0.67	0.87
600	0.46	0.24	0.30	0.44	0.51
700	0.20	0.14	0.17	0.24	0.25

T (°C)	$\alpha(T)\cdot 10^5$	$\mu(T)$	$\gamma_1(T)$ min^{-1}	$\log\gamma_2(T)$ min^{-1}	$n(T)$
20	0.88	1.00	0.01	10.1	7.5
100	0.95	1.00	0.03	12.1	7.5
300	1.14	1.00	0.08	14.1	7.5
400	1.24	0.98	0.21	15.5	7.5
500	1.33	0.86	0.82	18.4	7.5
600	1.43	0.77	1.95	21.1	7.5
700	1.52	0.68	5.17	24.7	7.5

Table C.1 Material properties at different temperatures

APPENDIX D. VERIFICATION EXAMPLES

D.1 General remarks

In this appendix some numerical examples are presented which concern geometric and material nonlinear problems under isothermal conditions. In addition, a linear analysis of a thermally loaded fixed bar is presented.

The purpose of these examples is not only to verify the validity of the theoretical procedure developed in the previous chapters but also to demonstrate the accuracy and the capability of the computer program.

The derivation of the nonlinear beam expressions in Chapter 4 results in an initial displacement stiffness matrix K^u. Special attention is therefore drawn to the influence of this matrix.

D.2 Influence of the initial displacement stiffness matrix K^u

In this section the influence of the initial displacement stiffness matrix K^u is demonstrated by an example. A cantilever beam with a transversal and an axial compression load is studied, see Fig. D.1.

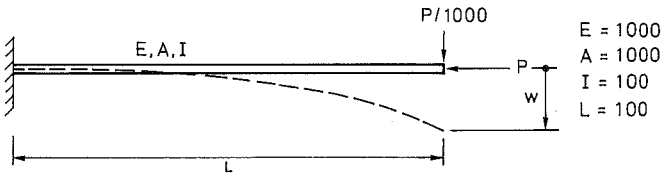

Figure D.1 Cantilever beam with a transversal and an axial compression load

The material is assumed to behave elastically. Exact solutions by means of elliptic integrals can be found in Refs. [110] and [111]. In Ref. [111] highly accurate results are presented in tabular form with five and six digits and are here used as comparative exact values. The solution of this large displacement

problem was performed by a true incremental procedure with the load step $\Delta P = L^2/200EI$. In Table D.1 the results for two different finite element discretizations are shown.

$\frac{PL^2}{EI}$	1 element		8 elements		Exact ($A=\infty$) [111]
	Without K^u	With K^u	Without K^u	With K^u	
0.2	0.00007	0.00007	0.00007	0.00007	0.00007
0.4	0.00016	0.00016	0.00016	0.00016	0.00016
0.6	0.00026	0.00026	0.00026	0.00026	0.00026
0.8	0.00038	0.00039	0.00039	0.00039	0.00039
1.0	0.00053	0.00055	0.00056	0.00056	0.00056
1.2	0.00072	0.00077	0.00077	0.00077	0.00077
1.4	0.00098	0.00106	0.00106	0.00107	0.00107
1.6	0.00134	0.00148	0.00149	0.00149	0.00150
1.8	0.00189	0.00215	0.00217	0.00218	0.00220
2.0	0.00283	0.00336	0.00343	0.00344	0.00345

Table D.1 Results for the normalized vertical displacement w/L

As can be seen from Table D.1 the results for the calculations performed with eight elements are very close to the exact solution.

In Fig. D.2 the error in the results for the vertical displacement in the calculation with one element only is shown.

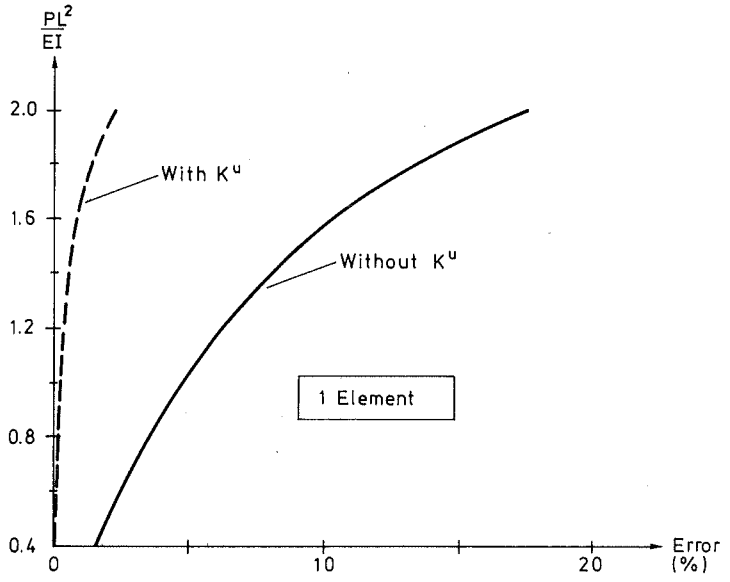

Figure D.2 Error in the vertical displacement w/L

The results indicate that if a coarse element subdivision is used (as normally applied in practice), the initial displacement stiffness matrix K^u should be taken into account in geometric nonlinear analysis.

D.3 Large displacement analysis of cantilever beam subjected to a concentrated moment

An example much used to check the accuracy of nonlinear programs is a cantilever beam subjected to a concentrated moment M at the free end (Fig. D.3).

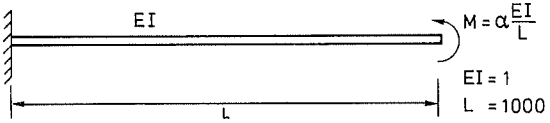

Figure D.3 Cantilever beam with end moment

The cantilever beam was divided into five equal beam elements and the load was applied in increments ($\Delta\alpha = 1/200$).

Exact solutions are represented by circular curves with radius R = EI/M. In Fig. D.4 calculated deformed configurations for four values of α are compared with exact ones.

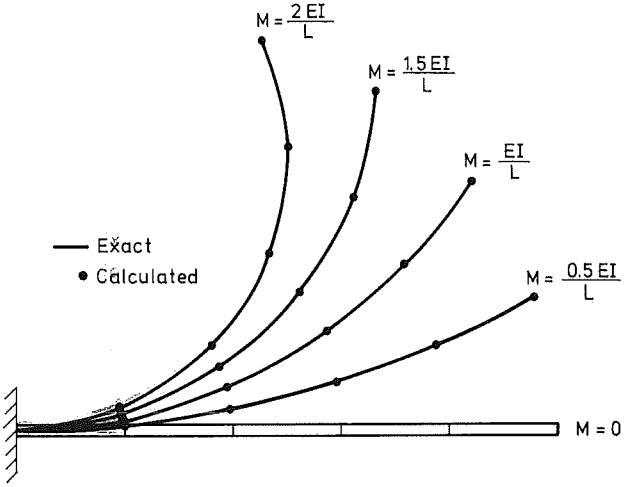

Figure D.4 Comparison between calculated configurations and exact ones

D.4 Cantilever beam with two transversal point loads

In previous sections, results from calculations were compared with exact values. In this section a cantilever beam with two transversal point loads is analysed (Fig. D.5).

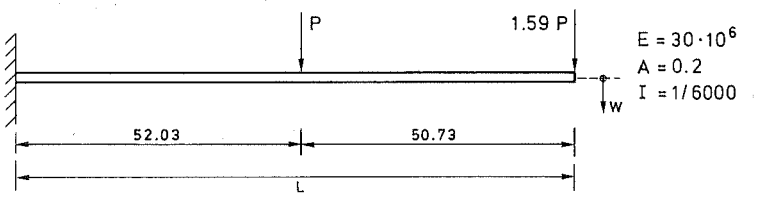

Figure D.5 Cantilever beam with two transversal point loads

This example is chosen because earlier comparisons of numerical results of different methods are available. The results for the transversal end displacement are shown in Table D.2.

Method	Number of elements	Number of increments	w/L	(Error) %
Exact [111]			0.655	0
Martin (TI)	20	100	0.687	4.9
Argyris (TI)	20	100	0,683	4.3
Jennings (TI)	20	100	0.498	24.0
Powell (TI)	20	100	0.433	33.9
Present (SCI)	4	25	0.649	0.9
Jennings (NR)	2	1	0.650	0.8
Powell (NR)	10	1	0.344	47.5
Bäcklund (NR) [82]	4	10	0.657	0.3
Wei et al (NR) [94]	2	20	0.711	8.6

Table D.2 Comparison of solution methods for the vertical displacement

The results corresponding to Jennings's, Powell's, Argyris's and Martin's method were transcribed from Ref. [112]. For further description of the theory see Refs. [77], [79], [113] and [114]. In Table D.2 the abbreviations TI, SCI and NR are used for true incremental, self-correcting incremental and Newton-Raphson methods respectively.

D.5 Williams's toggle

In the main part of the previously described examples either geometric softening or hardening behaviour occurred. However, the behaviour of the toggle in Fig. D.6 is characterized by a softening region followed by a hardening behaviour, see Williams [115].

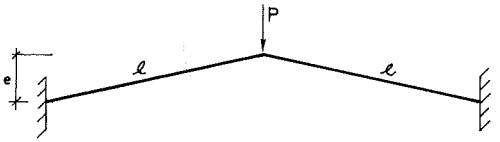

$E = 10.278 \cdot 10^6$ lb/in.^{2}
$A = 0.1829$ in.^{2}
$I = 9.0039 \cdot 10^{-4}$ in.^{4}
$\ell = 12{,}94$ in.
e = 0.320 in. and 0.380 in.

Figure D.6 Williams's toggle

The toggle has been analysed for two different values of the midpoint rise e. Because of the symmetry, it was only necessary to model one half of the toggle. Four beam elements have been used and a displacement incrementation has been performed. The displacement increment for the midpoint of the toggle is taken as 0.01.

The results from the calculations are shown in Fig. D.7 and compared with those obtained by Williams.

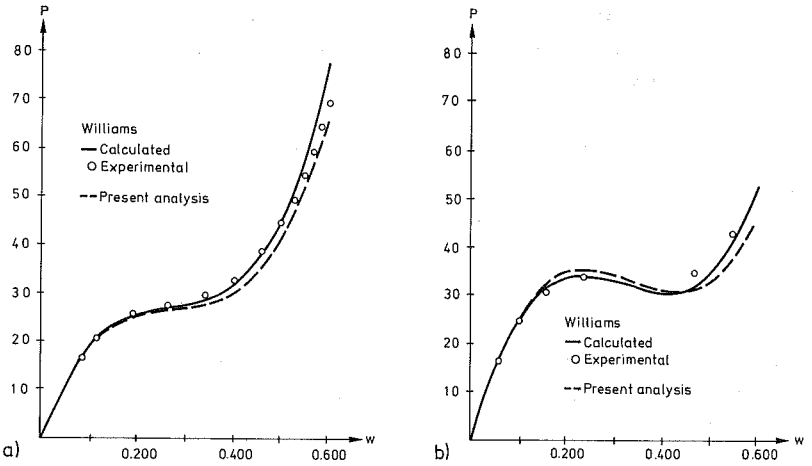

Figure D.7 Midpoint displacement for the toggle
a) e = 0.320 in.
b) e = 0.380 in.

D.6 Simply supported beam

D.6.1 Elastic beam with fixed supports

This is a classical large displacement problem with a closed form solution obtained by Timoshenko [116]. The beam in Fig. D.8 is subjected to a uniformly distributed load q and the supports are fixed, thereby allowing membrane forces.

Since the beam is symmetric about the midspan, one half of the beam was divided into four equal elements. A self-correcting incremental method was used with a loadstep $\lambda = 0.01$. The uniformly distributed load was approximated with vertical nodal loads only.

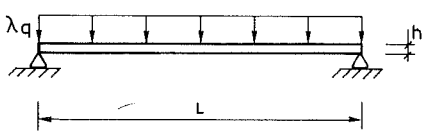

$E = 2.2 \cdot 10^5 MPa$
$L = 0.5 m$
$h = 0.01 m$
$A = 0.5 m^2$
$q = 1.5 MNm^{-2}$

Figure D.8 Simply supported beam

The results for the vertical displacement w, the moment M at the center of the beam and the support horisontal force are shown in Fig. D.9 and compared with theoretical values.

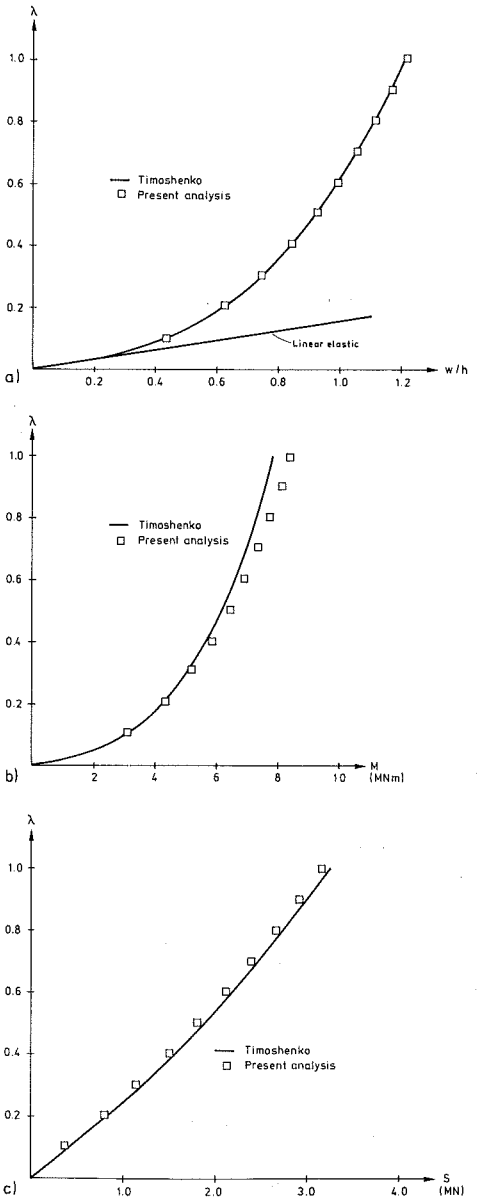

Figure D.9 Results obtained for the simply supported elastic beam in Fig. D.8
a) Midpoint displacement
b) Midpoint moment
c) Support horizontal force

D.6.2 Elastic-plastic beam

In Subsection D.6.1 a simply supported beam was analysed considering geometric nonlinearities only. In this section, the simply supported beam in Section D.6.1 is analysed taking into account nonlinear material behaviour only (no fixed supports). In addition to the parameters in Fig. D.8 a yield stress σ_y = 300 MPa was introduced to describe the material nonlinearity. The material was further assumed to be elastic-perfectly plastic.

The cross-sectional area was divided into 20 equal layers and a true incremental calculation was performed. In Fig. D.10 the central deflection w of the beam as a function of the applied load q is shown. The result is normalized to the conditions at the initial yield w_y and q_y respectively. In Fig. D.10 the analytical solution obtained by Prager and Hodge [117] is also shown.

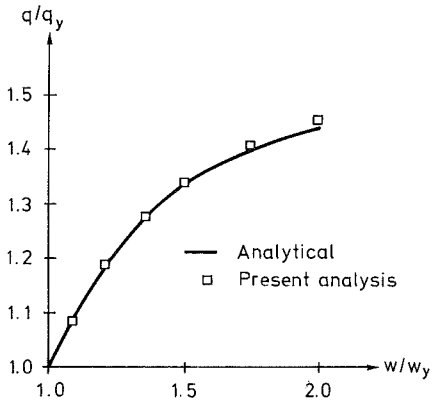

Figure D.10 Load-displacement curve for a simply supported elastic-plastic beam

D.6.3 Elastic-plastic beam with fixed supports

The elastic-plastic beam described in Subsection D.6.2 has also been analysed assuming fixed supports (combined geometric and material nonlinearities). A true incremental solution procedure was adopted with a load step λ = 0.01. The calculated results are shown in Fig. D.11 and compared with values reported by other investigators.

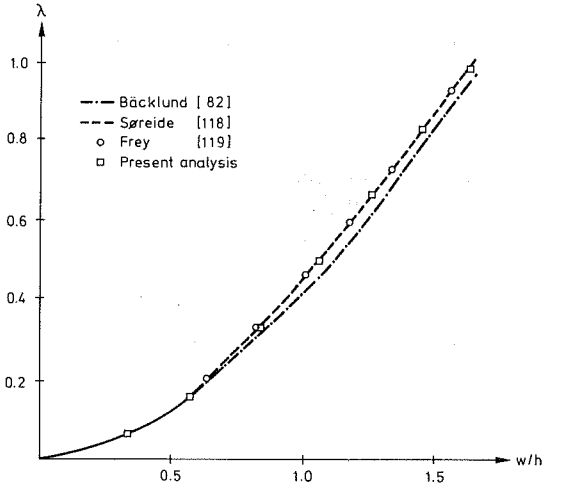

Figure D.11 Load-displacement curve for simply supported elastic-plastic beam with fixed supports

D.7 Thermal expansion of fixed bar

A bar with linearly varying cross sectional area A(x) is restrained at the ends x = 0 and x = L (Fig. D.12). The bar is subjected to a linear temperature variation T(x).

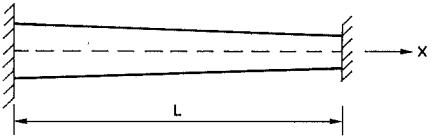

$T(x) = T_0 (1 - \frac{x}{L})$
$A(x) = A_0 (2 - \frac{x}{L})$
$L = 0.5\,m$
$E = 2.1 \cdot 10^5\,MPa$
$\alpha = 10^{-5}\,°C^{-1}$
$T = 100\,°C$
$A_0 = 10^{-3}\,m^2$

Figure D.12 Fixed bar

The analysis was performed with five elements of equal length. The mean values of temperature and cross sectional area were used for each element.

In Table D.3 the calculated displacements in the nodes and the stresses in the center of each element are compared with analytical solutions.

Node	Location x	Displacement (mm) Calculated	Analytical	Stress (MPa) Calculated	Analytical
1	0	0	0	- 79.87	- 79.73
2	0.10	0.0520	0.0520	- 89.27	- 89.11
3	0.20	0.0795	0.0795	-101.17	-100.99
4	0.30	0.0813	0.0814	-116.73	-116.53
5	0.40	0.0557	0.0558	-137.96	-137.71
6	0.50	0	0		

Table D.3 Analytical and calculated values

D.8 Summary and conclusions

In this appendix a number of problems have been analysed in order to verify the theoretical base considering isothermal conditions. In geometric nonlinear problems an initial displacement stiffness matrix is used. It is shown that this matrix is important when a coarse element subdivision is used.

The results obtained are generally in good agreement with analytical ones or results obtained by other investigators.

APPENDIX E. PROBLEM INDEPENDENT COMMANDS IN THE COMPUTER PROGRAM CAMFEM

STOP

Stop execution

PRON

Turn printing on. Output is written on terminal

PROFF

Turn printing off. No output is written on terminal

LOAD A N1 N2

Define a numeric matrix A with N1 rows and N2 columns.

N1 and N2 may be given either as digits or as scalar variables.

The matrix values are given after questions, or, if the command is included in a macro, matrix A becomes a zero matrix.

If matrix A is previously defined and N1 and N2 are omitted in the command the elements of A are changed according to input. If matrix A is not previously defined, or if A is a text matrix, A is defined as a scalar if N1 and N2 are omitted in the command.

The following specifications can be given in place of numerical input:

ZERO
Assign zero to the rest of the matrix.

DIAG
Assign values only to the diagonal elements. If only one value is given all diagonal elements are assigned that value.

GO TO N1 N2

Continue input from row N1 and column N2.

GO TO END

Stop input to matrix.

SYM

Make the matrix symmetric, based on the upper-right part.

LTEXT A N1

Define a text matrix A with N1 rows of 80 characters.

N1 may be given either as a digit or as a scalar variable.

The character rows are given after questions, or, if the command is included in a macro, matrix A becomes a blank matrix.

If matrix A is previously defined it is possible to change its character rows by omitting N1 in the command.

If matrix A is not previously defined, or if A is a numeric matrix, A is defined as a one row matrix if N1 is omitted in the command.

The following specifications can be given in place of input of character rows:

*BLANK

Assign blanks to the rest of the matrix.

*GO TO N1

Continue input from row N1.

*GO TO END

Stop input to matrix.

PRINT A1 [A2 A3...] [N1 [N2 [N3 N4]]]

Print matrices A1, A2 etc.

If N1 is given, only row N1 of the matrices are printed.

If N1 and N2 are given, only rows N1 to N2 of the matrices are printed.

If N3 and N4 are given, only columns N3 and N4 of numeric matrices are printed.

If any of N1, N2, N3 or N4 is negative, or none of the rows (and columns) specified are inside a matrix only the name and size of that matrix are printed.

If ALL is written instead of a matrix name, all matrices are printed.

SAVE A F

Store matrix A on file F. If ALL is written instead of a matrix name all matrices are saved.

OLD A F

Read matrix A from file F. If ALL is written instead of a matrix name all matrices on file F are read.

EMACRO A [N1 [B1 B2...]]

Execute the commands stored in text matrix A N1 times (execute macro A). If N1 is omitted the macro is executed one time.

N1 may be given as a digit or as a scalar variable.

A macro may include calls for other macros (EMACRO) to a maximum level of 10.

B1, B2 etc are actual arguments of the macro A. If actual arguments are given, corresponding formal parameters must be defined in the macro by the command PMACRO. The maximum number of actual arguments is 10.

PMACRO P1 P2...

Define formal parameters of a macro.

P1, P2 etc are formal parameters of the macro. All operations in the macro dealing with P1, P2 etc are carried out for the matrices given as actual arguments in the command EMACRO. The maximum number of formal parameters is 10.

BMACRO L

Break execution of a macro. If the integer scalar L is greater than or equal to 1, execution of the macro is broken, otherwise execution is continued.

ADD A B C

Add matrices A and B. The result is stored in matrix C.

SUB A B C

Subtract matrix B from matrix A. The result is stored in C.

MULT A B C

Multiply matrices A and B. The result is stored in C. A or B may be a scalar.

ELIN A EM EN [J]

Assembly of the element matrix EM into the global structure matrix A as described by the topology matrix EN.

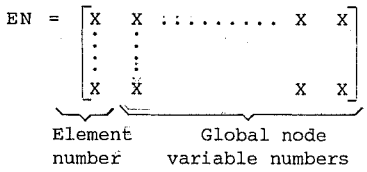

When J is omitted the assembly of EM is executed for all elements specified in matrix EN.

If J is specified the assembly of EM is performed for row number J in the topology matrix EN.

The command

ELIN P EL EN [J]

is used to assemble element load vector EL into the global vector P.

SOLVES A X P B [C]

Solves the symmetric system of equations

A X = P

where A is a symmetric matrix

P is the "load vector"

Prescribed rows in matrix X are specified in matrix B

[N X X . . . X]

Number of prescribed rows — Row numbers

C is a predefined scalar given the value
0 if the system of equations is positive definite and
1 if the system of equations is negative definite.

SOLVTR A B PIV [C]

Triangularize the matrix A in the system of equations

A X = P

Prescribed rows in matrix X are specified by matrix B

[N X X . . . X]

Number of prescribed rows — Row numbers

Matrix PIV is created and contains the Gaussian reduction factors.

Matrix C is a predefined scalar given the value
0 if the system of equations is positive definite and
1 if the system of equations is negative definite.

SOLVLM A X P B PIV

Modify the right hand side P ("load vector") in the system of equations

A X = P

The matrix B contains the prescribed rows in matrix X

[N X X . . . X]

N: Number of prescribed rows

X X . . . X: Row numbers

Matrix PIV contains the Gaussian reduction factors created by the command SOLVTR when matrix A has been triangularized.

SOLVBS A X P B [D]

Perform back-substitution in the system of equations

A X = P

The matrix B contains the prescribed rows in matrix X

[N X X . . . X]

N: Number of prescribed rows

X X . . . X: Row numbers

Matrix D contains calculated "reactions".

CONDES A B C D E

The symmetric system of equations

A X = B

is condensed to

$C \cdot \bar{X} = D$

The row (column) numbers to be condensed are specified in matrix E.

[N X X . . . X]

N: Number of rows to be condensed

X X . . . X: Row numbers

APPENDIX F. REFERENCES

[1] MALVERN. L.E.: Introduction to the mechanics of a continuous medium, Prentice-Hall, Englewood Cliffs, New Jersey 1969.

[2] FUNG, Y.C.: Foundations of solid mechanics, Prentice-Hall, Englewood Cliffs, New Jersey 1965.

[3] WASHIZU, K.: Variational methods in elasticity and plasticity, Third edition, Pergamon Press, Oxford 1982.

[4] ERINGEN, C.A.: Mechanics of continua, John Wiley and Sons, New York 1967.

[5] ODEN, J.T.: Finite elements of nonlinear continua, McGraw-Hill, New York 1972.

[6] BATHE, K-J.: Finite element procedures in engineering analysis, Prentice-Hall, Englewood-Cliffs, New Jersey 1982.

[7] SPENCER, A.J.M.: Continuum mechanics, Longman Mathematical Texts, London 1980.

[8] MATTIASSON, K.: Continuum mechanics principles for large deformation problems in solid and structural mechanics, Publ. 81:6, Chalmers University of Technology, Department of Structural Mechanics, Göteborg 1981.

[9] ZIENKIEWICZ, O.C.: The finite element method, Third edition, McGraw-Hill, London 1977.

[10] HUEBNER, K.H.: The finite element method for engineers, John Wiley and Sons, New York 1975.

[11] SEGERLIND, L.J.: Applied finite element analysis, John Wiley and Sons, New York 1976.

[12] BECKER, E.B., CAREY, G.F. and ODEN, J.T.: Finite elements, an introduction, Volume I, Prentice Hall, Englewood Cliffs, New Jersey 1981.

[13] COOK, R.D.: Concepts and applications of the finite element analysis, Second Edition, John Wiley and Sons, New York 1982.

[14] GALERKIN, B.G.: Reihenentwicklung für einige Fälle des gleichgewichts von Platten und Balken, Wjestwik Ingenow, No. 10, Petrograd 1915 (In Russian).

[15] BATHE, K-J., RAMM, E. and WILSON, E.L.: Finite element formulation for large deformation dynamic analysis, International Journal for Numerical Methods in Engineering, Vol. 9, pp. 353-386, 1975.

[16] HIBBIT, H.D., MARCAL, P.V. and RICE, J.R.: A finite element formulation for problems of large strain and large displacement, International Journal of Solids and Structures, Vol. 6, pp. 1069-1086, 1970.

[17] YAGMAI, S. and POPOV, E.P.: Incremental analysis of large deflections of shells of revolution, International Journal of Solids and Structures, Vol. 7, pp. 1375-1393, 1971.

[18] YAMADA, Y.: Incremental formulation for problems with geometric and material nonlinearities, Advances in Computational Methods in Structural Mechanics and Design, Second U.S.-Japan Seminar on Matrix Methods of Structural Analysis and Design, University of Alabama Press, pp. 325-355, 1972.

[19] STRICKLIN, J.A., VON RIESEMANN, W.A., TILLERSSON, J.R. and HAISLER, W.E.: Static geometric and nonlinear analysis, Advances in Computational Methods in Structural Mechanics and Design, Second U.S.-Japan Seminar on Matrix Methods of Structural Analysis and Design, University of Alabama Press, pp. 301-324, 1972.

[20] McMEEKING, R.M. and RICE, J.R.: Finite element formulations for problems of large elastic-plastic deformation, International Journal of Solids and Structures, Vol. 11, pp. 601-616, 1975.

[21] BATHE, K.J. and OZDEMIR, H.: Elastic-plastic large deformation static and dynamic analysis, International Journal of Solids and Structures, Vol. 6, pp. 81-92, 1976.

[22] HORRIGMOE, G.: Nonlinear finite element models in solid mechanics, Report No. 76-2, Division of Structural Mechanics, The Norwegian Institute of Technology, Trondheim 1976.

[23] WOOD, R.D. and ZIENKIEWICZ, O.C.: Geometrically nonlinear analysis of beams, frames, arches and axisymmetric shells, Computers and Structures, Vol 7, pp. 725-735, 1977.

[24] FREY, F. and CESOTTO, S.: Some new aspects of incremental total Lagrangian description in nonlinear analysis, Finite Elements in Nonlinear Solid and Structural Mechanics, Tapir, Trondheim 1978.

[25] ARGYRIS, J.H., BALMER, H., DOLTSINIS, J.ST., DUNNE, P.C., HAASE, M., KLEIBER, M., MALEJANNAKIS, G., MLEJNEK, H.-P., MÜLLER, M. and SCHARPT, D.W.: Finite element method - the natural approach, Computer Methods in Applied Mechanics and Engineering 17/18, pp. 1-106, 1979.

[26] CESOTTO, S., FREY, F. and FONDER, G.: Total and updated Lagrangian descriptions in nonlinear structural analysis: a unified approach, Energy Methods in Finite Element Analysis, pp. 283-296, Edited by R. Glowinsky, E. Rhodin and O.C. Zienkiewicz, John Wiley and Sons, 1979.

[27] NAGTEGAAL, J.C. and DE JONG, J.E.: Some computational aspects of elastic-plastic large strain analysis, International Journal for Numerical Methods in Engineering, Vol. 17, pp. 15-41, 1981.

[28] MATTIASSON, K.: On the co-rotational finite element formulation for large deformation problems, Publ. 83:1, Chalmers University of Technology, Department of Structural Mechanics, Göteborg 1983.

[29] CESOTTO, P.J.S., DE VILLE DE GOGET, V. and FREY, F.: Improved nonlinear finite elements for oriented bodies using an extension of Marguerre's theory, Computers and Structures, Vol. 17, pp. 129-137, 1983.

[30] HILL, R.: The mathematical theory of plasticity, Clarendon Press, Oxford 1950.

[31] MENDELSON, A.: Plasticity: Theory and Applications, Mac-Millan, New York 1968.

[32] MROZ, Z.: Mathematical models for inelastic material behaviour, Solid Mechanics Division, University of Waterloo, Waterloo Ontario 1973.

[33] AXELSSON, K.: On constitutive modelling in metal plasticity with special emphasis on anisotropic strain hardening and finite element formulation, Publ. 79:2, Chalmers University of Technology, Department of Structural Mechanics, Göteborg 1979.

[34] OWEN, D.R.J. and HINTON, E.: Finite elements in plasticity: Theory and practice, Pineridge Press Ltd., Swansea 1980.

[35] ODQVIST, F.K.G.: Mathematical theory of creep and creep rupture, Oxford Mathematical Monographs, Oxford University Press, Oxford 1966.

[36] HULT, J.: Creep in engineering structures, Blaisdell, 1966.

[37] RABOTNOV, Y.N.: Creep problems in structural members, English translation edited by F.A. Leckie, North-Holland, Amsterdam 1969.

[38] CRISTESCU, N. and SULICIU, I.: Viscoplasticity, Matrinus Nijhoff Publishers, The Hague 1982.

[39] BOLEY, B. and WEINER, J.: Theory of Thermal Stresses, John Wiley and Sons, New York 1967.

[40] BOYLE, J.T. and SPENCE, J.: Stress Analysis for creep, Butterworths, 1983.

[41] UEDA, Y. and YAMAKAWA, T.: Thermal nonlinear behaviour of structures, Advances in Computational Methods in Structural Mechanics and Design, University of Alabama Press, pp. 375-392, 1971.

[42] CYR, N.A. and TETER, R.D.: Finite element elastic-plastic-creep analysis of two-dimensional continuum with temperature dependent material properties, Computers and Structures, Vol. 3, pp. 849-863, 1973.

[43] HAISLER, W.E. and SANDERS, D.R.: Elastic-plastic-creep-large strain analysis at elevated temperature by the finite element method, Technical Report No. 3275-78-1, Aerospace Engineering Department, Texas A&M University, 1973.

[44] SHARAFI, P. and YATES, D.N.: Nonlinear thermo-elastic-plastic and creep analysis by the finite element method, AIAA Journal, Vol. 12, No. 9, pp. 1210-1215, 1974.

[45] CHENG, W-G.:Creep analysis of steel structures at elevated temperatures, Dr. Thesis, University of Notre Dame, Indiana 1975.

[46] YAMADA, Y.: Constitutive modelling of inelastic behaviour and numerical solution of nonlinear problems by the finite element method, Computers and Structures, Vol. 8, pp. 533-543, 1978.

[47] RUNESSON, K.: On non-linear consolidation of soft clay, Publ. 78:1, Chalmers University of Technology, Department of Structural Mechanics, Göteborg 1978.

[48] ALLEN, D.H. and HAISLER, W.E.: The application of thermal and creep effects to the combined isotropic-kinematic hardening model for inelastic structural analysis by the finite element method, Technical Report No. 3275-79-3, Aerospace Engineering Department, Texas A&M University, 1979.

[49] ALLEN, D.H. and HAISLER, W.E.: The prediction of response of solids to thermal loading using the finite element code AGGIE I, Technical Report 3275-80-1, Aerospace Engineering Department, Texas A&M University, 1980.

[50] SNYDER, M.D. and BATHE, K-J.: A solution for thermo-elastic-plastic and creep problems, Nuclear Engineering and Design 64, pp. 40-80, 1981.

[51] ALLEN, D.H. and HAISLER, W.E.: A theory for analysis of thermo-plastic materials, Computers and Structures, Vol. 13, pp. 125-135, 1981.

[52] LEVY, A.: High-temperature inelastic analysis, Computers and Structures, Vol. 13, pp. 249-256, 1981.

[53] ARGYRIS, J.H., SZIMMAT, J. and WILLIAM, K.J.: Computational aspects of welding stress analysis, Computer Methods in Applied Mechanics and Engineering, pp. 635-666, 1982.

[54] CHENG, W-C.: Theory and application of the behaviour of steel structures at elevated temperatures, Computers and structures, Vol. 16, pp. 27-35, 1983.

[55] RUNESSON, K.: Conventional finite element analysis of elastic-viscoplastic solids subjected to quasistatic and thermal load, Publ. 80:5, Chalmers University of Technology, Department of Structural Mechanics, Göteborg 1980.

[56] THELANDERSSON, S.: On the multiaxial behaviour of concrete exposed to high temperature, Nuclear Engineering and Design, Vol. 75, No. 2, pp. 271-282, 1983.

[57] von MISES, R.: Mechanik für plastischen formänderung von kristallen, Zeitschrift für angewandte Matematik und Mechanik, Vol. 8, 1928.

[58] GREEN, A.E. and NAGHDI, F.M.: A general theory of an elastic-plastic continuum, Archive for Rational Mechanics and Analysis, Vol. 18, pp. 251-281, 1965.

[59] GREENSTREET, W.L., CORUM, J.M., PUGH, C.E. and LIU, K.C.: Currently recommended constitutive equations for inelastic design analysis for FFTF components, ORNL-TM-3602, Oak Ridge National Laboratory, Tennessee 1971.

[60] PUGH, C.E. and ROBINSON, D.N.: Some trends in constitutive equation model development for high-temperature behaviour of fast-reactor structural alloys, Nuclear Engineering and Design, pp. 269-276, 1978.

[61] ALLEN, D.H.: A survey of current temperature dependent elastic-plastic-creep constitutive laws for applicability to finite element computer codes, Technical Report No. 3275-80-2, Aerospace Engineering Department, Texas A&M University, 1980.

[62] CORUM, J.M.: Future needs for inelastic analysis in design of high-temperature nuclear plant components, Computers and Structures, Vol. 13, pp. 231-240, 1981.

[63] KONTER, A.W.A. and KUSTERS, G.M.A.: Influence of constitutive equations on the results of inelastic analysis of Benchmark problems, Transactions, 6th SMiRT conference, Paris 1981.

[64] LEVY, A. and PIFKO, A.B.: On computational strategies for problems involving plasticity and creep, International Journal of Numerical Methods in Engineering, Vol. 17, pp. 747-771, 1981.

[65] FUJIMOTA, M., FURUMURA, F., AVE, T. and SHINOHARA, Y.: Primary creep of structural steel at high temperatures, Laboratory of Engineering Materials, Tokyo Institute of Technology, Number 4, 1979.

[66] NIKITENKO, A.F.: Effect of prior creep strain on instantaneous elastoplastic deformation of a material, Strength of Materials, No. 13, Vol. 2, pp. 155-158, 1981.

[67] ALAN, D.H.: Thermodynamic and computational aspects of a thermoplastic constitutive theory, Transactions, 6th SMiRT conference, Paris 1981.

[68] ALLEN, D.H.: A thermodynamic framework for comparison of current thermoviscoplastic constitutive models for metals at elevated temperature, Proceedings, International Conference on Constitutive Laws for Engineering Materials, Theory and Application, Editors C.S. Desai and R.H. Gallagher, pp. 61-69, Tuscon 1983.

[69] SCHMIDT, C.G. and MILLER, A.K.: A unified phenomenological model for non-elastic deformation of type 316 stainless steel - part I: Development of the model and calculation of the material constants, Res Mechanica (3), pp. 109-129, 1981.

[70] WENG, G.J.: A unified self-consistent theory for plastic-creep deformation of metals, Journal of Applied Mechanics, Vol. 49, pp. 728-734, 1982.

[71] CESOTTO, S. and LECKIE, F.: Determination of unified constitutive equations for metals at high temperature, Proceedings, International Conference on Constitutive Laws for Engineering Materials, Theory and Application, Editors C.S. Desai and R.H. Gallagher, pp. 105-111, Tuscon 1983.

[72] HARMATHY, T.Z.: A comprehensive creep model, Journal of Basic Engineering, Transaction of the ASME, Vol. 89, 1967.

[73] FESSLER, H. and HYDE, T.H.: Creep deformation of metals, Creep of Engineering Materials, A Journal of Strain Analysis Monograph, Edited by C.D. Pomeroy, pp. 85-110, Mechanical Engineering Publications, London 1978.

[74] BJURSTEN, J.: Steel reinforcement at transient conditions, Graduate work, Lund Institute of Technology, Lund 1980 (in Swedish).

[75] THOR, J.: Deformations and critical loads of steel beams under fire exposure conditions, Document D16:1973, National Swedish Building Research, 1973.

[76] ANDERBERG, Y.: Mechanical behaviour of steel reinforcement at high temperature, Tekniska Meddelanden nr 36, Halmstads Järnverk, 1978, (in Swedish).

[77] JENNINGS, A.: Frame analysis including change of geometry, Journal of the Structural Division, ASCE 94, No. ST3, pp. 627-644, 1968.

[78] MALLET, R.H. and MARCAL, P.V.: Finite element analysis of nonlinear structures, Journal of the Structural Division, ASCE 94, No. ST9, pp. 2081-2105, 1968.

[79] POWELL, G.H.: Theory of nonlinear elastic structures, Journal of the Structural Division, ASCE 95, No. ST12, pp. 2687-2701, 1969.

[80] MARTIN, H.C.: Finite elements and the analysis of geometrically nonlinear problems, Recent Advances in Matrix Methods and Structural Analysis and Design, University of Alabama Press, pp. 343-377, 1971.

[81] ORAN, C.: Tangent stiffness in plane frames, Journal of the Structural Division, ASCE 99, No. ST6, pp. 973-985, 1973.

[82] BÄCKLUND, J.: Finite element analysis of nonlinear structures, Dr. Thesis, Chalmers University of Technology, Department of Structural Mechanics, Göteborg 1973.

[83] BELYTSCHKO, T. and HSIEH, B.J.: Nonlinear transient finite element analysis with convected coordinates, International Journal for Numerical Methods in Engineering, Vol. 7, pp. 255-271, 1973.

[84] ÅLSTEDT, E.: Nonlinear analysis of reinforced concrete frames, Report No. 75-1, The Norwegian Institute of Technology, Division of Structural Mechanics, The University of Trondheim, Trondheim 1975.

[85] KANG, Y-J.: Nonlinear geometric, material and time-dependent analysis of reinforced and prestressed concrete frames, Dr. Thesis, University of California, Berkeley 1977.

[86] RAMSETH, S.N.: Nonlinear static and dynamic analysis of framed structures, Computers and Structures, Vol. 10, pp. 879-897, 1979.

[87] BATHE, K-J. and BOLURCHI, S.: Large displacement analysis of three-dimensional beam structures, International Journal of Numerical Methods in Engineering, Vol. 14, pp. 961-986, 1979.

[88] KARAMANLIDIS, D., HONECKER, A. and KNOTHE, K.: Large deflection finite element analysis of pre- and post-critical response of thin elastic frames, Nonlinear Finite Analysis in Structural Mechanics, Springer Verlag, 1981.

[89] BANOVEC, J.: An efficient finite element method for elastic-plastic analysis of plane frames, Nonlinear Finite Element Analysis in Structural Mechanics, Springer Verlag, 1981.

[90] TANG, S.C., YEUNG, K.S. and CHON, C.T.: On the tangent stiffness in a convected coordinate system, International Journal of Computers and Structures, Vol. 12, pp. 849-856, 1980.

[91] ARGYRIS, J.H., BONI, B., HINDENLANG, V. and KLEIBER, M.: Finite element analysis of two- and three-dimensional elasto-plastic-frames - the natural approach, Computer Methods in Applied Mechanics and Engineering 35, pp. 221-248, 1982.

[92] ZANATHY, M.H. and MURRAY, D.W.: Nonlinear finite element analysis of steel frames, Journal of Structural Engineering, Vol. 109, No. 2, pp. 353-368, 1983.

[93] KASSIMALI, A.: Large deformation analysis of elastic-plastic frames, Journal of Structural Engineering, Vol. 109, No. 8, 1983.

[94] WEN, R.K. and RAHIMZADEK, J.: Nonlinear elastic frame analysis by finite element, Journal of Structural Engineering, Vol. 109, No. 8, pp. 1952-1971, 1983.

[95] WENNERSTRÖM, H.: Numerical and computer techniques in finite element analysis, Publ. 81-7, Chalmers University of Technology, Department of Structural Mechanics, Göteborg 1981.

[96] WICKSTRÖM, U.: TASEF-2, A computer program for temperature analysis of structures exposed to fire, Report 79-2, Department of Structural Mechanics, Lund Institute of Technology, Lund 1979.

[97] BECKER, J.M., BIZRI, H. and BRESLER, B.: FIRES-T, A computer program for the fire response of structures - thermal, Report No. UCB FRG 74-1, University of California, Berkeley 1974.

[98] BATHE, K-J.: ADINAT - A finite element program for automatic dynamic incremental nonlinear analysis of temperatures, Report 82448-5, Acoustic and Vibration Laboratory, Mechanics Engineering Department, Massachusetts Institute of Technology, 1977.

[99] BERGAN, P.G. and SØREIDE, T.: A comparative study of different numerical solution techniques as applied to a nonlinear structural problem, Computer Methods in Applied Mechanics and Engineering, Vol. 2, pp. 1-17, 1973.

[100] STRICKLIN, J.A., HAISLER, W.E. and RIESMANN, W.A.: Evaluation of solution procedures for material and/or geometrically nonlinear structural analysis, AIAA Journal, Vol. 11, No. 3, pp. 292-299, 1973.

[101] BERGAN, P.G., HORRIGMOE, G., KRÅKELAND, B. and SØREIDE, T.: Solution techniques for nonlinear finite element problems, International Journal for Numerical Methods in Engineering, Vol. 12, pp. 1677-1696, 1978.

[102] CRISFIELD, M.A.: A faster modified Newton-Raphson iteration, Computer Methods in Applied Mechanics and Engineering, Vol. 20, pp. 267-278, 1978.

[103] ARNESSEN, A.: Analysis of reinforced concrete shells considering material and geometric nonlinearities, Report No. 79-1, Division of Structural Mechanics, The University of Trondheim, Trondheim 1979.

[104] PRZEMIENIECKI, J.S.: Theory of matrix structural analysis, McGraw-Hill, New York 1968.

[105] PETERSSON, H. and POPOV, E.P.: Substructuring and equation system solutions in finite element analysis, Computers and Structures, Vol. 7, pp. 197-206, 1977.

[106] DAHLBLOM, O. and PETERSON, A.: CAMFEM - Computer aided modelling based on the finite element method, Report TVSM-3001, Lund Institute of Technology, Division of Structural Mechanics, Lund 1982.

[107] DAHLBLOM, O.: CAMFEM applied to nonlinear structural analysis, Report TVSM-7016, Lund Institute of Technology, Division of Structural Mechanics, Lund 1983.

[108] OLSSON, M.: Finite element analysis of structures subjected to moving loads, Report TVSM-3004, Lund Institute of Technology, Division of Structural Mechanics, Lund 1983.

[109] SANDBERG, G.: Fluid-structure interaction - numerical studies, Lund Institute of Technology, Division of Structural Mechanics, to be published.

[110] FRISCH-FAY, R.: Flexible bars, Butterworths, London 1962.

[111] MATTIASSON, K.: Numerical results from elliptic integral solutions of some elastic problems of beams and frames, Publ. 79-10, Department of Structural Mechanics, Chalmers University of Technology, Göteborg 1979.

[112] EBNER, A.M. and UCCIFERRO, J.J.: A theoretical and numerical comparison of elastic nonlinear finite element methods, Computers and Structures, Vol. 2, pp. 1043-1061, 1972.

[113] ARGYRIS, J.H.: Recent Advances in Matrix Methods of Structural Analysis, Progress in Aeronautical Sciences, Vol. 4, Pergamon Press, 1964.

[114] MARTIN, H.C.: On the derivation of stiffness matrices for the analysis of large deflection and stability problems, Proceedings, Conference of Matrix Methods in Structural Mechanics, Wright-Pettersson Air Force Base, Ohio 1965.

[115] WILLIAMS, F.W.: An approach to the nonlinear behaviour of the members of a rigid jointed plane frame work with finite deflections, Quarterly Journal of Mechanics and Applied Mathematics, Vol. XVII, pp. 451-469, 1964

[116] TIMOSHENKO, S.P. and WOINOWSKY-KRIEGER, S.: Theory of plates and shells, McGraw-Hill, Second edition, 1970.

[117] PRAGER, W. and HODGE, P.G.: Theory of perfectly plastic solids, John Wiley and Sons, New York 1951.

[118] SØREIDE, T.: Collapse behaviour of stiffened plates using alternative finite element formulations, Report No. 77-3, The Norwegian Institute of Technology, Division of Structural Mechanics, The University of Trondheim, Trondheim 1977.

[119] FREY, F.: L'analyse statique non lineare des structures par la methode des elements finis et son application a la construction metallique, These de doctorat, Universite de Liege, Liege 1978, (in French).

[120] REYER, E. and NÖLKER, A.: Zum Brandverhalten von Gesamtkonstruktionen des Stahl- und Stahlverbundbaues, 1. Teil Verfahren, Eignungstests und Vegleichberechnungen zur experimentellen Untersuchung mit Grossmodellen, Der Stahlbau Heft 1, pp. 1-10, 1983, (in German).

[121] FORSÉN, N.E.: Steelfire, finite element program for nonlinear analysis of steel frames exposed to fire, Multiconsult AS, Oslo 1983.

[122] STANZAK, W.W. and HARMATHY, T.Z.: Effect of deck on failure temperature of steel beams, Research Paper No. 388, Division of Building Research, National Research Council of Canada, Ottawa 1968.

[123] HARMATHY, T.Z. and STANZAK, W.W.: Elevated-temperature tensile and creep properties of some structural and prestressing steels, Research Paper No. 424, Division of Building Research, National Research Council of Canada, Ottawa 1970.

[124] HARMATHY, T.Z.: Creep deflection of metal beam in transient heating process, with particular reference to fire, Research Paper No. 673, Division of Building Research, National Research Council of Canada, Ottawa 1976.

[125] FURUMURA, F. and SHINOHARA, Y.: Inelastic behaviour of protected steel beams and frames in fire, Report of the Research Laboratory of Engineering Materials, Tokyo Institute of Technology, Number 3, pp. 1-14, Tokyo 1978.

[126] FORSÉN, N.E.: A theoretical study of the fire resistance of concrete structures, Cement and Concrete Research Institute, The Norwegian Institute of Technology, STF65 A82062, Trondheim 1982.

[127] Regulations for Steel Structures, 1970, The National Swedish Committee on Regulations for Steel Structures, (In Swedish with an English summary).